UNIVERSIDAD POLITÉCNICA DE CARTAGENA

ESCUELA TÉCNICA SUPERIOR DE INGENIERÍA DE TELECOMUNICACIÓN

Proyecto Fin de Carrera

Investigación sobre antenas impresas RFID UHF para uso en soporte óptico, CDs, DVDs

Investigation on printed antennas for RFID UHF systems for application in optical devices, CDs, DVDs

AUTOR:	José Antonio García Pérez
DIRECTOR:	Alejandro Álvarez Melcón
CODIRECTOR:	Fernando D. Quesada Pereira

Cartagena, Octubre 2013

Acknowledgements

First I would like to thank all the persons involved in this project, specially to professors Dr. Alejandro Alvarez Melcon and Dr. Fernando D. Quesada Pereira. They have provided me the inspiration and motivation to do this project and get involved in microwaves world.

I would like to acknowledge too the support provided by my family and all my friends during all these years. It couldn't have been possible without their help .

Author	José Antonio García Pérez
Author's email	josse89@gmail.com
Director	Alejandro Álvarez Melcón
Director's email	alejandro.alvarez@upct.es
Co-director	Fernando Quesada Pereira
Title	Investigación sobre antenas impresas RFID UHF para uso en soporte óptico, CDs, DVDs

Summary

Los sistemas de RFID han experimentado una expansión considerable en las últimas décadas debido principalmente a su capacidad para reducir la intervención humana en los procesos de identificación. Este potencial ha provocado el desarrollo de muchas aplicaciones de RFID utilizadas en las empresas como la trazabilidad alimentaria y el control de inventario. Uno de los problemas de esta tecnología aparece cuando las antenas se sitúan cerca de materiales metálicos o líquidos, reduciendo su alcance y fiabilidad de lectura. En este proyecto se ha investigado el desarrollo de nuevas antenas RFID UHF para ser utilizadas en dispositivos ópticos como CDs y DVDs. Para ello hemos desarrollado una interfaz gráfica de usuario en MATLAB para reducir el tiempo de desarrollo de las antenas.

RFID systems have experienced a considerable expansion in the recent years due mainly to their ability to reduce human intervention on identification processes. This potential have caused the development of many RFID applications to be used in companies as food traceability and control inventory. One problem of RFID UHF antennas is when they are situated near metallic materials or liquids, reducing their reading range and reliability. In this project we have investigated the development of novel RFID UHF antennas to be used on optical devices as CD's and DVD's. For this purpose we have developed a MATLAB GUI to highly reduce the geometric design time of the antennas.

Degree	Ingeniero de Telecomunicación
Department	Tecnologías de la Información y la Comunicación
Submission date	Octubre 2013

Contents

1 Introduction **15**

2 Concepts and Theory **19**

2.1 Antenna Characterization Parameters 19

2.1.1 Impedance Matching 19

2.1.2 Radiation Efficiency 20

2.1.3 Mono-static Radar Cross Section (Mono-static RCS) 21

2.2 CD characteristics 22

2.3 RFID chip characteristics 24

3 GUI for Antenna Design **27**

3.1 Graphic User Interface 27

3.2 Antenna Parameters 29

3.2.1 Meanders Antenna 30

3.2.2 Commercial Ring Antenna 33

3.2.3 Arms Antenna 35

3.3 HFSS Options 37

3.3.1 General 37

3.3.2 Setup 37

3.3.3 Sweep 38

3.3.4 Dielectric 38

3.3.5 CD . . . 39
3.3.6 Loading . . . 41
3.3.7 Analysis Buttons . . . 42
3.4 Plot and Save . . . 48
3.5 Directories and Video . . . 50

4 Simulations and Results Before Software Development 51
4.1 Previous Research . . . 52
4.1.1 Bent Dipole . . . 53
4.1.2 Compact Printed-On-CD UHF RFID Tag Antennas . . . 54
4.2 First Antennas . . . 56
4.2.1 Ring-Type Antenna . . . 56
4.2.2 Longitudinal Meanders Antenna . . . 57
4.2.3 Transverse Meanders Antenna . . . 58
4.2.4 Antennas efficiency . . . 59
4.2.5 Study on polycarbonate . . . 60
4.2.6 Study on CD . . . 63
4.2.7 RCS Study . . . 65
4.2.8 Commercial Linear Antenna . . . 69
4.3 New Proposal for Antennas for CDs . . . 75

5 Simulations and Results with GUI Software 83
5.1 First Examples . . . 83
5.2 New Design Strategies . . . 87
5.2.1 Free Space Meanders Antenna . . . 88
5.2.2 Meanders Antenna on Dielectric . . . 91
5.2.3 Meanders Antenna on CD . . . 93
5.2.4 Ring Antenna . . . 96
5.2.5 Arms Antenna . . . 98
5.3 Meanders Antenna Improvement . . . 101

5.3.1 Meanders Antenna on Dielectric Cylinder 101
5.3.2 Meanders Antenna on Dielectric Foam 103
5.3.3 Meanders Antenna on Available Dielectric 105
5.3.4 Meanders Antenna with 4 Arms 107
5.4 Ideal CD Dilema 109
5.4.1 Tapered Antenna 110
5.4.2 Ground Plane Antennas 111
5.5 Last Meanders Antenna 118
5.5.1 Large Meanders Antenna 119
5.5.2 Small Meanders Antenna 121

6 Conclusions and Future Research Lines **125**

List of Figures

2.1 Classic CD dimensions 23

3.1 Final GUI 28
3.2 General panel 29
3.3 Commercial linear antenna 30
3.4 Meanders antenna 30
3.5 Meanders antenna parameters panel 31
3.6 Meanders antenna parameters 31
3.7 Commercial ring antenna 33
3.8 Commercial ring antenna parameters panel 34
3.9 Commercial ring antenna parameters 34
3.10 Arms antenna 36
3.11 Arms antenna parameters panel 36
3.12 HFSS General sub-panel 37
3.13 HFSS Setup sub-panel 38
3.14 Sweep sub-panel 38
3.15 Dielectric sub-panel 39
3.16 Dielectric Inclusion 39
3.17 CD sub-panel 40
3.18 Complete CD 40
3.19 Only Polycarbonate 40

3.20 Only Aluminium . . . 41
3.21 Loading Error . . . 41
3.22 Loading sub-panel . . . 41
3.23 Loading Inclusion . . . 42
3.24 Stacked Impedance Result Example . . . 43
3.25 Smith Chart Result Example . . . 43
3.26 Axial Ratio Result Example . . . 44
3.27 Reflection Coeficient Result Example . . . 44
3.28 Efficiency Error Window . . . 45
3.29 Efficiency Result Example . . . 45
3.30 RCS Designs . . . 46
3.31 RCS Error . . . 46
3.32 RCS Result Example . . . 47
3.33 RCS Subtract Error . . . 48
3.34 RCS Subtract Example . . . 48
3.35 Plot and Save Panel . . . 49
3.36 Final directory tree . . . 50

4.1 CD center typically used for placing the antenna . . . 52
4.2 Bending dipole antenna . . . 53
4.3 Bending dipole impedance . . . 54
4.4 Meander-Type Antenna (Left) and Ring-Type Antenna (Right) . . . 55
4.5 Longitudinal Meanders Antenna (Left) and Transverse Meanders Antenna (Right) . . . 56
4.6 Ring-Type Antenna S_{11} coefficient . . . 57
4.7 Longitudinal Meanders Antenna S_{11} coefficient . . . 58
4.8 Transverse Meanders Antenna S_{11} coefficient . . . 59
4.9 Antenna efficiency comparison . . . 60
4.10 Ring-Type on polycarbonate . . . 61
4.11 Longitudinal Meanders Antenna on polycarbonate . . . 61

4.12 Transverse Meanders Antenna on polycarbonate 62
4.13 Antenna efficiency comparison on polycarbonate 62
4.14 Ring-Type Antenna on CD 63
4.15 Longitudinal Meanders Antenna on CD 64
4.16 Transverse Meanders Antenna on CD 64
4.17 Antenna efficiency comparison on CD 65
4.18 Phi and Theta components when reader interrogates with Theta polarization in $\phi = 0$ deg plane 66
4.19 Phi and Theta components when reader interrogates with Theta polarization in $\phi = 90$ deg plane 67
4.20 Phi and Theta components when reader interrogates with Phi polarization in $\phi = 0$ deg plane 67
4.21 Phi and Theta components when reader interrogates with Phi polarization in $\phi = 90$ deg plane 68
4.22 Commercial Ring Antenna dimensions 69
4.23 Commercial Ring Antenna S_{11} coefficient 70
4.24 Commercial Antenna radiation efficiency 71
4.25 Reflected component (Phi) when reader interrogates with Phi polarization for both planes $\phi = 0$ deg and $\phi = 90$ deg 72
4.26 Reflected component (Theta) when reader interrogates with Phi polarization for both planes $\phi = 0$ deg and $\phi = 90$ deg 73
4.27 Reflected component (Theta) when reader interrogates with Theta polarization for both planes $\phi = 0$ deg and $\phi = 90$ deg 73
4.28 Reflected component (Phi) when reader interrogates with Theta polarization for both planes $\phi = 0$ deg and $\phi = 90$ deg 74
4.29 New antenna model proposed for CDs 76
4.30 Antenna model proposed for CDs with meanders connected in feeding loop border 77

4.31 Antenna model proposed for CDs with meanders connected in feeding loop center 78
4.32 Radiation efficiency for new proposed antennas depending on meanders number 79
4.33 Reflected component (Phi) when reader interrogates with Phi polarization for both planes $\phi = 0$ deg and $\phi = 90$ deg 79
4.34 Reflected component (Theta) when reader interrogates with Phi polarization for both planes $\phi = 0$ deg and $\phi = 90$ deg 80
4.35 Reflected component (Theta) when reader interrogates with Theta polarization for both planes $\phi = 0$ deg and $\phi = 90$ deg 81
4.36 Reflected component (Phi) when reader interrogates with Theta polarization for both planes $\phi = 0$ deg and $\phi = 90$ deg 81

5.1 New optimized antenna at RFID UHF frequency 84
5.2 Optimized antenna with less meanders and increasing tapering 85
5.3 Optimized antenna with one arm shortened 85
5.4 Optimized antenna with one arm shortened on polycarbonate 86
5.5 Optimized antenna with one arm shortened on CD 87
5.6 Optimized antenna with short-circuited arms 87
5.7 8 meanders antennas with open arms (Left) and closed arms (Right) . 88
5.8 8 meanders antenna with open arms results on free space 89
5.9 8 meanders antenna with closed arms results in free space 90
5.10 Meanders antennas on dielectric with open arms (Left) and closed arms (Right) 91
5.11 Meanders antenna with open arms results on dielectric 92
5.12 Meanders antenna with open arms results on dielectric 93
5.13 Meanders antennas on CD model 1 (Left) and model 2 (Right) 94
5.14 Meanders antenna model 1 results on CD 95
5.15 Meanders antenna model 2 results on CD 95
5.16 Commercial Ring Antenna on CD 96

5.17 Commercial Ring antenna results on CD 97
5.18 Ring antenna variations example 98
5.19 Arms antenna on dielectric (Left) and on CD (Right) 99
5.20 Arms antenna results on dielectric 100
5.21 Arms antenna results on CD 100
5.22 Meanders antenna on a dielectric cylinder 102
5.23 Meanders antenna results on a dielectric cylinder 102
5.24 Meanders antenna on a dielectric foam 103
5.25 Meanders antenna results on a dielectric foam 104
5.26 Meanders antenna on dielectric and CD (with available dielectric of $\epsilon_r = 2.2$ and 0.13 mm) 105
5.27 Meanders antenna with short-circuited arms results 106
5.28 Meanders antenna with open-circuited arms results 106
5.29 Meanders antenna with 4 arms on dielectric and CD model 1 (left) and model 2 (right) 107
5.30 Meanders antenna with 4 arms on dielectric and CD results 108
5.31 Meanders antenna with 4 arms on dielectric and CD results 109
5.32 Tapering antenna 110
5.33 Tapering antenna results 111
5.34 Thick dielectric ground plane antenna 112
5.35 Thick dielectric ground plane antenna results 113
5.36 Thick dielectric ground plane antenna RCS results on XZ plane . . . 113
5.37 Thick dielectric ground plane antenna RCS results on YZ plane . . . 114
5.38 Antenna examples on thin dielectric of 13 mm (Left) and 4 mm (Right) 115
5.39 Antenna on 13 mm and $\epsilon_r = 10.2$ dielectric results 115
5.40 Antenna on 4 mm and $\epsilon_r = 10.2$ dielectric results 116
5.41 Thin dielectric (4 mm and $\epsilon_r = 10.2$) ground plane antenna RCS results on XZ plane 117

5.42 Thick dielectric (4 mm and $\epsilon_r = 10.2$) ground plane antenna RCS results on YZ plane 118
5.43 Last antenna meanders models with large meanders (Left) and small meanders (Right) 118
5.44 Last antenna meanders with large meanders results (dielectric 0.13 mm and $\epsilon_r = 2.2$) 119
5.45 Last antenna meanders with large meanders RCS results on XZ plane 120
5.46 Last antenna meanders with large meanders RCS results on YZ plane 121
5.47 Last antenna meanders with small meanders results (dielectric 0.13 mm and $\epsilon_r = 2.2$) 122
5.48 Last antenna meanders with small meanders RCS results on XZ plane 122
5.49 Last antenna meanders with small meanders RCS results on YZ plane 123

6.1 Thick antenna example 127

Chapter 1

Introduction

During the last years, RFID systems have experienced a considerable expansion in a lot of business areas, from people and items control to the development of complex product traceability systems in many companies. The main advantage of RFID systems in comparison with the previous barcode based systems, is their ability to read and detect a lot of different objects automatically without human intervention. This has allowed the development of efficient electronic systems which are very useful to improve many processes in many companies, replacing the old barcode based systems much less efficient.

Despite of all those benefits, RFID systems have some drawbacks that have delayed their deployment on small and medium-sized businesses. On the one hand the high cost associated to the systems, due to the specific hardware needs (tags on the products and readers all along the reading area). On the other hand the complexity of the integration of new RFID systems with old installed systems.

In addition to the aforementioned difficulties there is a problem not yet solved which is the massive use of RFID systems in many applications. The problem appears if RFID tags are in proximity of metallic or liquid materials such as cans, bottles, etc. In those cases, the radiation produced by the antenna is deteriorated

and the RFID tag become useless.

One interesting application for RFID technology would be the CD/DVD or Blue-Rays identification. In this case, the problem described appears due to the metallization of some layers of the disc and the reading reliability is reduced. One solution for this problem is placing the tag outside the CD box but this is not a good solution because in many places such as libraries the CD cases are not sealed and therefore people could steal them very easily.

The main objective of this project is the investigation of techniques to solve this problem and increase the RFID tags reliability when they are placed on the most common optical devices such as CDs, DVDs or Blue-Rays and the extrapolation of results to other applications like glass bottles, cans or any other problematic surface. For this purpose HFSS software [1] is used to design and analyze the antennas and to store the desired results. To reduce the design time a MATLAB GUI has been implemented so the creation of the whole structure is done automatically and also the results exportation.

To achieve this goal the following parameters have been analyzed:

- *Antenna to RFID chip matching.* Important to use the maximum reader power.

- *Radiation Efficiency.* This is an obviated parameter in previous investigations which is very important specially when working with electrically small antennas. Even if there is a good power matching, it is important to check which percentage is going to be radiated and which absorbed by the lossy structure surrounding the antenna due to non ideal materials.

- *Mono-static Radar Cross Section* (Monostatic RCS). It is another common obviated parameter in previous investigations and very important for RFID

applications since these RFID systems are based on the *backscattering* principle. When the reader interrogates the tag, it answers reflecting the received incident wave power. Such reflection is received back by the reader so the amount of reflected power will be determined by the tag RCS. For this reason this parameter is so important to determine the performance of the designed antennas.

Chapter 2

Concepts and Theory

In this chapter the theoretical background and all the concepts studied previously before starting the project will be explained. These concepts have been studied from bachelor and master degree and reference books such as [2], [3], [4].

2.1 Antenna Characterization Parameters

2.1.1 Impedance Matching

As previously stated in the introduction chapter, the first important parameter for the antenna characterization is the power matching between the antenna and the chip. It should be noted that RFID chips generally present a strong capacitive impedance. In this project we have chosen an Impijn chip [5]. The formula used to obtain the power matching is the power reflection coefficient commonly defined, for complex impedances, as shown in equation 2.1 from [6].

$$\rho_{11} = \frac{Z_{ant} - Z^{\star}_{chip}}{Z_{ant} + Z_{chip}} \tag{2.1}$$

Where Z_{ant} is the antenna impedance and Z_{chip} the chip impedance. The star superscript on the numerator denotes the complex conjugated impedance. A high module on negative dBs of this parameter will indicate that there is a good matching

between the antenna and the chip, so the chip will use the the maximum available power to make the antenna radiates.

2.1.2 Radiation Efficiency

This is a very important parameter when working with electrically small antennas. It is desirable to maximize the radiation efficiency of the designed antennas in order to assure than the input power in the antenna is actually radiated, and is not dissipated due to the internal losses of materials. This parameter measures the relationship between the power that is actually radiated by the antenna and the total power delivered by the generator.. Obtaining it theoretically through simulation is a complex problem. Typically efficiency is calculated comparing directivity and gain with regard to calibrated antennas. To calculate the radiation efficiency we have used a variant of the *Wheeler Cap Method* described in [7]. This method is based on the calculation of the antenna radiated power and power delivered by the source which in this case is the RFID chip, differentiating the loss resistance R_{loss} from the total antenna resistance R_{ant}. In [7] a metallic sphere is employed in order to eliminate the radiation and so it is possible to calculate the dissipated power. In [8] this sphere is also investigated and is indicated that using this sphere is not always easy because it presents inner resonances which give rise to a strong interaction with the antenna. Following the above procedure, the efficiency could be calculated as shown in equation 2.4.

$$\eta = \frac{P_{rad}}{P_{chip}} = \frac{P_{chip} - P_{loss}}{P_{chip}} \tag{2.2}$$

Where P_{rad} is the power radiated by the antenna and P_{chip} is the power delivered from the chip to the antenna. The power delivered by the chip can be calculated by using circuit theory 2.3

$$P_{chip} = \tfrac{1}{2}|I|^2 Re(Z_{ant}) \quad I = \tfrac{V_g}{Z_{chip}+Z_{ant}} \tag{2.3}$$

Where V_g it the available voltage in the chip. The lost power P_{loss} is calculated in

the same way but using the metallic sphere around the antenna in order to eliminate the radiated power. In this project, to avoid the complexity of using the metallic sphere, we have simplified the process. So we also avoid the undesired effects that the auxiliary sphere causes on the antenna. The technique we have implemented eliminates the dissipated power P_{loss} from the total delivered power P_{chip}. In this manner the efficiency can be expressed as 2.4.

$$\eta = \frac{P_{rad}}{P_{chip}} = \frac{P_{rad}}{P_{rad} + P_{loss}} \tag{2.4}$$

If we remove the structure losses in the simulation, then the delivered power 2.3 will be equal to the radiated power P_{rad} since the power can not be dissipated in the antenna or the CD structure because they have been considered without losses and $P_{loss} = 0$. The second step is to simulate again the structure introducing the previously removed losses and calculate the power with 2.3, so in this case this power corresponds to the delivered power by the chip $P_{chip} = Prad + Ploss$, since one part will be dissipated by the lossy materials and the other one radiated.

The simplification introduced in this technique is that we suppose that in both simulations (lossy and lossless), the radiated power does not change. This is true whenever the losses do not affect the reactive part of the antenna impedance which is usually met if the corresponding losses are not very large.

2.1.3 Mono-static Radar Cross Section (Mono-static RCS)

The last studied parameter for the antennas is the *Mono-static Radar Cross Section*, of which importance results to the working principle of RFID-UHF systems that is the backscattering modulation principle. The RCS of an object measures the relationship between the reflected power in the object and the incident power. In this case the RCS has to be mono-static, since the reader interrogates and receives the answer essentially from the same direction. If we use the electric field square value to state those powers, the equation used to calculate the RCS is 2.5.

$$\sigma = \lim_{R \to \infty} 4\pi R^2 \frac{|E_r|^2}{|E_i|^2} \tag{2.5}$$

Where E_r is the reflected electric field by the object and E_i is the incident electric field. In this case R is the distance between the reader and the tag. Generally a high RCS is desirable because it entails more reflected power to the RFID reader which allows a longer reading distance.

The last point to consider is the polarization property of the electromagnetic waves. Normally, both reader and antenna could operate with different polarization schemes. This means that the transmitted wave could be an electric field in two orthogonal polarizations combinations θ and ϕ. On the other hand, the tag can also reflect power in both polarizations. Consequently, the RCS shown in 2.5 must be calculated using the 4 possibles polarization combinations which allows the reader interrogation and the tag response.

2.2 CD characteristics

It is essential to know the characteristics of the structure that will be studied and simulated [9]. Therefore the first thing that is going to be done is studying the CD properties. In figure 2.1 it is depicted the classical CD dimensions. As can be seen in the figure, the CD structure consists of a central air hole of 15 mm of diameter, followed by a polycarbonate circle of 39 mm of diameter. This part does not contains information and is used by CD readers to hold stable the CD. The external part of this central circle reaches the 40 mm. From this point the information section starts, which extends from 40 mm up to 120 mm where the CD limit is found.

The structure has a lot of area to be used for sticking the tag, however the information section has a metalized layer which has negative effects on the tag radiation so, in general, it can not be used for placing the antenna. This is due to the high

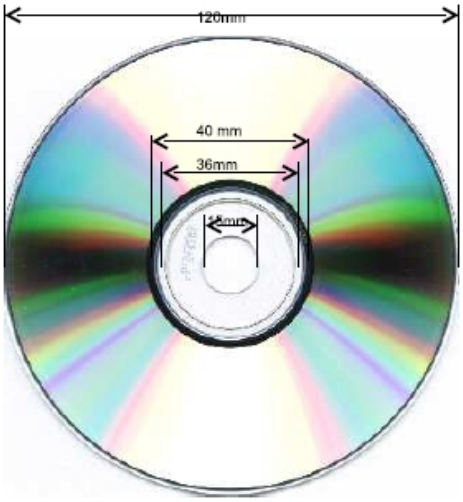

Figure 2.1: Classic CD dimensions

conductivity of this layer that tends to short-circuiting any antenna placed on its surface. This is the reason that existing solutions for RFID tag antennas try to use only the central polycarbonate part of 39 mm of diameter.

Otherwise, for a correct antenna modeling, it is necessary to know the electromagnetic properties of the polycarbonate plastic used on CD fabrication. The most interesting electromagnetic characteristics for our project due to their impact on antenna design are:

- Width 1.2 mm
- Relative dielectric constant $\varepsilon_r = 2.6 - 2.9$
- Permittivity $\varepsilon = 2.567 \cdot 10^{-11} \frac{F}{m}$
- Relative permeability $\mu_r = 0.866$
- Permeability $\mu = 1.089 \frac{\mu H}{m}$

2.3 RFID chip characteristics

It is very important for the project development to select an appropriate RFID chip for the designed antenna.

Currently there are different types of RFID chips for sale, working on different frequency bands (HF, UHF or even microwave bands). This project is focused on the RFID tags improvement working on UHF band which is of 866 MHz in Europe. At this frequency the wavelength is $\lambda = 0.3464$ meters so it will be very important the electrical size of the antenna depending on the working wavelength.

One of the latest chips covering the above requirements is the Monza 4 chip manufactured by Impinj. This chip also meets the GEN 2 EPCGlobal specifications standard. This was the reason to have chosen this chip model for the project.

From the standpoint of the antenna design, the chip is very important since it is the key element which the antenna has to transfer the received reader power. This power sent by the reader must be captured by the antenna and be transferred to the RFID chip. The chip then uses this power to feed itself by a AC-DC rectifying process. This is the reason that the most important design parameter is going to be the inner chip impedance which will be responsible for the chip-antenna matching. For this purpose the antenna and the chip must comply the Maximum Power Transfer Theorem.
As can be seen at the RFID chip datasheet [5], the chip has a frequency dependent impedance shown in table 2.1.

Such chip impedance does not vary very much depending on the frequency. In this project as has been said before, we will use the European band of 866 MHz. At this frequency the chip impedance is $13 - j151\Omega$, so the antenna will require an impedance of $Z_{ant} = Z^{\star}_{chip} = 13 + j151\Omega$ to accomplish the Maximum Power Transfer Theorem. Therefore, one of the objectives will be to obtain such antenna

Frequency	Chip Impedance
866 MHz	$13 - j151\Omega$
915 MHz	$11 - j143\Omega$
956 MHz	$10 - j137\Omega$

Table 2.1: Chip Impedance

impedance in order to match it to the chip and achieve the maximum transferred power.

Chapter 3

GUI for Antenna Design

The creation of the geometry of an antenna and the whole structure with the CD is very complicated and requires a lot of design time even for experienced users with CAD software. This causes the need to spend long times for creating each structure and that highly reduces the ability to optimize the designs and adjust them to the desirable specifications due to the need to adjust a lot of parameters. To avoid these drawbacks we have developed a Graphic User Interface by using MATLAB and the capability of HFSS for executing scripts. Thereby, by using this software it is possible to reduce the design time and test many different structures in a very simple way.

3.1 Graphic User Interface

The software basically creates a script using MATLAB functions in HFSS language with all the geometry and simulation parameters and then the program opens HFSS and runs the script automatically. As starting point we have used the MATLAB API available in [10] and it has been expanded with new specific functions for this project. The final GUI is shown in figure 3.1. This software allows to introduce a lot of parameters for the antenna to be designed, and exports the most important results to analyze and compare the response of the structure with other results. As can be seen at a glance in the GUI there are 3 panels:

- ***Antenna Parameters***: this panel is used to define the antenna geometry. It is possible to generate 3 types of antennas named *Meanders*, *Arms* and *Commercial Ring* which will be explained later. Each antenna has different sub-panels so they will be explained separately.

- ***HFSS Options***: this panel defines HFSS simulation configuration and is divided in *General*, *Setup* and *Sweep* which are used to set the simulation parameters and the folder where the results will be exported.

- ***Plot and Save***: This last panel is used to load a *.csv* file and plot it with the right axes. This is useful for comparing results from several antennas. This panel can also save the generated plots as a *.jpg* image.

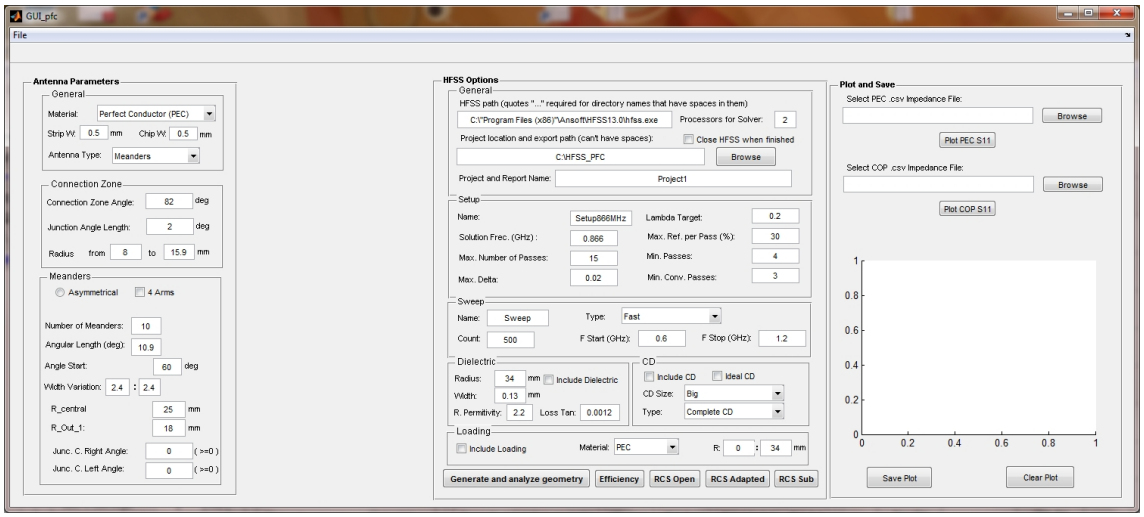

Figure 3.1: Final GUI

The software can automatically obtain different results which is very useful to determine the response of the antenna at first sight without wasting much time and save and load it with the file menu options as a *.mat* file. In the following sections it will be explained how to use the software and all its features.

3.2 Antenna Parameters

As it is said above, this panel allows the user to define the desired antenna geometry. For this aim, the panel has different parameters available depending on the selected antenna. In the following sub-section the different parameters for each antenna and how to generate each geometry will be described. The *General* sub-panel is always the same for all antennas (figure 3.2).

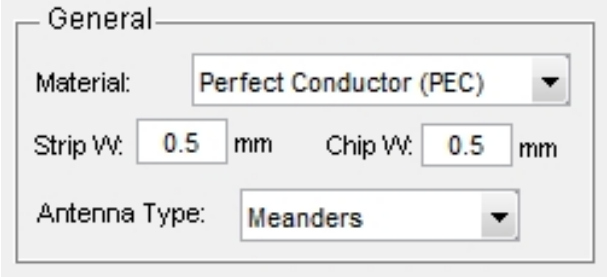

Figure 3.2: General panel

- ***Material:*** this option selects the antenna material. If we choose *Perfect Electric Conductor (PEC)* the antenna will be made of PEC so it won't have losses. If *Copper* is chosen the antenna will be made of copper and it will have losses. These two options will be important when computing antenna efficiency.
- ***Strip W:*** indicates the strip width of the antenna.
- ***Chip W:*** indicates the chip width to be connected to the antenna. It will leave more or less space in the connecting region depending on the chip size.
- ***Antenna Type:*** option for choosing the antenna type between the 3 available options: *Meanders*, *Arms* or *Commercial Ring*.

Depending on the selected antenna. The sub-panels below the general panel will be different in order to provide the proper geometry parameters for each antenna. Those are explained in more detail below.

3.2.1 Meanders Antenna

This one is the main studied antenna in the project. It is based on a linear RFID commercial tag depicted on figure 3.3. This antenna uses meanders to extend its electrical length and make it size similar to the wavelength of 0.3464 m at 866 MHz. Our modified meanders antenna, shown in figure 3.4, is based on the same meanders principle but is conformed to the circular shape of a conventional CD.

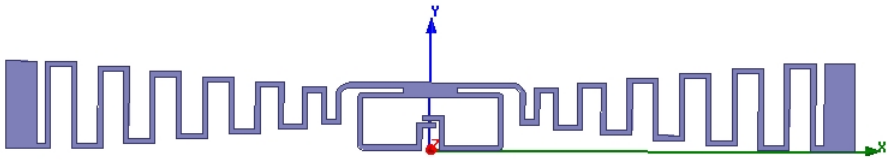

Figure 3.3: Commercial linear antenna

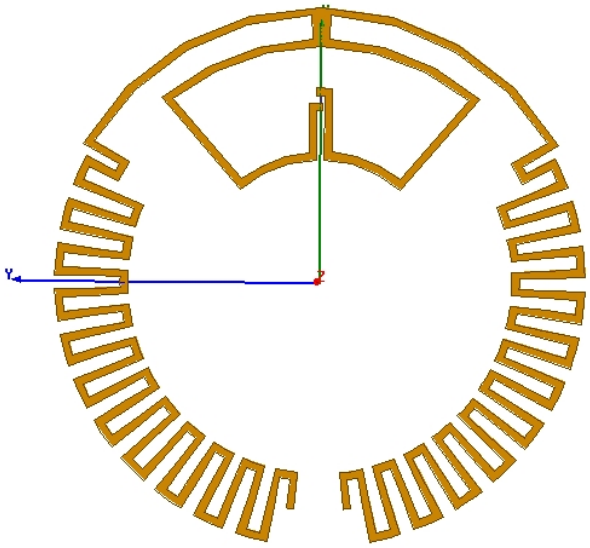

Figure 3.4: Meanders antenna

The GUI panel for generating this antenna is shown in figure 3.5.

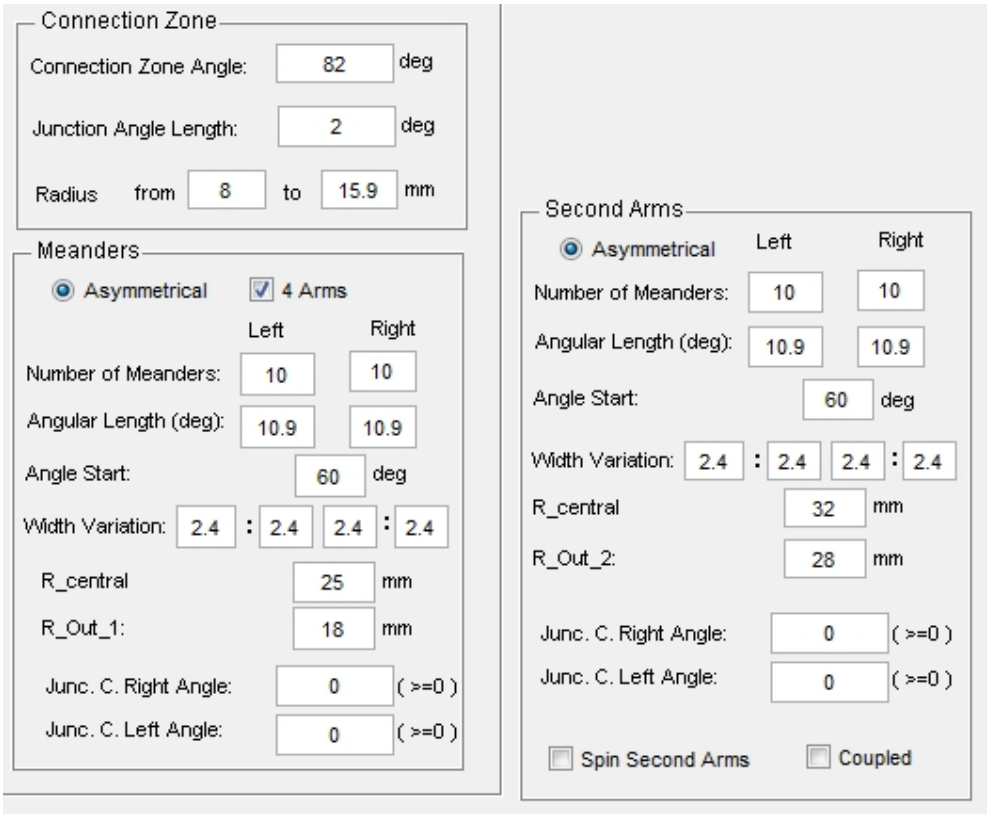

Figure 3.5: Meanders antenna parameters panel

As can be seen it has the following parameters shown in figure 3.6 :

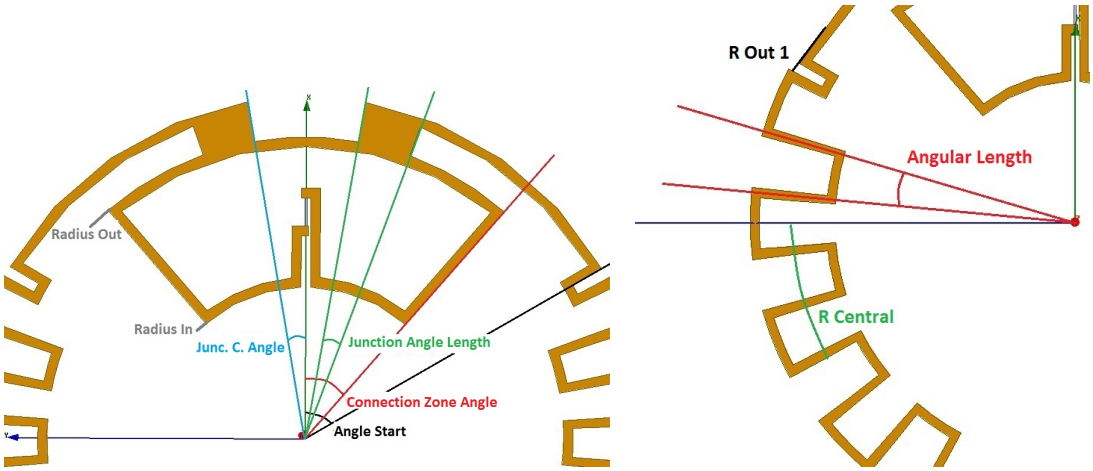

Figure 3.6: Meanders antenna parameters

- ***Connection Zone***

  This part is used to define the geometry parameters of the main loop where the chip connection zone is.

  - ***Connection Zone Angle:*** angular length of the main loop.
  - ***Junction Angle Length:*** angular length of the junction between the connection zone and the meanders.
  - ***Radius:*** defines the connection zone width from an inner radius to an outer radius.

- ***Meanders***

  This part defines the antenna meanders.

  - ***Asymmetrical:*** by default meanders are defined symmetrical but it is possible to select this option to do them asymmetrical. When this option is selected the left and right meander options become available so it will be possible to define each arm parameters separately.
  - ***4 Arms:*** If this option is selected it will appear another meander configuration panel which will allow to define another 2 arms for the antenna. This new panel has also the options *Spin* which flips the new meanders and *Coupled* which eliminates the union between the connection zone and the new meanders so they will be coupled to the first meanders.
  - ***Number of Meanders:*** number of meanders of the antenna.
  - ***Angular Length:*** length in degrees of each meander.
  - ***Angle Start:*** first meander start angle.
  - ***Width Variation:*** width variation from the first meander to the last meander. The meanders width will grow incrementally from the first value for the first meander to the last value for the last meander.
  - ***R central:*** central radius of the meanders arm.

- ***R Out 1 and 2:*** connection radius between the connection zone and the meanders.

- ***Junc. C. Right and Left Angle:*** connection angle for the union between the connection zone and the meanders (See figure 3.6.

As can be seen above this antenna can fit very well on a CD beacuse it has the same shape with a free space in its center and circular arms. The analysis and conclusions about this antenna will be discussed on following chapters.

3.2.2 Commercial Ring Antenna

This antenna is a commercial RFID tag studied and compared with the new ones and shown in figure 3.7. This antenna has different parameters respects to the previous one. The active panel when this antenna is selected is shown in figure 3.8. Its geometric parameters are depicted in figure 3.9 and explained below.

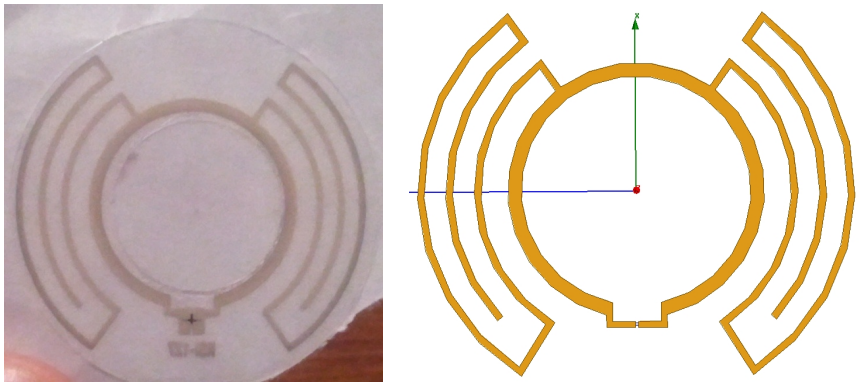

Figure 3.7: Commercial ring antenna

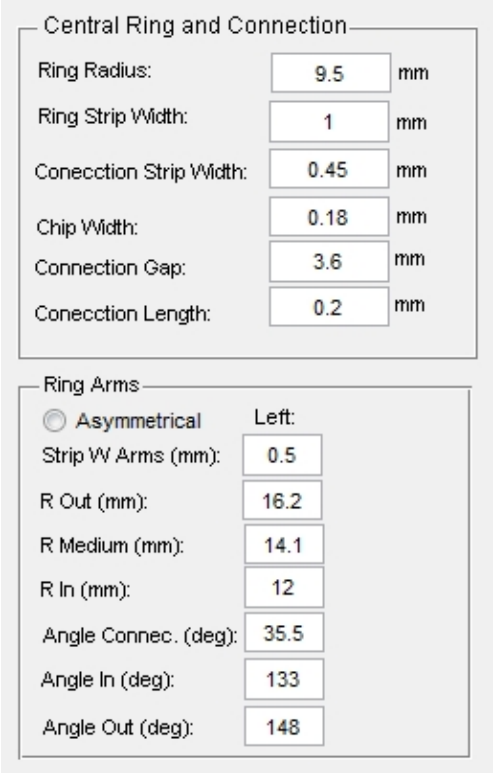

Figure 3.8: Commercial ring antenna parameters panel

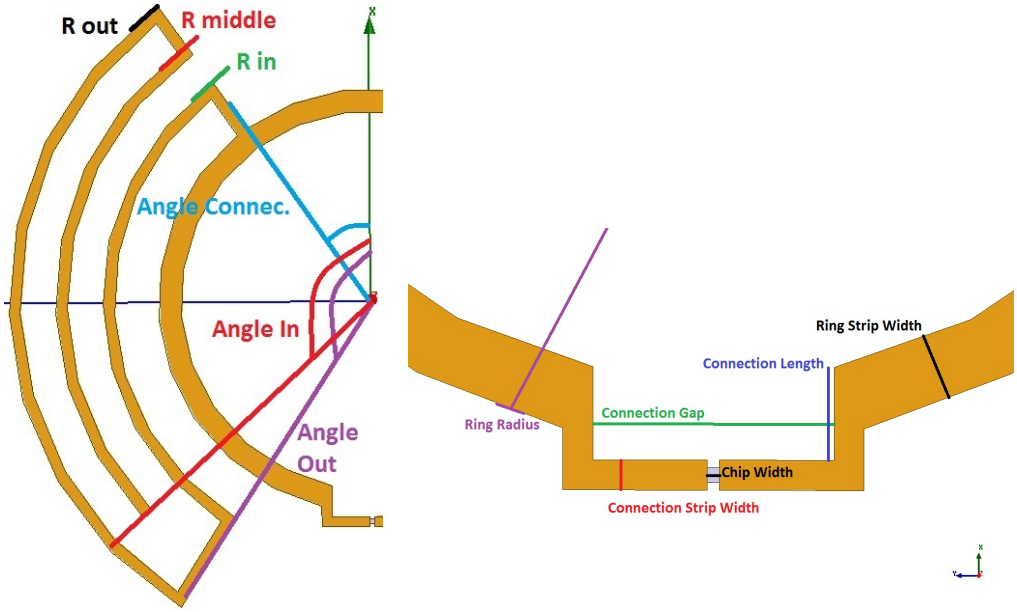

Figure 3.9: Commercial ring antenna parameters

- ***Central Ring and Connection***

  This part is used to define the geometric parameters of the main ring where the chip connection zone is.

  - ***Ring Radius:*** defines the outer radio of the main ring.
  - ***Ring Strip Width:*** strip width of the main ring.
  - ***Connection Strip Width:*** width of the strip where the chip is placed.
  - ***Chip Width***: width of the chip to be connected.
  - ***Connection Gap:*** gap which contains the connection strip and the chip.
  - ***Connection Length:*** separation between the connection strip and the main ring.

- ***Ring Arms***

  This part defines the antenna arms.

  - ***Strip W Arms:*** width of the arms strip.
  - ***R Out:*** radius of the outer arm.
  - ***R Middle:*** radius of the middle arm.
  - ***R in:*** radius of the inner arm.
  - ***Angle Connec:*** angle of connection of the whole arm.
  - ***Angle In:*** finish angle of the middle arm.
  - ***Angle Out:*** finish angle of the outer arm.

3.2.3 Arms Antenna

This antenna was designed as an hybrid between the meanders antenna and the commercial ring antenna. It is basically the union of the connection zone of the meanders antenna with the commercial ring antenna arms. The antenna is in figure

3.10 and the visible panel when this antenna is selected is shown in figure 3.11. As can be seen those parameters are the same as the meanders antenna for the connection zone and the same as the ring antenna for the arms so they will not be explained in detail again.

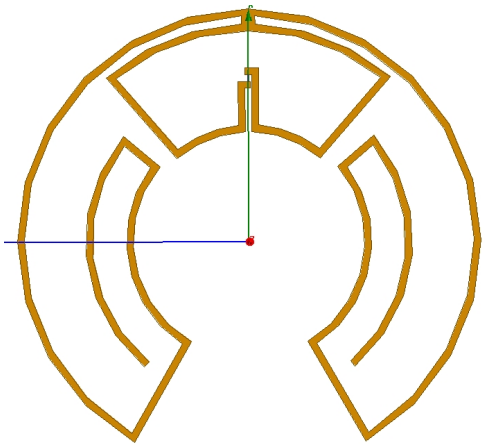

Figure 3.10: Arms antenna

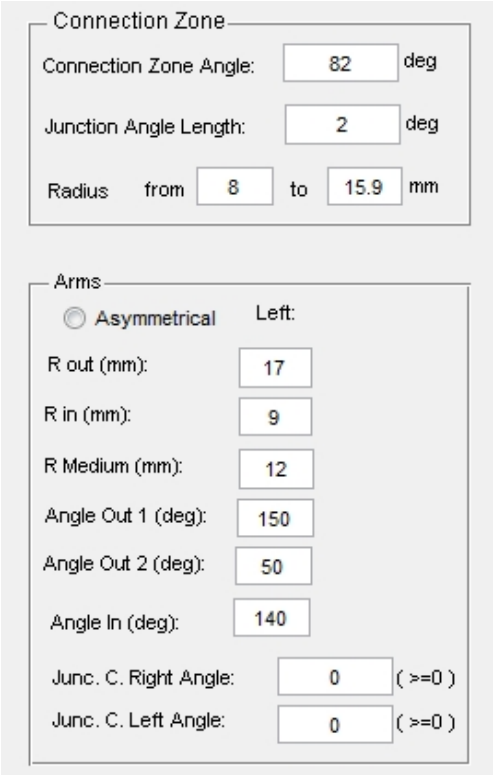

Figure 3.11: Arms antenna parameters panel

3.3 HFSS Options

This section of the GUI is created for defining all the HFSS configuration parameters. It also includes the *Dielectric*, *CD* and *Loading* options that are geometric options but are placed here because of the space constrains in the GUI. Inside this panel there are 6 sub-panels named *General*, *Setup*, *Sweep*, *Dielectric*, *CD* and *Loading* that are used to define the different parameters of the HFSS simulation and the last ones for including a dielectric, a CD or a loading in the dielectric. These sub-panels are described in detail below.

3.3.1 General

This sub-panel is used to define the HFSS.exe path and the project path and name. The *HFSS.exe* path is configured by default. The name of the project is very important because the software will create automatically a folder with this name and inside it will create all the sub-directories that will contain all the project and results files. This panel has also an option named *Close HFSS when finished* that if selected the software will close automatically HFSS when the simulation and the file exportation are finished. It is also possible to select the number of processors used for simulating the project. This panel is shown in figure 3.12.

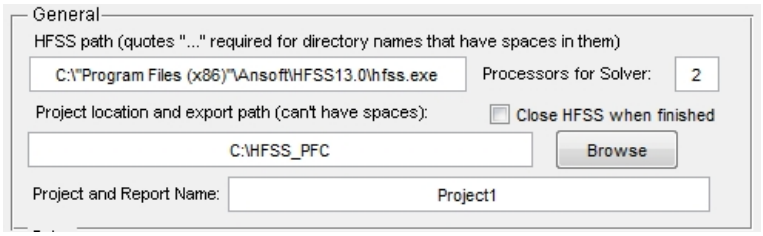

Figure 3.12: HFSS General sub-panel

3.3.2 Setup

This sub-panel configures all the simulation setup options for HFSS. It is very important to define properly the parameters to obtain the desired simulation results

with maximum reliability. This panel is shown in figure 3.13.

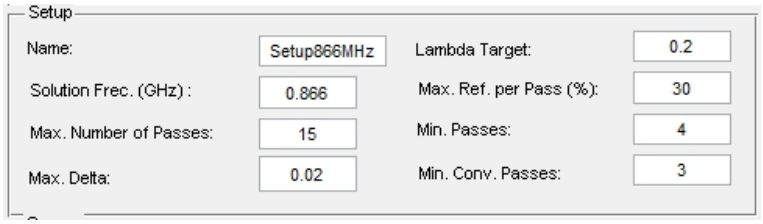

Figure 3.13: HFSS Setup sub-panel

3.3.3 Sweep

This sub-panel determines the name, type and properties of the frequency sweep for the analysis. It is important to define correctly the frequency range and the number of points to obtain a good report with relevant data. For example, if we need a good impedance matching around 866 MHz we should use a wide range from 500 MHz to 1.5 GHz for a good resolution and afterwards we can reduce this range to analyze the response in more detail. This panel is shown in figure 3.14.

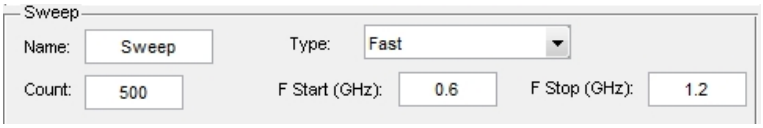

Figure 3.14: Sweep sub-panel

3.3.4 Dielectric

With this sub-panel we can include a dielectric substrate between the antenna and the CD. We can define the *Radius*, *Width*, *Relative Permittivity* and *Loss Tangent*. To include the dielectric it is only necessary to check the option *Include Dielectric* and it will be included automatically in the simulation with the introduced parameters. This panel is shown in figure 3.15 and in figure 3.16 an example snapshot of the dielectric is shown.

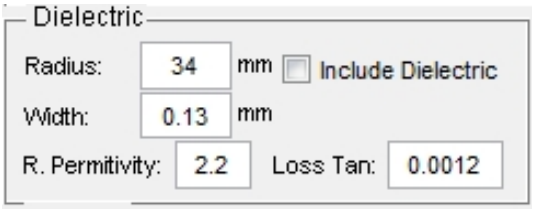

Figure 3.15: Dielectric sub-panel

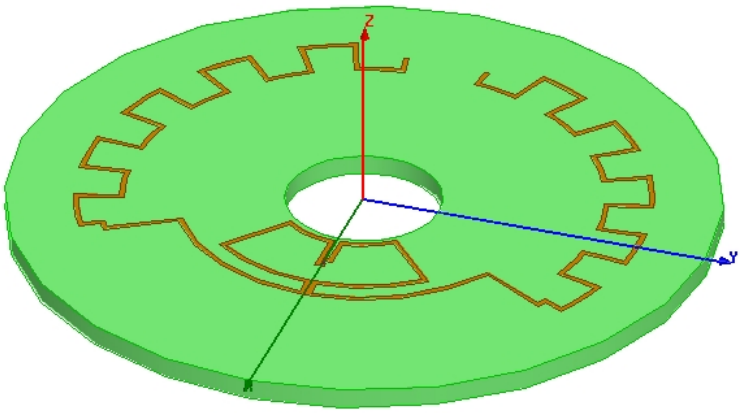

Figure 3.16: Dielectric Inclusion

3.3.5 CD

In the same way than the previous sub-panel, this one allows to include a CD. It is possible to include it as an ideal CD (all the CD materials will be lossless as the polycarbonate will have loss tangent 0 and the layer will be made of PEC). In the option *CD Size* it can be selected if the CD has a normal size (*Big* option, $Diameter = 120mm$) or a mini-CD size (*Small* option, $Diameter = 80mm$) and the *CD Type* which selects if the CD structure is *Complete* (figure 3.18), *Only Polycarbonate* (figure 3.19) or *Only Aluminum* (figure 3.20). This panel is shown in figure 3.17.

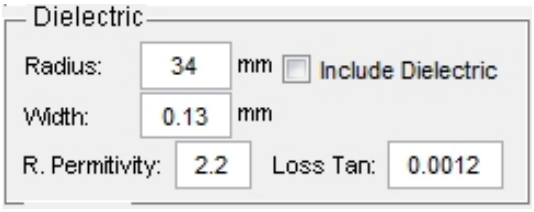

Figure 3.17: CD sub-panel

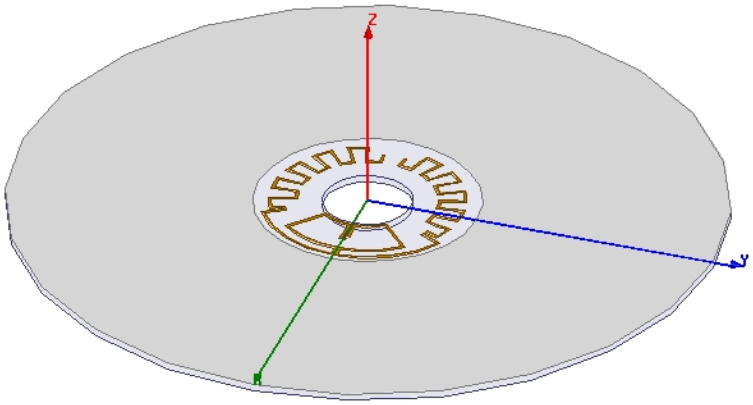

Figure 3.18: Complete CD

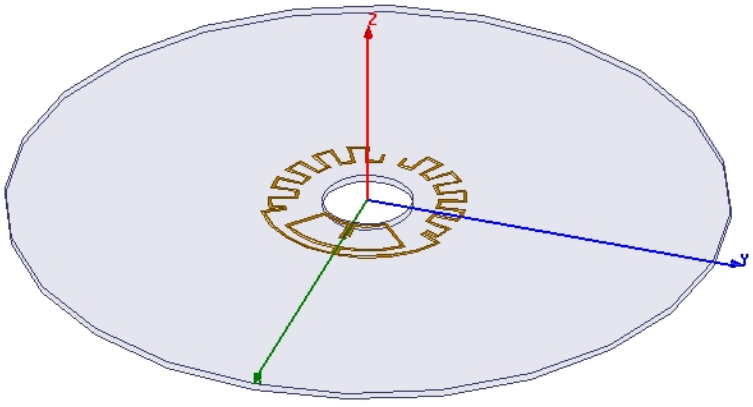

Figure 3.19: Only Polycarbonate

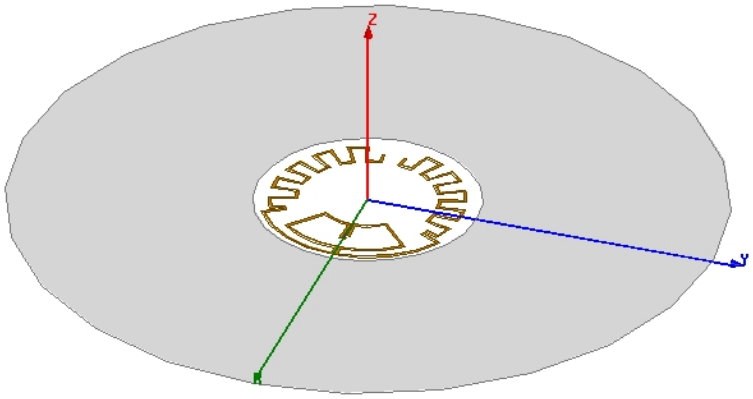

Figure 3.20: Only Aluminium

3.3.6 Loading

This sub-panel can be used to include a metallic layer in the middle of the dielectric for studying how the loading inclusion affects the antenna response. One can select the material (*PEC* or *Copper*) and the start and finish radius. If the include option is selected without including a dielectric, the software will show an error (figure 3.21) since the loading can not be modelled if a dielectric is not used in the structure. This panel is shown in figure 3.22, whereas in figure 3.23 an example capture of the dielectric is shown.

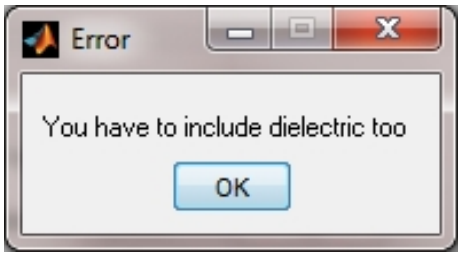

Figure 3.21: Loading Error

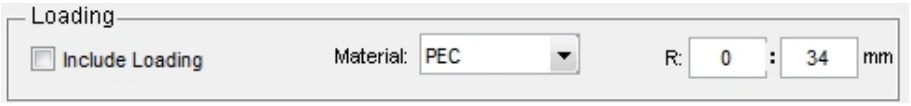

Figure 3.22: Loading sub-panel

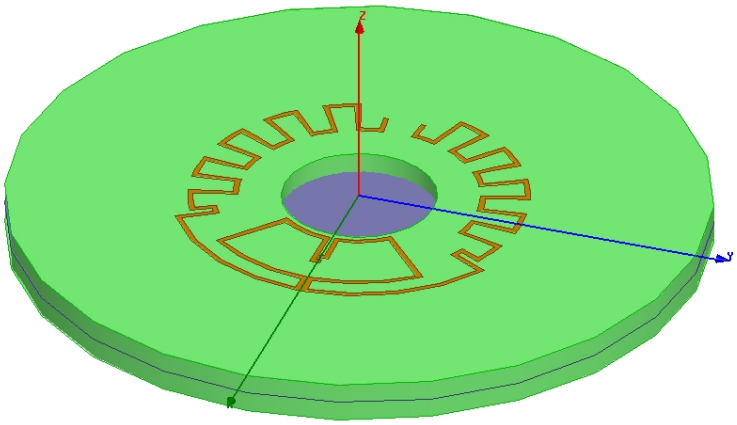

Figure 3.23: Loading Inclusion

3.3.7 Analysis Buttons

Those buttons run the simulations and export the results. There are 5 buttons named *Generate and analyze geometry*, *Efficiency*, *RCS Open*, *RCS Adapted*, *RCS Sub*. They will be explained below.

- ***Generate and analyze geometry***: This first button generates the antenna geometry and executes the electromagnetic analysis in HFSS. It is the first step to obtain results from a designed antenna. It should be noticed that depending on the selected material, the project files and the exported results in the selected directory will be *Lossless* for PEC material simulations or *Lossy* for Copper simulations. The project file will be saved at the *ProjectFiles* directory named as the project name and finished as Lossy or Lossless depending on the selected material. When this button is pressed down the software will start creating the HFSS script and then HFSS will be opened automatically and the script created in MATLAB will be loaded and executed by HFSS. The geometry will be the first thing that the script will create and then it will begin to define all the simulation parameters and the simulation will start to run. It is advisable to look at the simulation convergence by right-clicking in the setup name at the left tree in HFSS to be sure that the simulation is going

well and if not, stop it before wasting much time.

If the simulation is going properly it will converge and when finished the script will automatically show the *Stacked real and imaginary impedance* (figure 3.24), *Smith chart* (figure 3.25) and the *Axial ratio* (figure 3.26) and in background those results will be exported as a *.jpg* image and *.csv* file to the selected directory in the folder named *\ReportFiles\Z_S_Smith_AxialRatio_Efficiency*. Depending on the material type the name of those files will end in *-Lossless* or *-Lossy*. This button also saves a screen capture of the GUI in the *ReportFiles* directory.

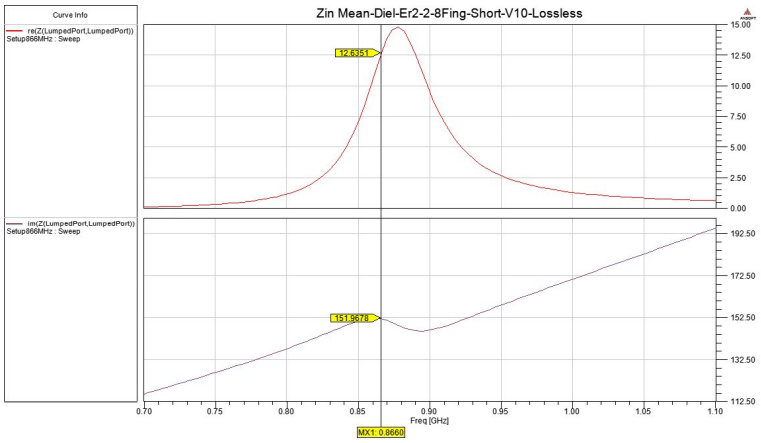

Figure 3.24: Stacked Impedance Result Example

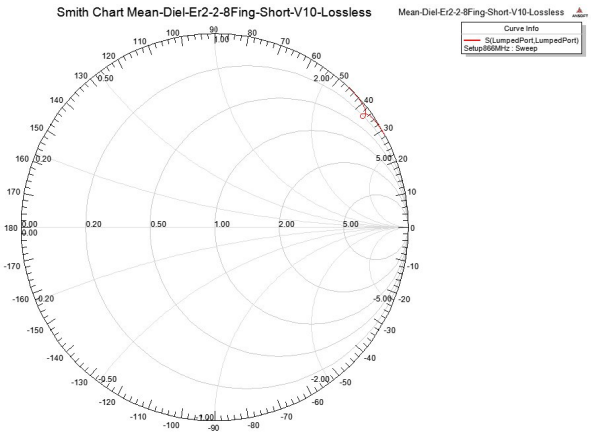

Figure 3.25: Smith Chart Result Example

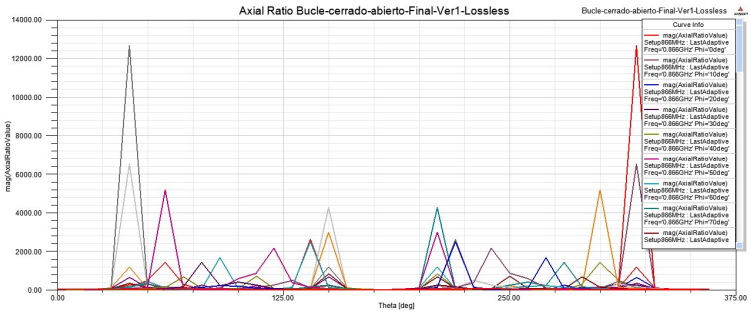

Figure 3.26: Axial Ratio Result Example

When HFSS is closed after a successful simulation the software will read the *.csv* impedance file and will calculate and plot the reflection coeficient S_{11} parameter in a MATLAB figure that will be saved in the same directory as the aforementioned results files as a *.jpg* image (figure 3.27).

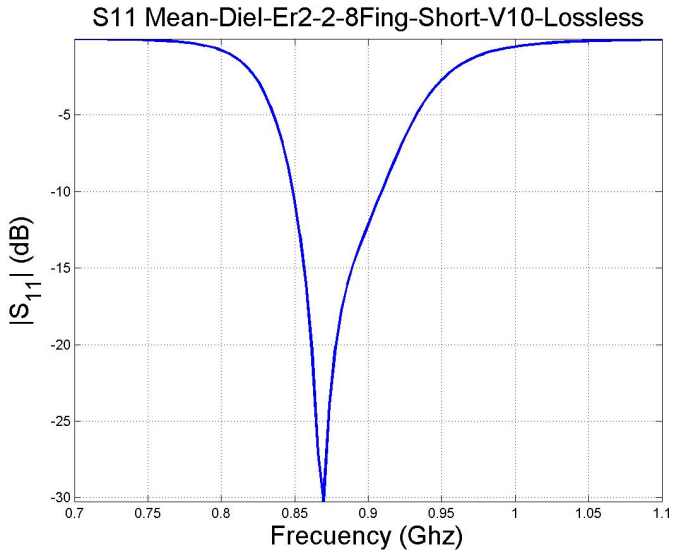

Figure 3.27: Reflection Coeficient Result Example

With all those results we are able to have a first opinion about the antenna response in the simulated structure and parameters configuration. It is obvious that the software saves a lot of time when it is necessary to simulate a lot of different antennas to compare their results or even if we want to check the influence of any parameter for improving the antenna performance.

- ***Efficiency***: Once we have simulated the two types of materials (*Lossy and Lossless*) we can obtain the efficiency results for the designed antenna. This result gives information about the antenna performance depending on the frequency since it indicates the ratio of the total power radiated by an antenna to the net power accepted by the antenna from the connected transmitter. Thererfore, as more power radiated less power is lost in the structure. If any of the two simulations are not run the software would notify it with an error window (shown in figure 3.28). A result plot example is shown in figure 3.29.

Figure 3.28: Efficiency Error Window

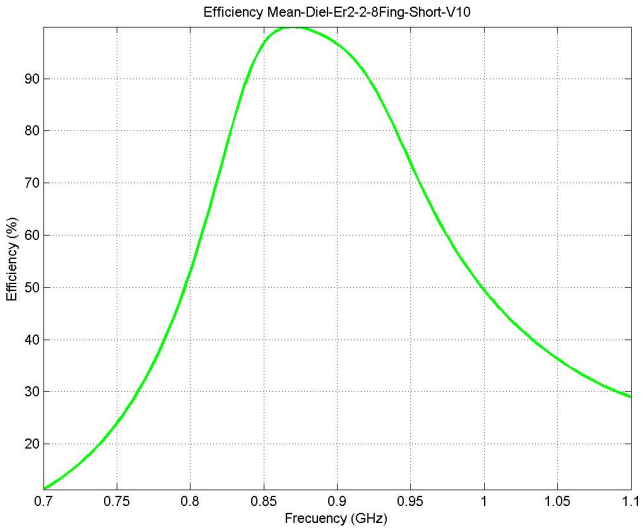

Figure 3.29: Efficiency Result Example

- ***RCS Open***: This button will create a new *.hfss* file named as the project name and finished with *-RCS-Open* in the *ProjectFiles* directory and will use

the lossy simulation, which must be run before pushing this button, for obtaining the RCS results with the antenna port as open circuit. The script simulates all the incident-reflected wave configuration which are interesting for this kind of antenna. Those are PHI-PHI, PHI-THETA, THETA-PHI, THETA-THETA all in XZ and YZ planes so in total it export 8 reports. For this purpose the script creates 4 designs in the project (figure 3.30 using the geometry loaded from the lossy simulation and configures the incident wave depending on the desired results. Once the simulation has finished the results are exported automatically to the directory named *\ReportFiles\RCS\Open* and they have the word *Open* at the end of their names. If the lossy simulation is not run the software would notify it with an error window (shown in figure 3.31) A result plot example for an incident PHI wave and PHI reflected in XZ plane is shown in figure 3.32.

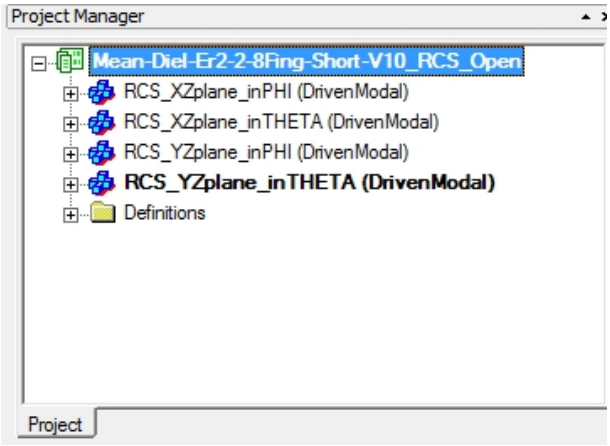

Figure 3.30: RCS Designs

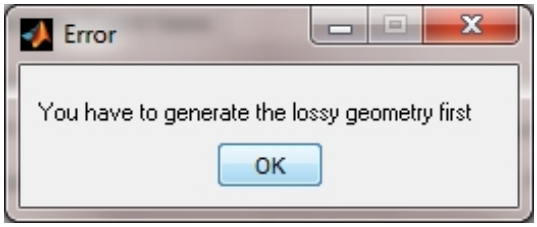

Figure 3.31: RCS Error

Figure 3.32: RCS Result Example

- ***Matched RCS***: This other button is for the same purpose than the previous one but this one assigns an matched impedance of $13 - j151\ \Omega$ to the port. So this button does the same as the *RCS Open* button but with the word *Adapt* at the end of each result file to identificate all the files and reports.

- ***RCS Sub***: This button subtracts the RCS results to obtain the level difference between the two possible configurations. This is important because the chip modulates the incident power by reflecting or absorbing it to make the 2 logical levels. The more difference between levels, the less error probability will produce, and so the reading range will improve. We have to take care when analyzing those levels because in some of them the level difference is so high because of the poor precision when levels are very low (about -80 dB). Therefore, we should notice that the only relevant results are those for which RCS levels are high enough (-10 to -30 dB). If any of the two RCS simulations are not found the software would notify it with an error window shown in figure 3.33. A result example is shown in figure 3.34.

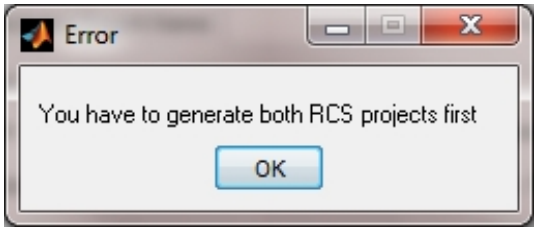

Figure 3.33: RCS Subtract Error

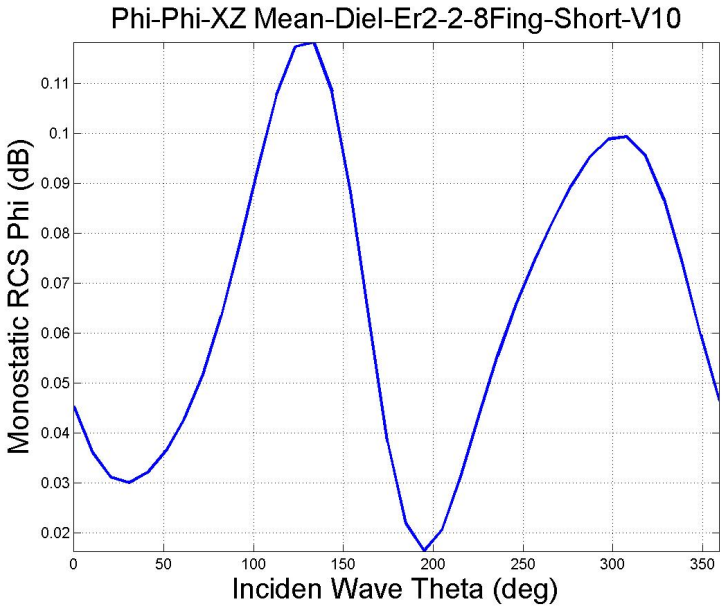

Figure 3.34: RCS Subtract Example

3.4 Plot and Save

This last panel is used for making plots of the S_{11} parameters for several antennas (commonly 2) and save it. Those plots help to compare the antenna response in different configurations. Those plots are generally created to compare the PEC solution and the copper solution.

The panel has 2 buttons that open a windows explorer to select the *.csv* impedance file. Then if the button *Plot PEC S11* or *Plot COP S11* is pushed the S_{11} parameter will be plotted in the axes. If we wanted to plot more than 2 S_{11} we would just have to browse another *.csv* with any of both windows explorers and push again the

corresponding plot button. When the final desired plot is made we can save it by pushing the *Save Plot* button. If we want to clear the plot we just have to push the *Clear Plot* button and the axes will be cleared. In figure 3.35 we can see the panel with a plot example for a comparison between PEC and copper S_{11} results for an antenna.

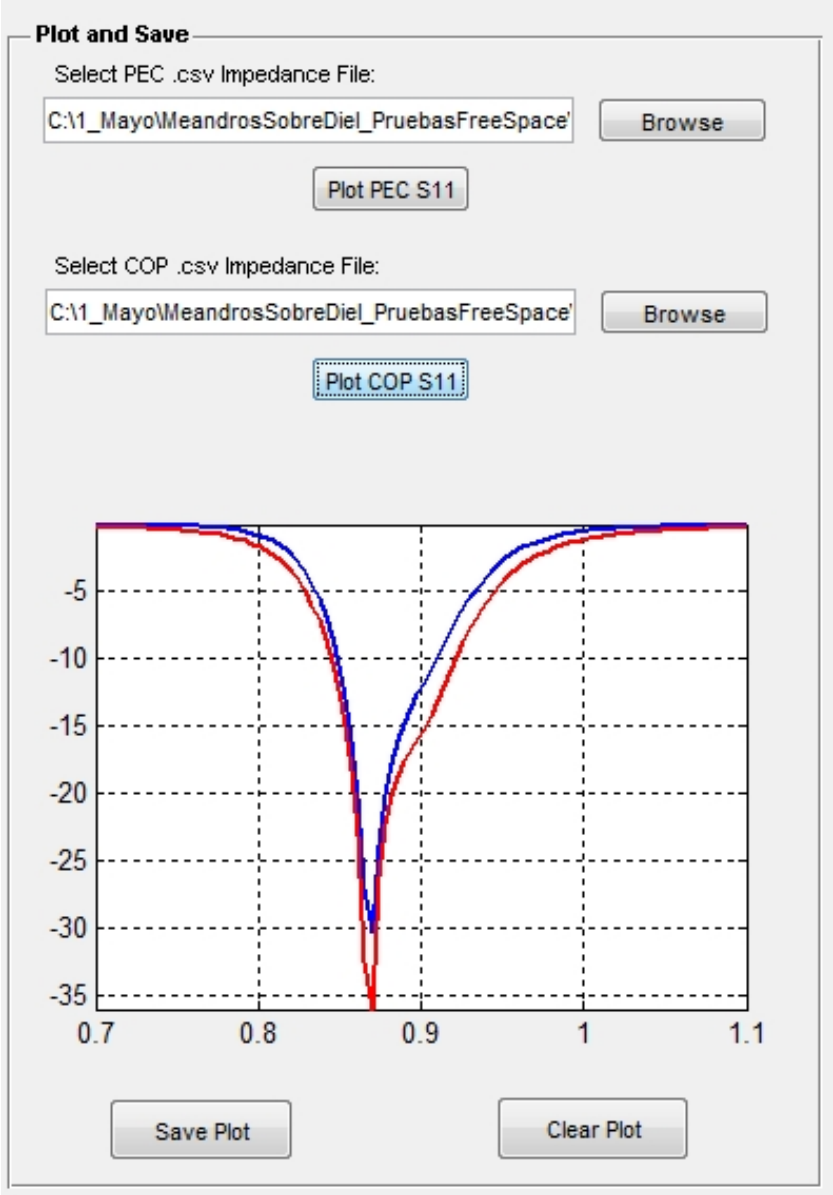

Figure 3.35: Plot and Save Panel

3.5 Directories and Video

In this last section we can see an example of the final directories created by the GUI after running all the simulations. This is shown in figure 3.36

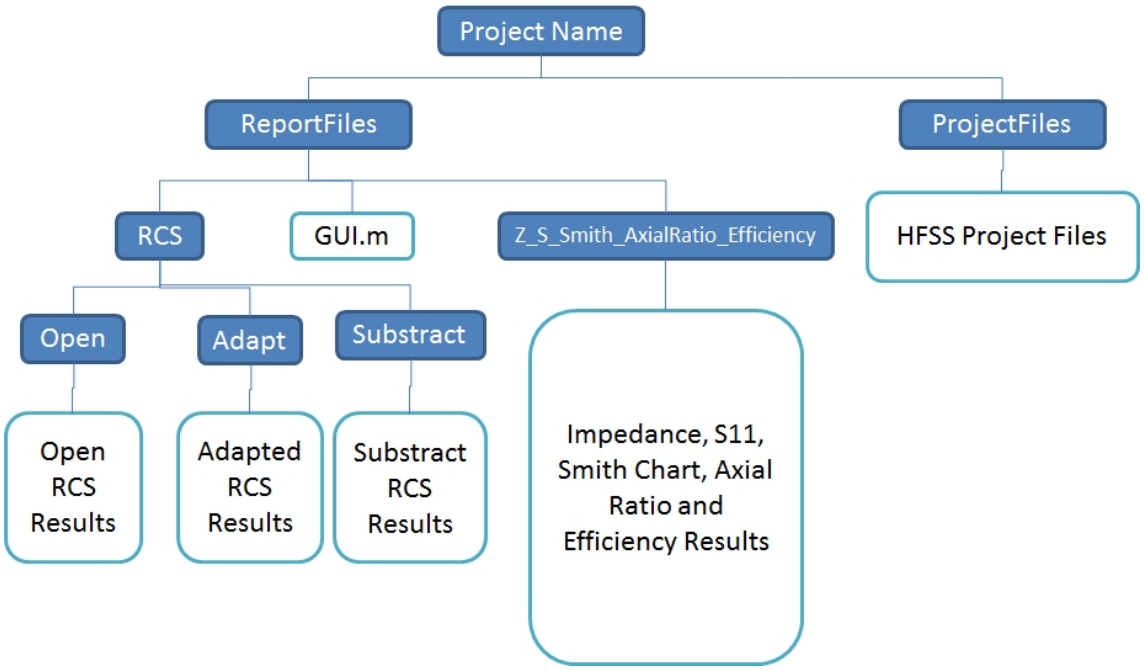

Figure 3.36: Final directory tree

Finally we have uploaded an example video of the GUI operation that can be seen in [11].

Chapter 4

Simulations and Results Before Software Development

In this chapter it is explained all the process followed to do the project simulations and analysis, from the previous research papers read about this topic to the first antennas studied and our conclusions about them after the deep investigation performed with the developed GUI software.

The first step when we started the project was looking for necessary information. Not only information about RFID systems but also about CD fabrication materials and methods and RFID tag actual solutions for being used on CDs. The RFID systems and CD found information have been explained in chapter 2 so this chapter is only focused on explaining the previous solutions for CDs with RFID technology. Once done this, we will explain all the designed antennas and the ideas that have been implemented and tested. Many of these ideas have produced several intermediate antennas, before obtaining the final prototype. In these cases we only show the last one because there would be a lot of non-definitive antennas which are not as important as the final one for each strategy.

4.1 Previous Research

As we have said before, in the initial phase of the project a first scientific literature review was carried out to understand the theory concepts and have a global vision of the actual solutions of antenna design for RFID tags for CD in UHF band.

In all the found papers about this topic, designs use the central plastic part of the CD of 39 mm of diameter (figure 4.1) as useful surface for placing the antenna. It was mentioned in chapter 2 that the reason of that placement region is the aim to avoid the metalized part where data are written on the CD that is between 18 and 60 mm of radius and causes that any antenna placed upon this zone tends to be short-circuited.

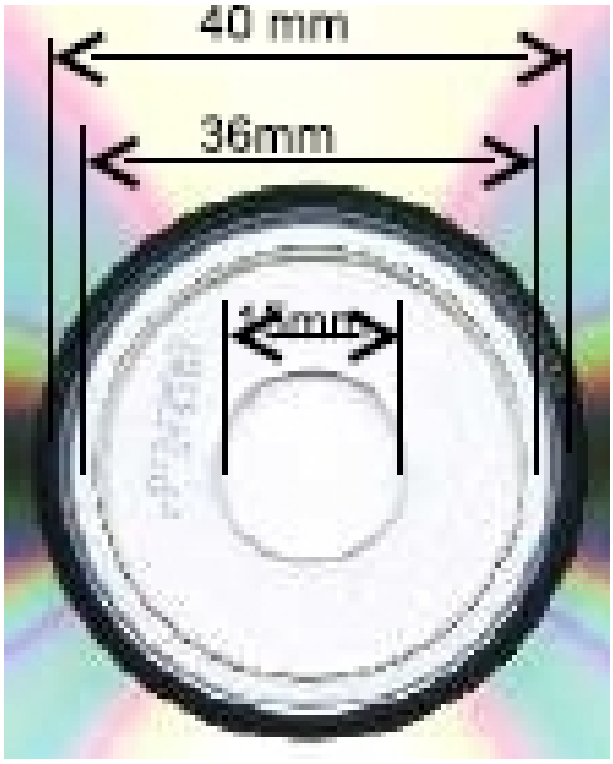

Figure 4.1: CD center typically used for placing the antenna

On the other hand, due to the small surface in the 39 mm diameter zone (we

Figure 4.2: Bending dipole antenna

have to subtract the central zone which is used to support the CD on a CD reader) the antennas present a very small electrical length. Therefore the antennas are very difficult to match to the chip, therefore they have very poor bandwidth and present low radiation efficiency (all of them very known problems of this kind of antennas).

4.1.1 Bent Dipole

One of the first papers reviewed was a bent dipole [12] which is placed at the aforementioned central part of the CD. This antenna is shown in figure 4.2.

The proposed steps for implement this design are the following:

1. *Select the application and define tag requirements*

2. *Determine the materials for antenna construction*

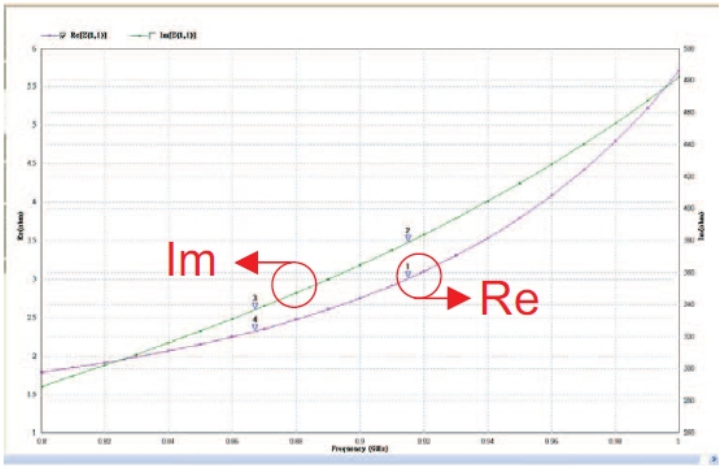

Figure 4.3: Bending dipole impedance

3. *Determine RF impedance of RFID chip*

4. *Identify the type of antenna and its parameters*

5. *Perform parametric study and optimization*

This paper presents the impedance results of the antenna that as we can see in figure 4.3 has a high imaginary part which indicates a strong inductive behavior and a low real part about 3Ω very common in electrically small antennas. This intends to illustrate the difficult design of these antennas when we want to achieve good impedance matchings with a good bandwidth. They also mention the commented properties for example that the tag antenna performance strongly depends on the impedance of the chip, the problems with the reflective layer and the small antenna size but they do not present any performance results as bandwidth or efficiency so we centered our investigation on the other paper studied and explained in the following subsection.

4.1.2 Compact Printed-On-CD UHF RFID Tag Antennas

This paper [13] is the main focus of our research. It proposes 2 types of antennas, both meander based, which makes them electrically longer. These 2 designs are

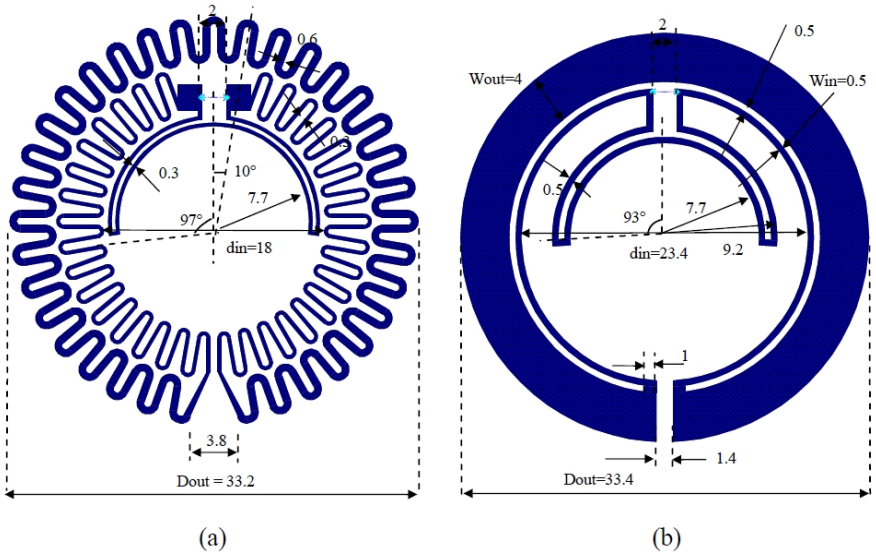

Figure 4.4: Meander-Type Antenna (Left) and Ring-Type Antenna (Right)

shown in figure 4.4.

As can be seen, the antennas are formed by loops that fit into the circular geometry of the central part of the CD. It is also important to notice that the antennas have only an electrical conductor. This is to make them inductive at lower frequencies because it will be necessary to achieve the impedance matching condition ($Z_{ant} = Z^{\star}_{chip} = 13 + j151\Omega$). We can also see that in the *Meander Type* antenna another technique has been used. This technique is to introduce meanders in the arms loops thus the current through the electric conductor has to flow a longer way and this makes electrical length to grow. However, these strategies have to be applied meticulously since if the conductors metallic surface is reduced the induced current densities dramatically increase and equally does the losses which is very negative for the gain and radiation efficiency.

After reading this paper we decide to carry out this meander strategy since we thought it was very important to make antennas with an important electrical length in a small surface. So we started creating by hand the first prototypes explained in the following section.

4.2 First Antennas

Mainly we designed 2 antennas by hand after developing the software that provided a faster designing and testing of each antenna. This two antennas are called *Longitudinal Meanders Antenna* and *Transverse Meanders Antenna* shown in figure 4.5

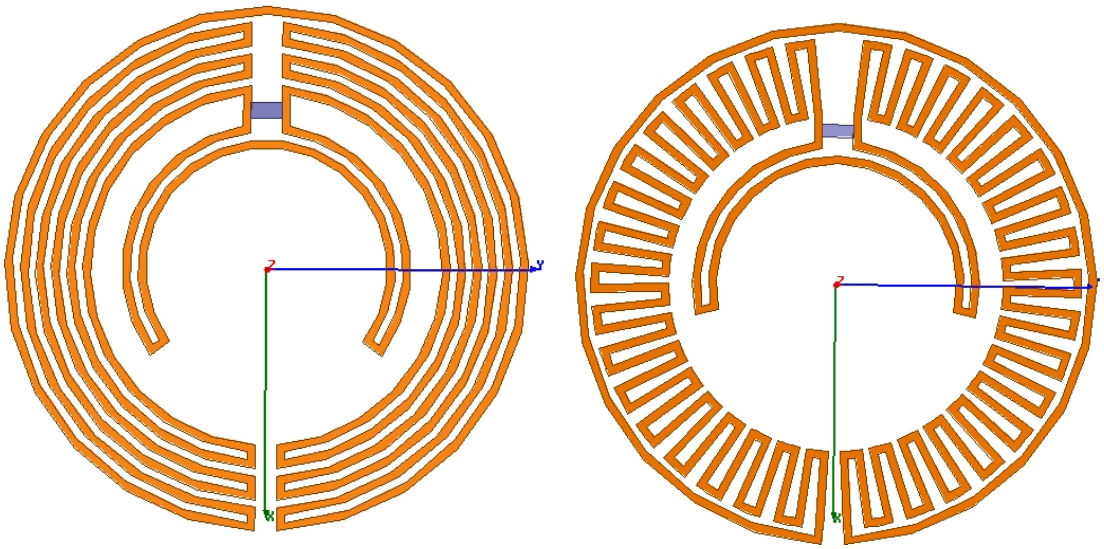

Figure 4.5: Longitudinal Meanders Antenna (Left) and Transverse Meanders Antenna (Right)

4.2.1 Ring-Type Antenna

We started studying the first antenna proposed in [13] whose name was *Ring-Type Antenna*. The first step was to study it in free space to check its operation from the point of view of impedance matching. The reflexion coefficient and the antenna is shown in figure 4.6

As can be seen in the figure, the reflection coefficient level is just $-0.07dB$ at 866 MHz which is a very poor value. There is also a better level when frequency grows. This indicates that the antenna is electrically small, hence it is necessary to use some strategy to increase the electrical length as introducing meanders.

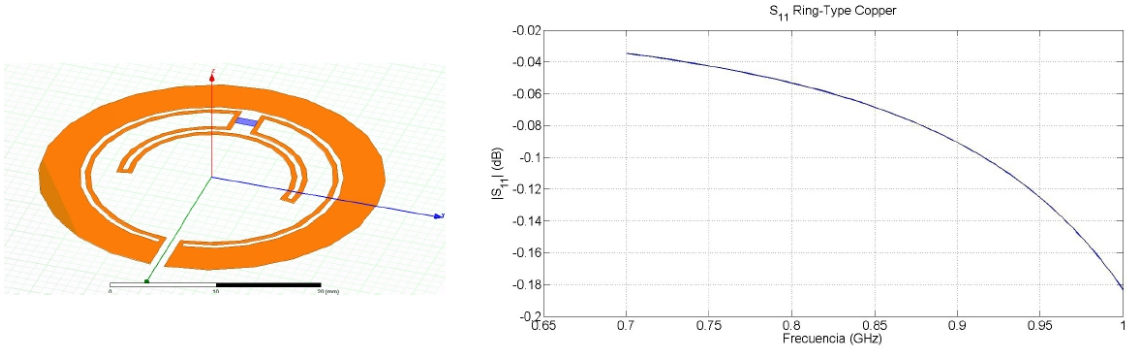

Figure 4.6: Ring-Type Antenna S_{11} coefficient

4.2.2 Longitudinal Meanders Antenna

In order to check if this meander theory is useful to increase the electrical length of the antenna we started the analysis of the *Ring-Type* antenna modification that we called *Longitudinal Meanders Antenna* which is simply the same antenna with its arms transformed in longitudinal meanders which are closed with the last one. This design was parametrized by hand which took a long time due to the complex geometry of the antenna. The main parameter studied was the angular length of the inner arm because it can shift the resonant frequency up (if the innner arm is shortened) or down (if the inner arm is elongated). The results obtained depending on the inner arm angular length for this antenna are shown in figure 4.7.

It can be seen that this theory is valid to increase the antenna electrical length since the resonant frequency has been displaced to smaller values. The parametric sweep shows inner arm angular length values from 125 deg to 130 deg. The aforementioned effect produced by this arm allows to do a fine adjustment of the antenna resonant frequency and as we can see, tune it to the frequency of interest (866 MHz) with a $-0.2dB$ matching level and with an angular length of 127 deg. Although we achieve the correct frequency, we observe an adverse effect: as the angular length grows, the matching level get worse due to the effect on the reactive part of the antenna impedance.

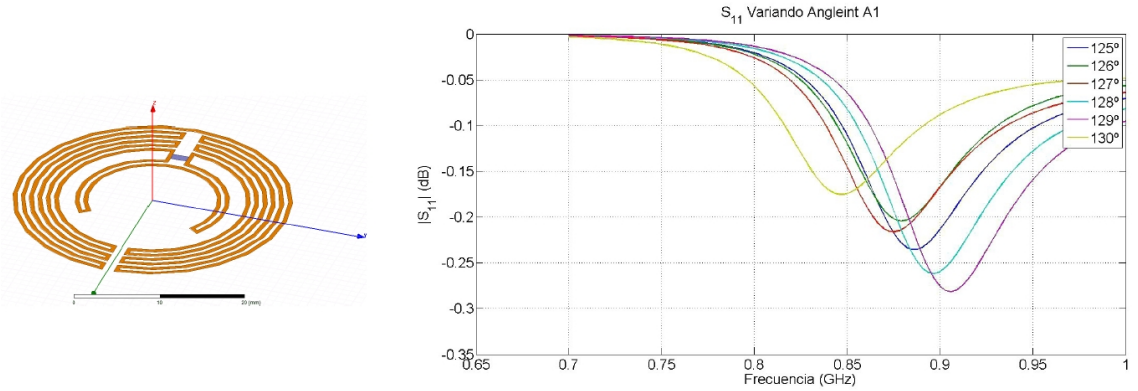

Figure 4.7: Longitudinal Meanders Antenna S_{11} coefficient

This analysis has revealed that such structures presents an important restriction when a good matching is needed. It is possible to adjust the resonant frequency varying the meanders size (coarse adjustment) and likewise varying the inner arm (fine adjustment). However, we don't have more parameters to properly adjust the reactive impedance in order to achieve better matching.

4.2.3 Transverse Meanders Antenna

After the first antenna study, we moved to explore the next antenna model which has transverse meanders instead of longitudinal thus this new model is very similar to the previous one except for the meanders orientation. The obtained results are shown in figure 4.8. Once again the meanders are effective to reduce the frequency of the matching maximum but this time we can see that the matching level has improved to $-0.6dB$ at 866 MHz which is an x6 increase compared to the base antenna (*Ring-Type*) and three times compared to the previous antenna (*Longitudinal Meander*). This better matching level denotes a better response of this antenna compared to the others but we should confirm it by calculating the radiation efficiency of both antennas. We can also see that the figure shows a parametric sweep for the inner arm angular length from 100 deg to 105 deg which causes the same effect than the previous one, if the arm is longer the resonant frequency decreases and so does the

matching level and vice versa.

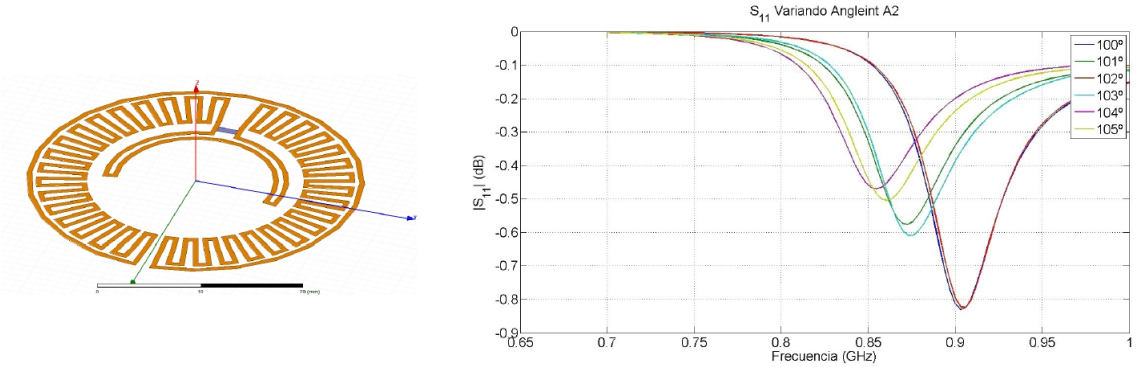

Figure 4.8: Transverse Meanders Antenna S_{11} coefficient

4.2.4 Antennas efficiency

The next step was to calculate the radiation efficiency using the method described in chapter 2. To this purpose we used 2 simulations, one considering ideal materials which is lossless (PEC) and other considering real materials which have losses (Copper). Using this two simulations it is possible to calculate the antennas radiation efficiency with the aforementioned approach. To do this study we compared the 3 previous antennas in order to determinate which one is better. These results are shown in figure 4.9

As can be seen, the ring-type antenna shows very low radiation efficiency at 866 MHz but it increases when frequency grows which confirm the interest in achieving a good electrical length for the structure. We also see that the radiation efficiency for the 2 new models is better than for the base antenna probably due to the best matching achieved at the working frequency. Other important point is that the transverse meander antenna is more efficient (15%) than the longitudinal meander antenna (7%) at the frequency of interest.

The explanation of this behavior can be based on the current cancellation that circulate through the meanders on both models. In the longitudinal model the currents circulating through the meanders are in opposite directions and so their

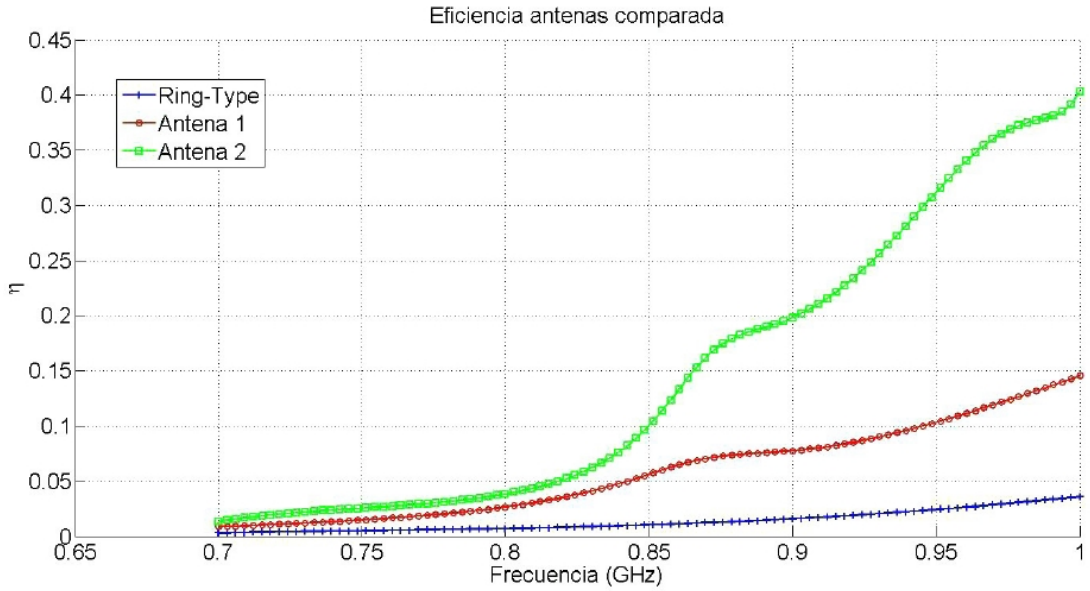

Figure 4.9: Antenna efficiency comparison

radiation tends to be canceled out in far field resulting in a less radiation efficiency.

On the other hand, the transverse antenna has currents circulating transversely through the meanders which are canceled out but it also has currents circulating on the same direction (those ones which are in longitudinal direction) so this radiation is not canceled resulting in a better radiation efficiency. As conclusion, the transverse meanders antenna should be the best antenna of the 3 studied because it has the best matching level.

4.2.5 Study on polycarbonate

Once the free space study of the three antennas was completed, the next step was to check the CD influence on the antennas performance. We decided to do an study in several steps. We first studied the effect of the polycarbonate and then we put the whole CD (including the reflecting aluminum layer). In general the polycarbonate effect on the antennas is favorable because a dielectric material tends to make antennas electrically longer which helps to our design.

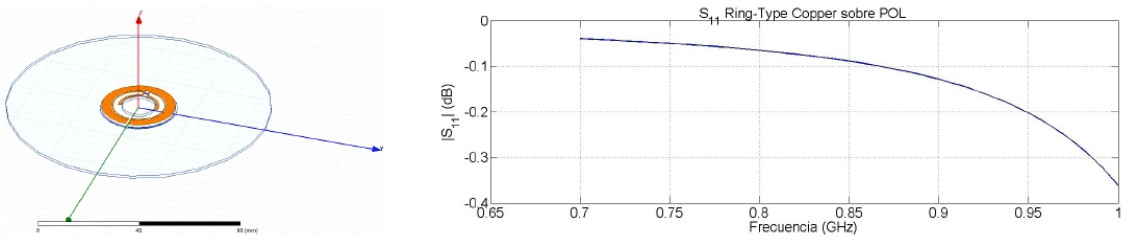

Figure 4.10: Ring-Type on polycarbonate

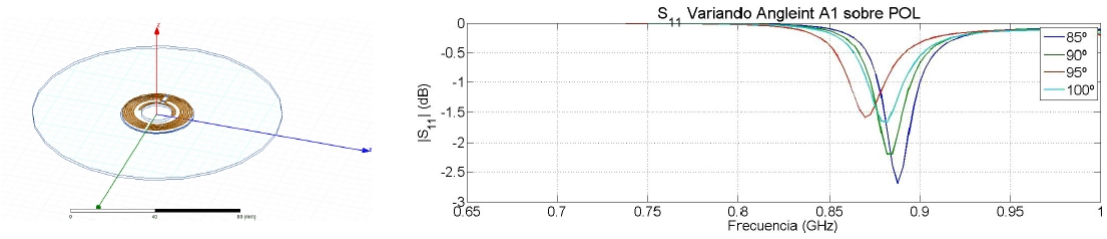

Figure 4.11: Longitudinal Meanders Antenna on polycarbonate

For the ring-antenna we have the results shown in figure 4.10. As can be seen the matching improves to $-0.1dB$ which is better value than in free space. The structure becomes electrically longer but not enough to obtain a matching maximum at the working frequency of 866 MHz.

The next step is studying the longitudinal meanders antenna response on polycarbonate. In general the positive polycarbonate effect will be seen in all the antennas. This results are shown in figure 4.11 with a parametric sweep for the inner arm between 85 and 100 obtaining much more higher matching levels about $-2dB$ which represents a great improvement with respect to the free space analysis. The polycarbonate makes the resonant frequency to decrease and the inner arms have to be bigger to compensate this effect.

A very similar case occurs when we analyzed the transverse meanders antenna. The results are shown in figure 4.12. In this case the parametric sweep is for the inner arm from 70 to 85. The arms has been reduced a lot and it reduces the imaginary antenna impedance so matching levels of $-6dB$ are achieved. This is almost

3 times the matching level of the longitudinal meander antenna.

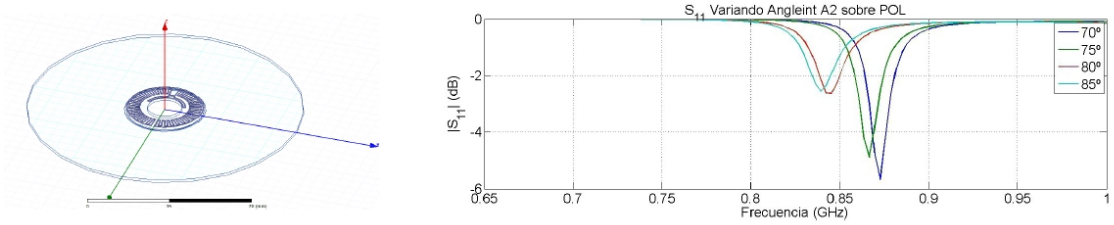

Figure 4.12: Transverse Meanders Antenna on polycarbonate

Finally, the efficiency of the 3 antennas on polycarbonate is shown in figure 4.13. We can appreciate that the ring-type antenna efficiency is still very low but there are very good improvements in the other 2, reaching 40% for the longitudinal meanders antenna and almost 90% for the transverse meanders antenna. Once again the best antenna response is the 3 one.

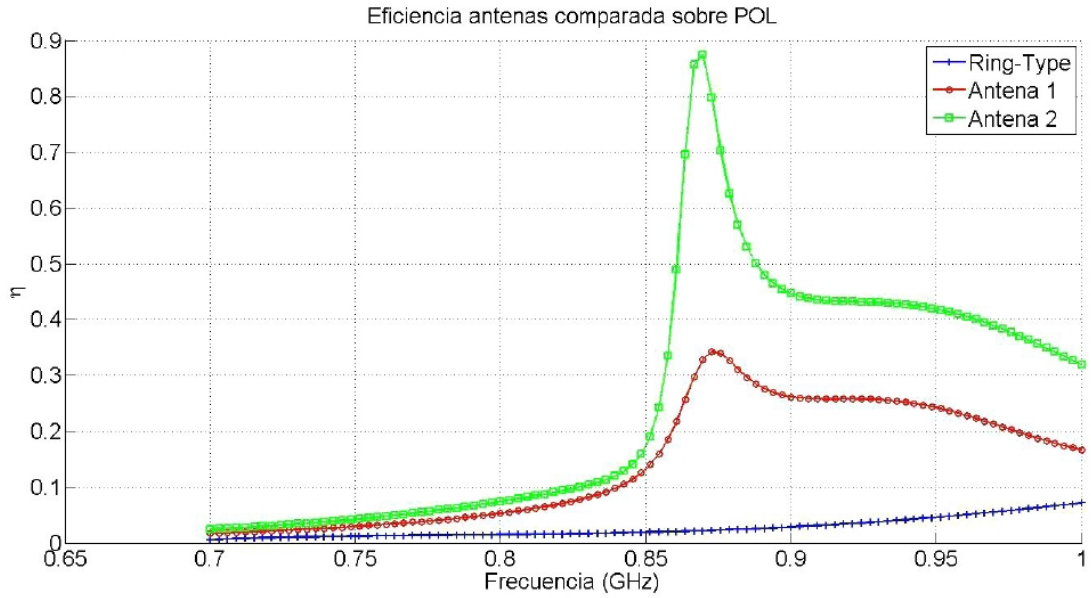

Figure 4.13: Antenna efficiency comparison on polycarbonate

4.2.6 Study on CD

The next step was placing the antennas on a complete CD. We expected that the reflective layer would affect negatively to the antenna radiation, but as the antennas were placed on the central part of the CD where there are no aluminum, they could still work.

The first study was done with the ring-type antenna, shown in figure 4.14. It is obvious that the reflective layer has a negative effect on the antenna. Even though the antenna is placed on the central part where there are no aluminum, the proximity with it causes strong couplings which tends to ruin the antenna radiation.

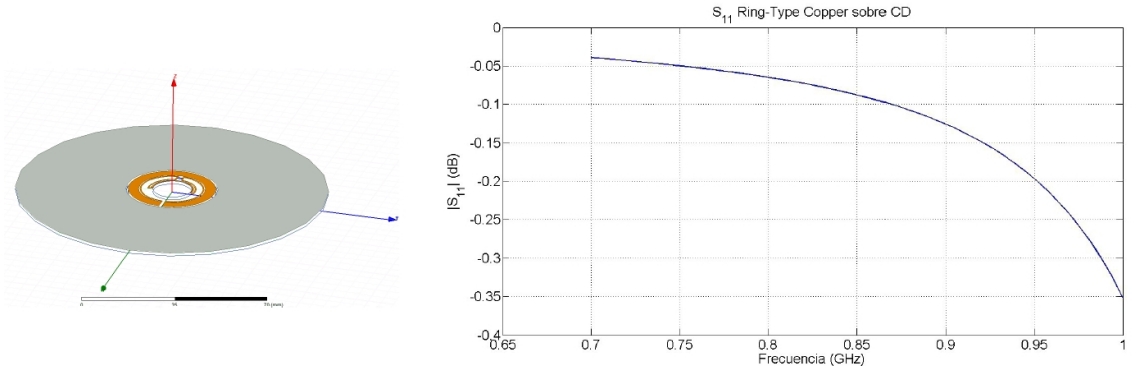

Figure 4.14: Ring-Type Antenna on CD

The next antenna is the longitudinal one. In this case there is a very strong coupling between the antenna and the reflective layer which affects on the resonant frequency moving it to higher frequencies. Even making the inner arms bigger it is impossible to take back the resonant frequency to 866 MHz. This effects can be seen in figure 4.15 where a parametric sweep for the inner arm from 155 deg to 175 deg is shown. We can see that the operation frequency is very high around 950 MHz even with the inner arm almost totally opened. This big coupling effect is due to the longitudinal arms orientation which propitiates the coupling with the reflective layer. This makes this antenna model nonviable for using it on CD.

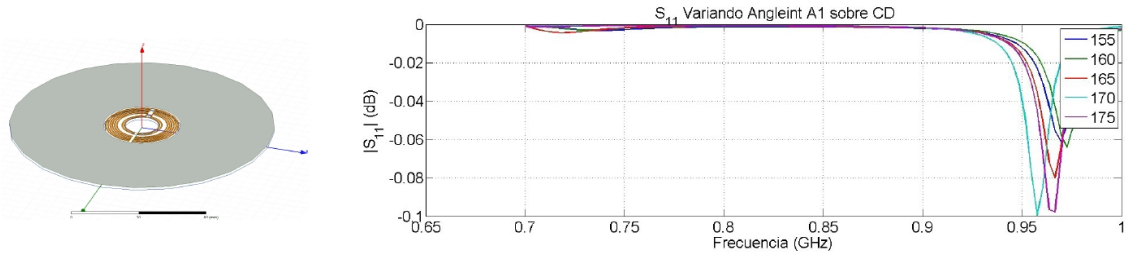

Figure 4.15: Longitudinal Meanders Antenna on CD

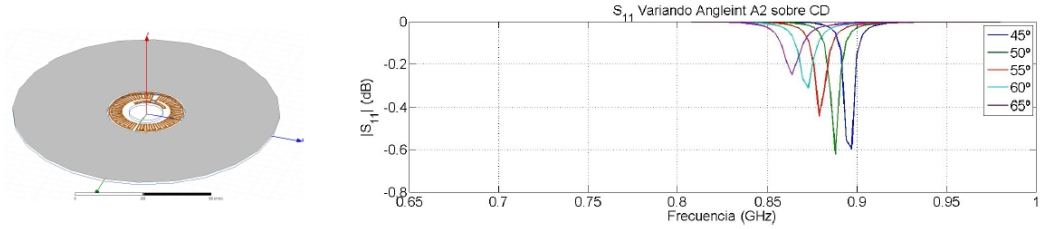

Figure 4.16: Transverse Meanders Antenna on CD

The next step is studying the last antenna with transverse meanders. The reflection coefficient is shown in figure 4.16. In this case the coupling with the reflective layer tends to load the antenna capacitively which reduces the resonant frequency. This makes necessary to reduce the inner arms to adjust the correct frequency. In the last referred figure are shown results for inner arm angular lengths between 45 deg and 65 deg. In this case it can be appreciated that the coupling between the reflective layer and the antenna does not prevent a fine adjustment of the resonant frequency. However, the interaction is still very strong and the matching level is just around $0.4dB$. Additionally, this antenna does not have other parameter to vary the imaginary impedance part of the antenna in order to improve the matching level.

As final result, we can see in figure 4.17 the radiation efficiency for the 3 antenna models on CD. Once again we can see that the base antenna efficiency is very low. The longitudinal meanders antenna has a maximum but a higher frequency than the operation frequency of 866 MHz and the transverse meanders antenna has a maximum efficiency of 14%. This maximum is at the correct frequency but

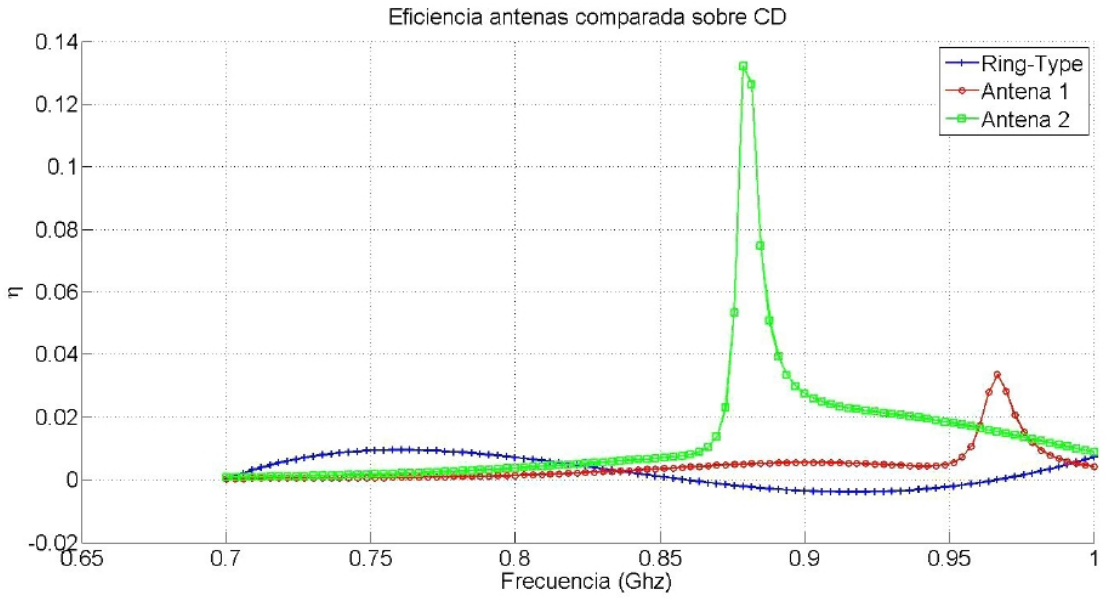

Figure 4.17: Antenna efficiency comparison on CD

is difficult to improve these values since as we have mentioned above, there are no parameters in the structure which allows to adjust the resonant frequency and the imaginary impedance separately. Despite this disadvantage, the results for the transverse meanders antenna are promising and this antenna could be a candidate to experiment with on real CDs.

4.2.7 RCS Study

Once done the study from the point of view of matching and radiation efficiency we studied the mono-static RCS in all the possibles polarization combinations and in the two main planes of the structure which are the $\phi = 0$ deg plane and $\phi = 90$ deg. Due to it higher viability the study has been done with the transverse meanders antenna. As it has been commented, the main idea is studying if the back-scattering is important and also check which antenna polarization works better. In figure 4.18 we can see that this antenna reflects much better the co-polar polarization (Theta in this case). The difference between both polarization reflections is around 50 dB. Except in end-fire directions the reflection levels are uniform in all directions but

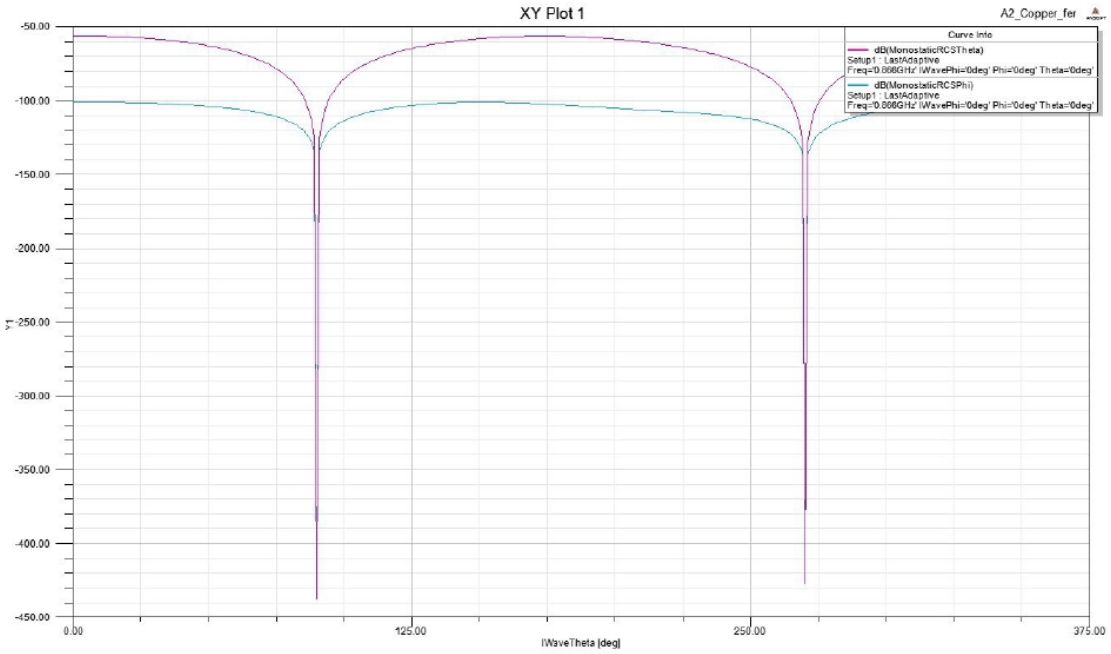

Figure 4.18: Phi and Theta components when reader interrogates with Theta polarization in $\phi = 0$ deg plane

the values are in general very low (around -50 dB) compared with the incident wave.

In figure 4.19 we can see the same result but this time in plane $\phi = 90$ deg. In this case the level difference between both polarizations is much lower indicating that in this plane there is not a clear difference for neither polarization. In any case the reflection level power is also around -50 dB compared with the incident power.

The next study corresponds to the same configuration but now the reader interrogates with phi polarization. Results for plane $\phi = 0$ deg are shown in figure 4.20.

As we can see in this plane both polarizations also have similar levels so that indicates that there is not a clear polarization. This behavior is due to the curved shape of the tag which tend to increment the coupling between both orthogonal polarizations. We can also see that the reflected phi component does not have any zero in all directions. This is because the phi vector (incident and reflected) does not

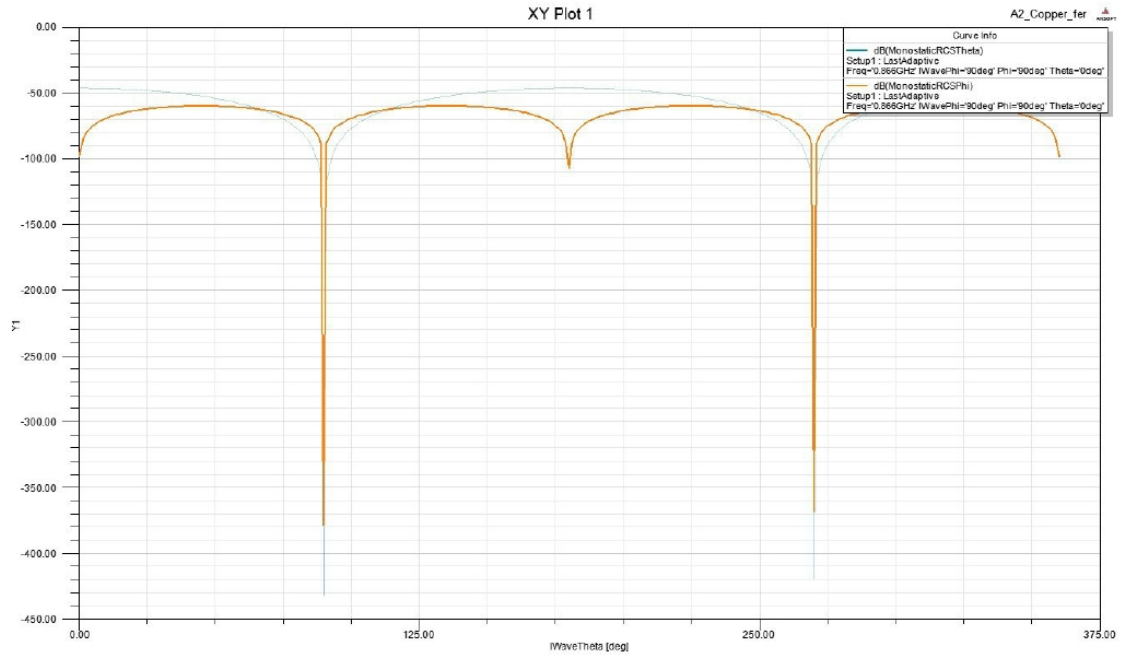

Figure 4.19: Phi and Theta components when reader interrogates with Theta polarization in $\phi = 90$ deg plane

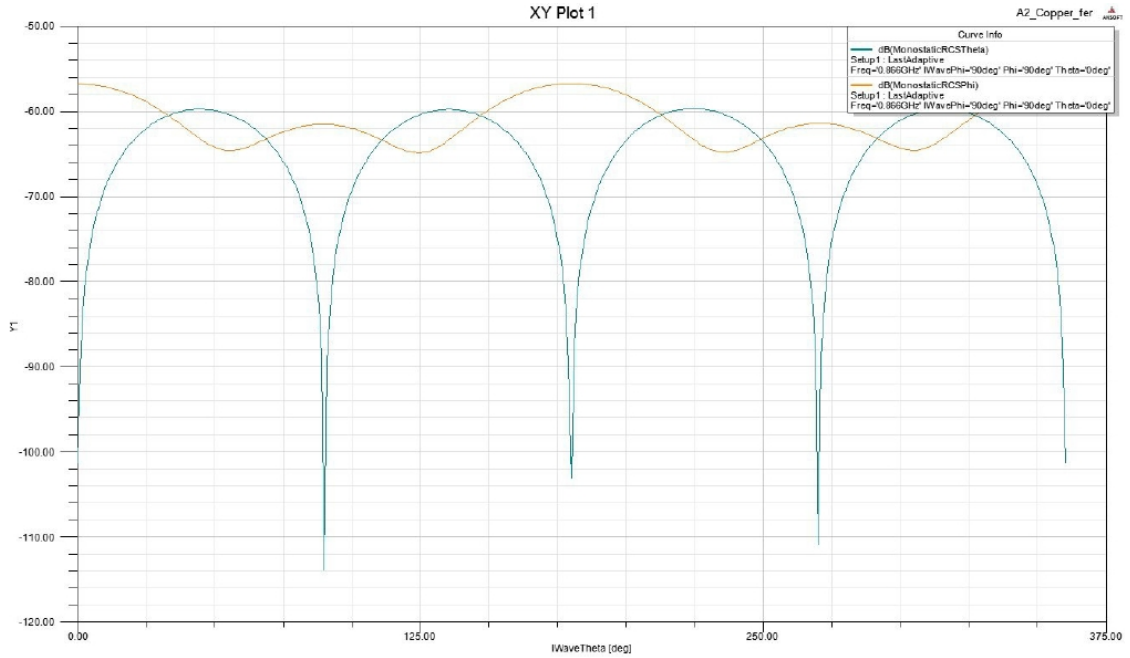

Figure 4.20: Phi and Theta components when reader interrogates with Phi polarization in $\phi = 0$ deg plane

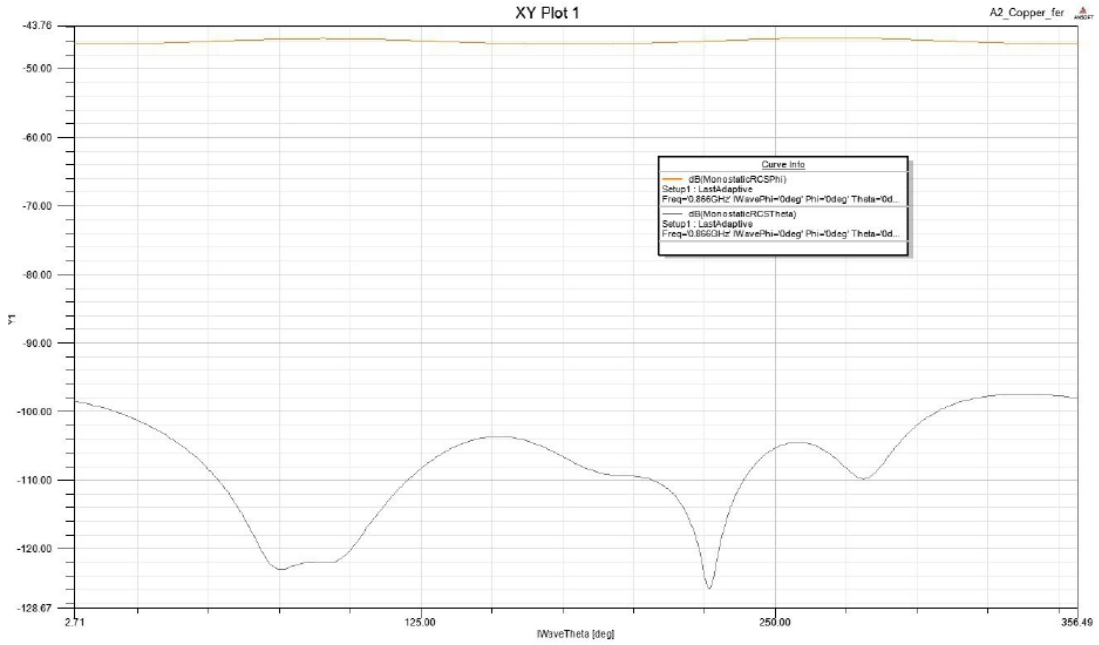

Figure 4.21: Phi and Theta components when reader interrogates with Phi polarization in $\phi = 90$ deg plane

change it direction when elevation plane is swept with a constant phi angle ($\phi = 0$). In any case, the reflected power level are $50dB$ below the incident power.

The last result for the same configuration than the previous one but in plane $\phi = 90$ deg is shown in figure 4.21. We can observe that in this plane there is a strong difference between both polarizations. The co-polar component (Phi in this case) is much higher than the cross-polar (theta). This is due to the chip connection point respect to this plane and confirms that one current component radiation effect tends to be canceled out in far field destroying theta component while the other current component is not canceled so the phi component is much higher. In any case the power levels are still very low (44 dB).

4.2.8 Commercial Linear Antenna

In the first study , we have obtained some electric parameters which characterize the antennas response such as impedance matching, radiation efficiency and mono-static RCS. However, it is difficult to determine if the obtained performance is better or not compared with existing solutions. Therefore, instead of starting with the development of the selected solution (transverse meanders antenna model) we first studied an existing commercial tag to compare it to our antenna.

The selected model to do this comparison is shown in the aforementioned linear tag which is for general use (not for CDs) shown in figure 4.22. The dimensons of this tag have been extracted using a manual micrometer with a precision of 0.1 milimeters. We estimate that this precision is enough for the frequency band of 866 MHz.

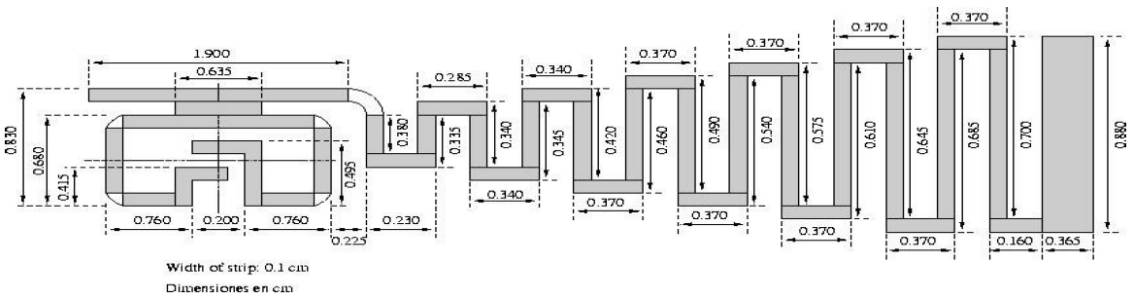

Figure 4.22: Commercial Ring Antenna dimensions

The first thing studied was the impedance matching in free space. This result is shown in figure 4.23 and is obtained for 3 mesh densities to check the convergence of these results.

We can see that the antenna has a very good impedance matching in the desired frequency band reaching values around 12 dB. We can also notice that there are 2 resonances, that means that this kind of antennas has a dual resonant behavior respect to the complex chip impedance. This characteristic is very interesting since this dual resonance significantly improves the bandwidth of the antenna as well as

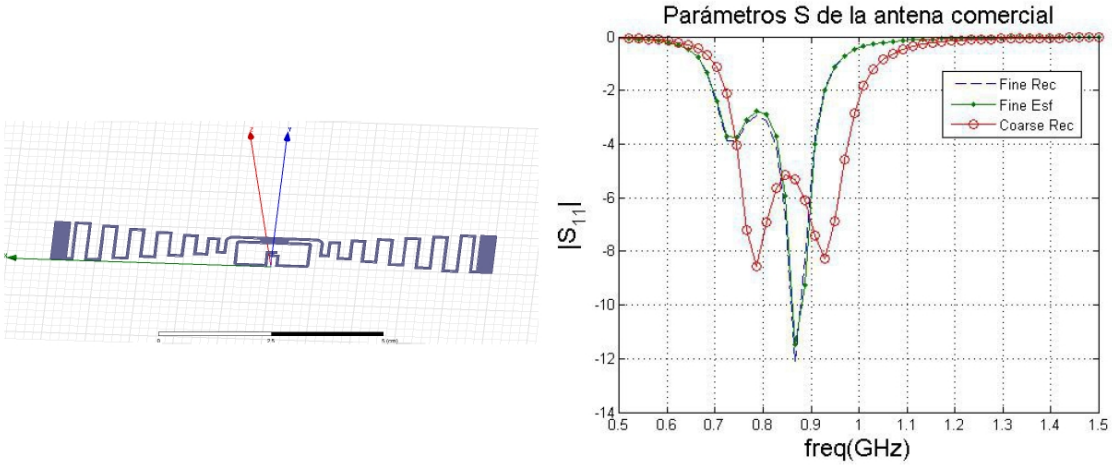

Figure 4.23: Commercial Ring Antenna S_{11} coefficient

it keeps very good matching levels.

Comparing this result with the previous results for the studied antennas we realized that this commercial antennas has much better impedance matching. As mentioned above, the commercial design has also a dual resonance which improves the working bandwidth of the antenna.

The next step was to check the radiation efficiency for this commercial antenna. This result is shown in figure 4.24. First we can notice that using this method, described in chapter 2, the result is above 100% in some points. This is because of the greater sensibility of this structure due to the dual coupled resonance. This increased sensitivity makes the structure losses affecting the reactive part of the impedance of the antenna, thus the method used is no longer precise. Despite not having a precise measure in this case, we can be sure that it will be high. This behavior is also better than the previous antennas which achieved a radiation efficiency around 15% in free space.

The last parameter of interest for comparing the commercial antenna with our proposed ones is the mono-static RCS. The first component calculated is the Phi

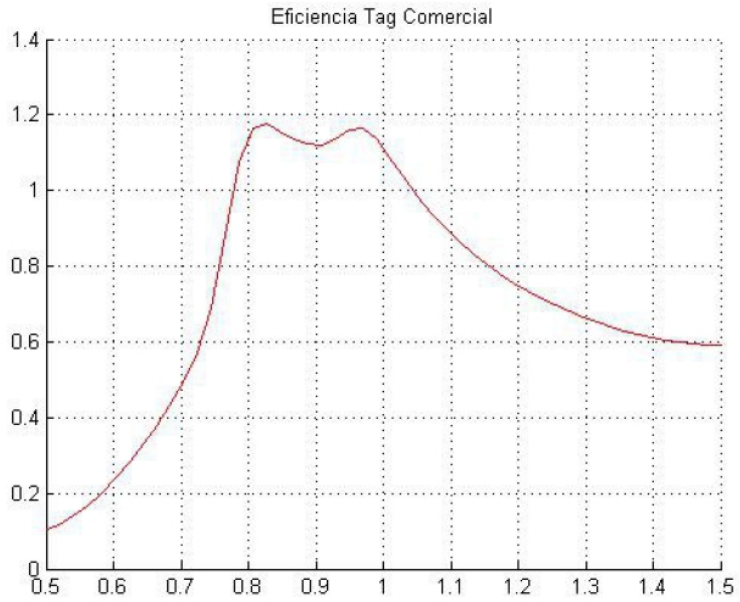

Figure 4.24: Commercial Antenna radiation efficiency

response when reader interrogates with Phi polarization (so is the co-polar component). This result is shown in figure 4.25 where is depicted this component for both planes ($\phi = 0$ deg and $\phi = 90$ deg). We can see that this antenna has a very strong reflection of the co-polar component in plane $\phi = 90$ deg because in this plane the component is aligned with the antenna arms. The reflected power in this plane is just 12 dB below the incident power. This value can be compared with that obtained for the transverse meanders antenna in the previous sections which had much lower values (the best case was -44 dB). We can also notice that the Phi component in the other plane ($\phi = 0$ deg) is very low because in this plane the phi component is orthogonal to the antenna arms. These results indicate that this antenna has a clear linear polarization through the antenna arms. However, for the proposed antenna is mixed because of the circular shape of the antenna.

The next studied component is the Theta one when reader interrogates with Phi polarization. Therefore, now we are going to measure the crossed coupling between polarizations. Figure 4.26 shows this case for the main considered planes ($\phi = 0$

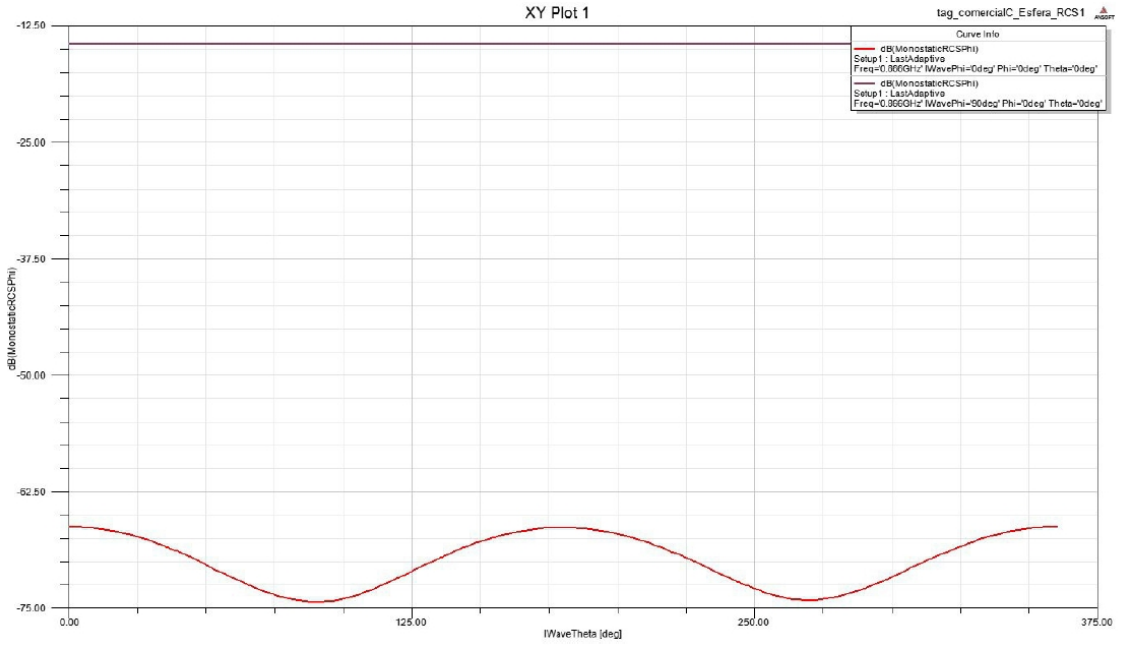

Figure 4.25: Reflected component (Phi) when reader interrogates with Phi polarization for both planes $\phi = 0$ deg and $\phi = 90$ deg

deg and $\phi = 90$ deg). In this figure we can clearly observe that theta component is always very low around -60dB. This means that the commercial antenna response is clearly linear polarized with very low cross polarization coupling.

The next step is checking the antenna performance when reader interrogates with a Theta polarized wave. Figure 4.27 shows this case for the main considered planes ($\phi = 0$ deg and $\phi = 90$ deg) for the co-polar component (Theta reflected).

We can notice that the reflected component (Theta) has a very high value in plane $\phi = 0$. This reflected power level is around 12 dB below the incident wave power which is a very good level. This performance confirms the linear polarization of this antenna throughout it arms. Indeed, we have to realize that Theta component is aligned with the antenna arms in plane $\phi = 0$. On the other hand, this component Theta is orthogonal to the antenna arms in plane $\phi = 90$ as we can see in this figure where it has a very poor power level below -60 dB (this indicates that

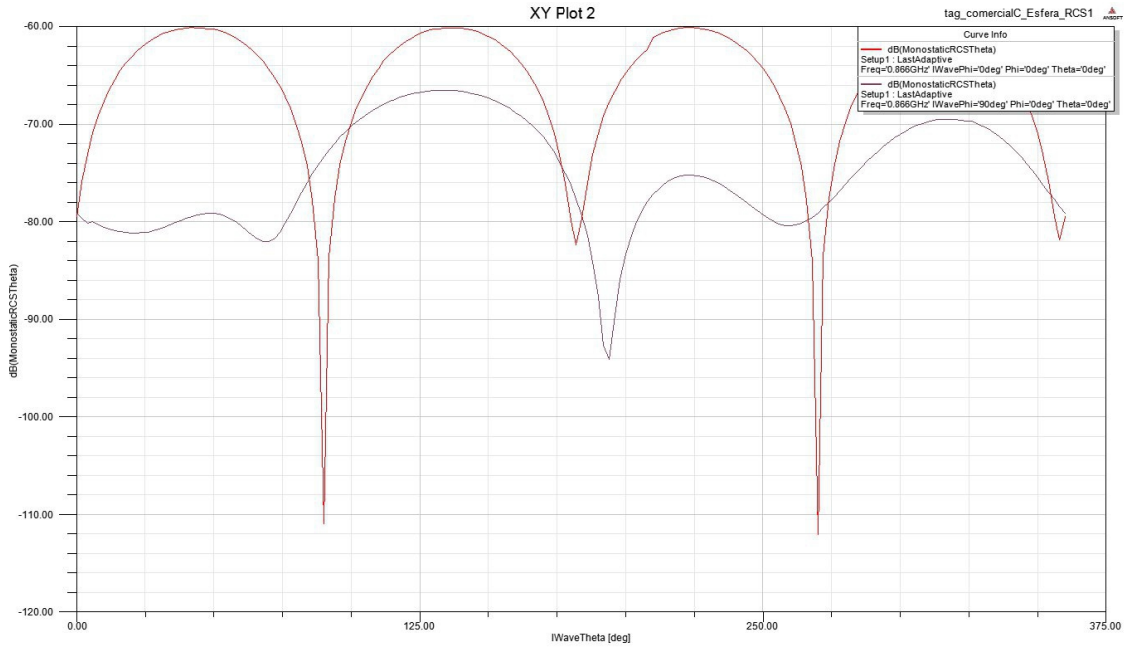

Figure 4.26: Reflected component (Theta) when reader interrogates with Phi polarization for both planes $\phi = 0$ deg and $\phi = 90$ deg

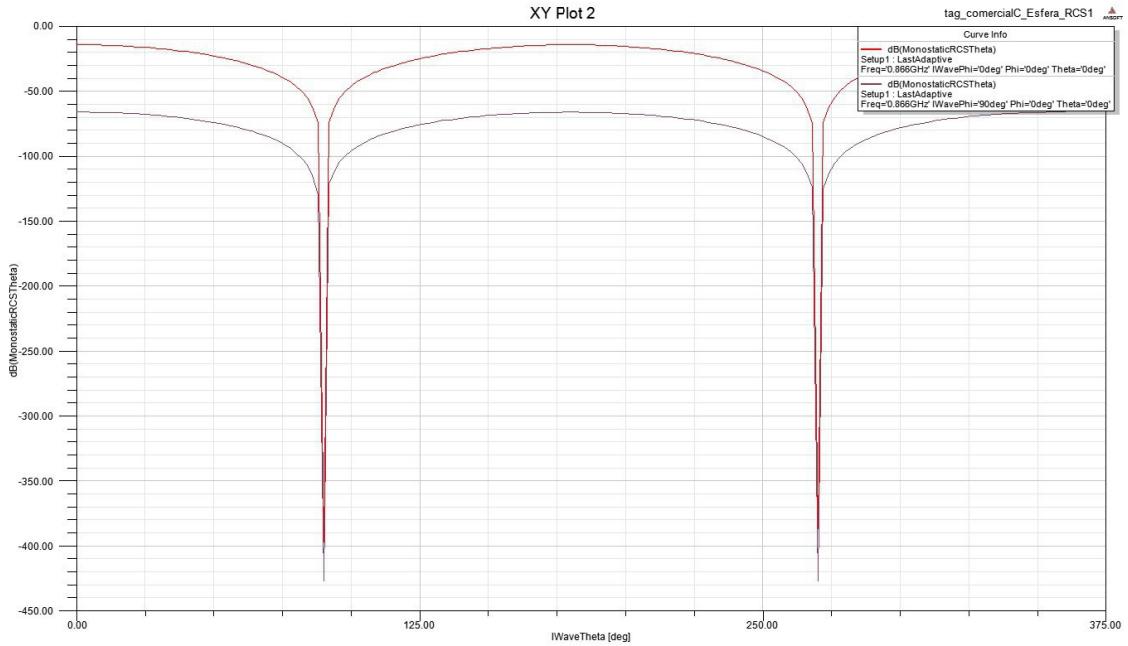

Figure 4.27: Reflected component (Theta) when reader interrogates with Theta polarization for both planes $\phi = 0$ deg and $\phi = 90$ deg

there is not almost response).

Finally, the last component to study is Phi when reader interrogates with a Theta polarized wave (in this case is a cross-polar component). In figure 4.28 we can see what was expected. As cross-polar component, the reflected power level for both planes is very low, indicating once again that this antenna has a clear linear polarization with very low cross-coupled polarization.

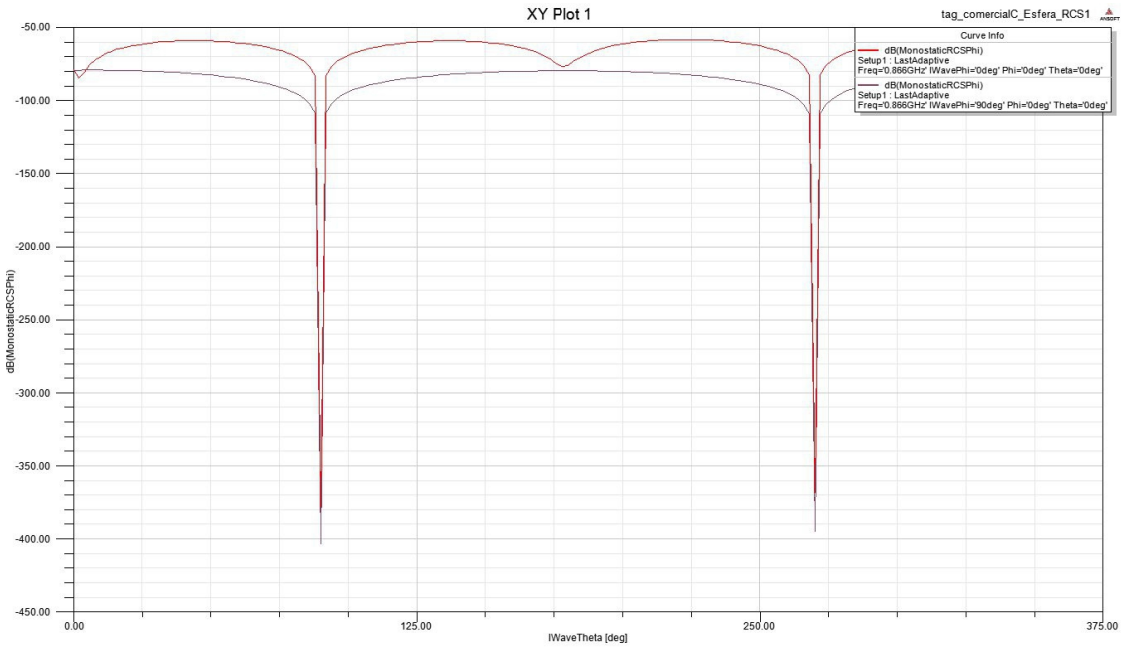

Figure 4.28: Reflected component (Phi) when reader interrogates with Theta polarization for both planes $\phi = 0$ deg and $\phi = 90$ deg

As we have seen, differences between this commercial antenna compared to the proposed before for CD use are very large even from the point of view of back-scattering. Indeed, while our antenna tends to couple polarizations and does not have a clear polarization direction, the commercial antenna do the opposite presenting a clear linear polarization in it arms direction. Such situation makes that the reflection levels of our antenna are always similar and very low (in the best case we achieved -44 dB) and this is as consequence of the circular shape of our antenna.

4.3 New Proposal for Antennas for CDs

After concluding these two studies about the proposed antennas and the commercial antenna some conclusions can be extracted that have allowed us to develop new ideas to improve the antennas performance when they are put on CDs.

The commercial antenna advantages compared with our proposed antenna are mainly based on 3 factors:

- The antenna operating on CD has to reduce it size to be placed on the central part of the CD in order to minimize the interactions with the reflective layer. This is a natural impediment that can not be get over because of the CD structure so we have to accept this restriction and try to design the antennas in the available space. The commercial antenna does not have this restriction so it can use more space to improve it radiation efficiency.

- The commercial antenna has a structure formed by a central feeding loop and 2 arms that generates a dual coupled resonance. Contrary to this antenna, our proposed antenna does not have this advantage so we could design a new antenna that take advantage of this benefit.

- The aforementioned geometric structure formed by a central loop and 2 arms adds a degree of freedom compared with the proposed antenna for CD. The antenna arms adjust the resonance frequency while the loop size allows an independent adjustment of the reactive part of the antenna impedance. This allows the improvement of the matching level since it is possible to do a fine compensation of the strong negative reactance of the RFID chip. In principle, we do not have an important restriction regarding this characteristic so we could do an antenna that take advantage of it.

Regarding the mono-static RCS, the commercial antenna has also advantages as it is able to reflect some components with very good power levels when these components are aligned with the antenna arms and when the component is not aligned

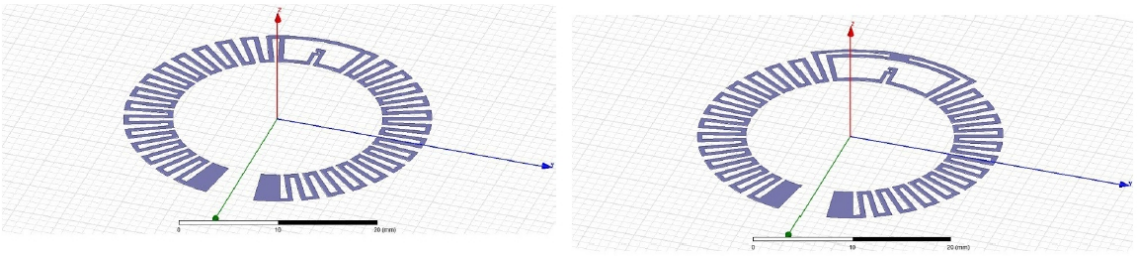

Figure 4.29: New antenna model proposed for CDs

the reflected power levels are very low. Therefore, there is a drawback with this design, in some cases the communication between the reader and the tag would be very good but if the reader or the tag is not oriented properly the communication could be interrupted so this tag has a strong dependence on the tag orientation.

Our antenna does not have this direction dependence and has a very similar response for different incident electric field orientations. The inconvenient is the power level achieved by our antenna that is much lower and so the reading range. The advantage of this antenna is the less dependence on the reader-tag orientation which is due to the circular shape of this antenna which causes induced currents that does not have a strong component in a single direction. Therefore, we can consider that this restriction is also unavoidable given the CD circular structure, and especially the available space in the central area of polycarbonate, unaffected by the aluminum layer.

Based on the previous considerations, we proposed a new antenna design which could be compatible with the unavoidable restrictions in such environment but with the commercial antenna advantages. In figure 4.29 the new proposed models are shown.

As can be seen these antennas also have circular structure and are still placed on the central polycarbonate part. It has also preserved the idea of transverse cuts studied since it has been demonstrated that its behavior is far superior to the ob-

tained with longitudinal cuts. The new antenna structure incorporates an internal feeding loop. It seeks to independently adjust the operating frequency of the antenna, and the reactive part of its input impedance. With this structure it is also wanted to obtain the effect of coupled dual resonance present in the commercial tag.

Preliminary results obtained in this stage of the project to this new concept of antenna have proven to be quite promising. Here we present these preliminary results, including the three relevant parameters studied.

First, in figure 4.30 is shown the power reflection coefficient of the antenna. As we can see, with this structure it is possible to obtain the coupled dual resonance, although the coupling is still not adequate, because the two resonance frequencies are very separated. However, in the band of interest we achieve very satisfactory matching levels, reaching values of -7 dB.

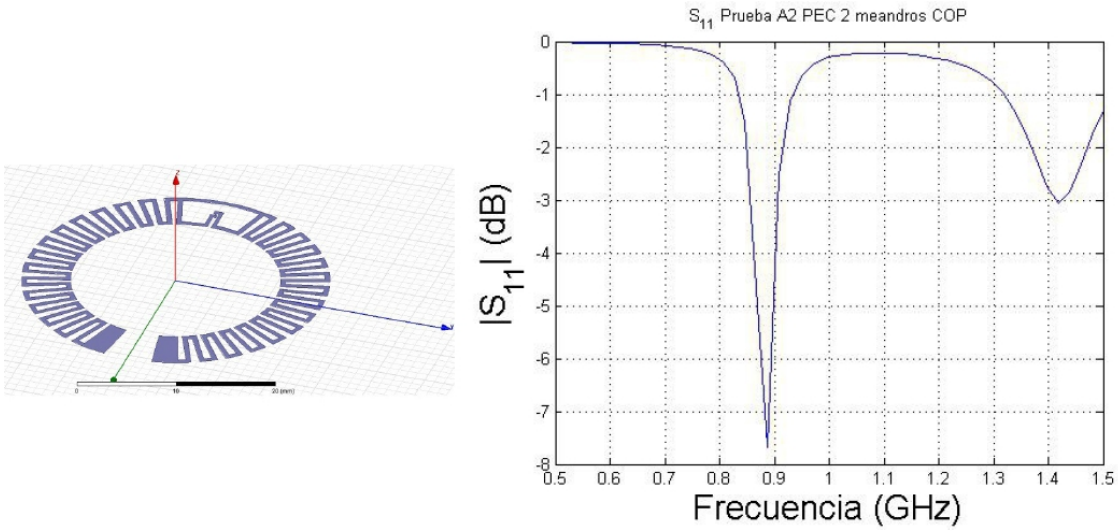

Figure 4.30: Antenna model proposed for CDs with meanders connected in feeding loop border

The dual resonance effect appears to be confirmed also in the other model shown in figure 4.31where the reflection coefficient is depicted for several feeding loop sizes.

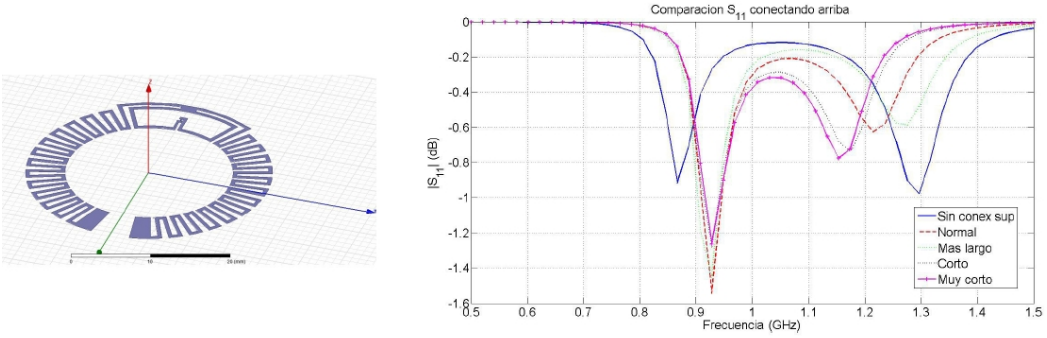

Figure 4.31: Antenna model proposed for CDs with meanders connected in feeding loop center

We can clearly see how the two resonances tend to improve it coupling, although the level of matching is not yet adequate. However, this level in principle could be improved by acting on the central loop to achieve a higher compensation of the reactive part of the chip impedance.

The next parameter of interest is the radiation efficiency for this new antennas. Figure 4.32 shows the radiation efficiency for this new antennas depending on the meanders numbered from 2 to 5. As can be noticed for all the results there are clearly 2 efficiency maximums that correspond with the 2 resonances of the antennas. These 2 zones are not yet optimum since the 2 resonances are very separated in frequency. Anyway, the efficiency improves in some zones to 40 % and even reaching some peaks of 90 %. These data are very promising, and indicate that these antennas could be a great alternative to operate in CDs.

The next study is to check the RCS results for this new antenna model. The reflected Phi component when reader interrogates with a Phi polarized wave is shown in figure 4.33 for both planes ($\phi = 0$ deg and $\phi = 90$ deg).

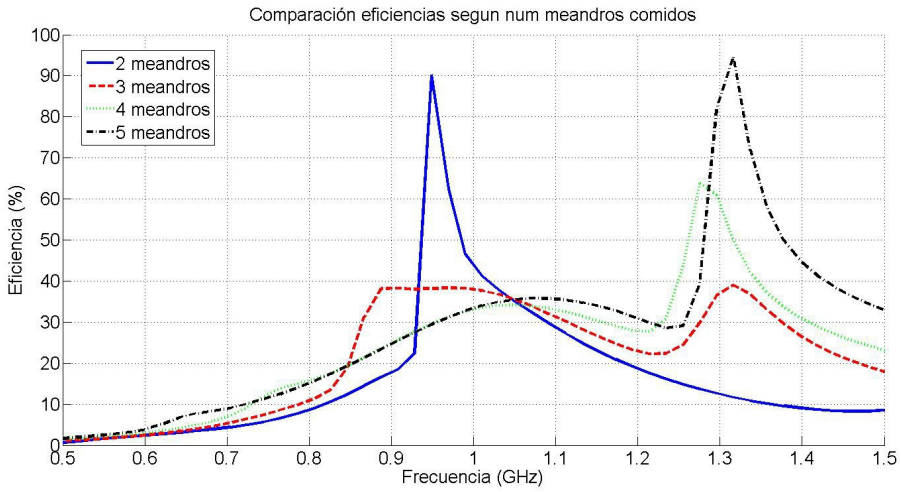

Figure 4.32: Radiation efficiency for new proposed antennas depending on meanders number

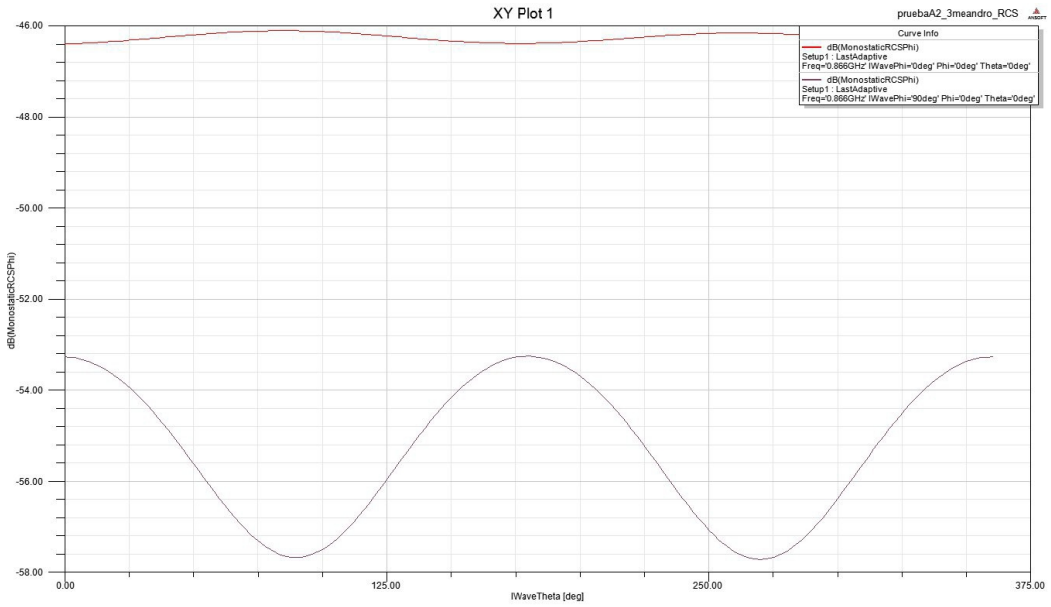

Figure 4.33: Reflected component (Phi) when reader interrogates with Phi polarization for both planes $\phi = 0$ deg and $\phi = 90$ deg

We can see that the reflected power in both planes is very similar with levels between -46 dB and -52 dB. This indicates that this antenna reflects in a similar way when electric field is in any spatial direction. Moreover the obtained levels are very low, comparable to those obtained in the first proposal. This seems to confirm

that this behavior is due to the intrinsic curvature of the antenna.

The next result is the reflected Theta component when reader interrogates with a Phi polarized wave is shown in figure 4.34 for both planes ($\phi = 0$ deg and $\phi = 90$ deg).

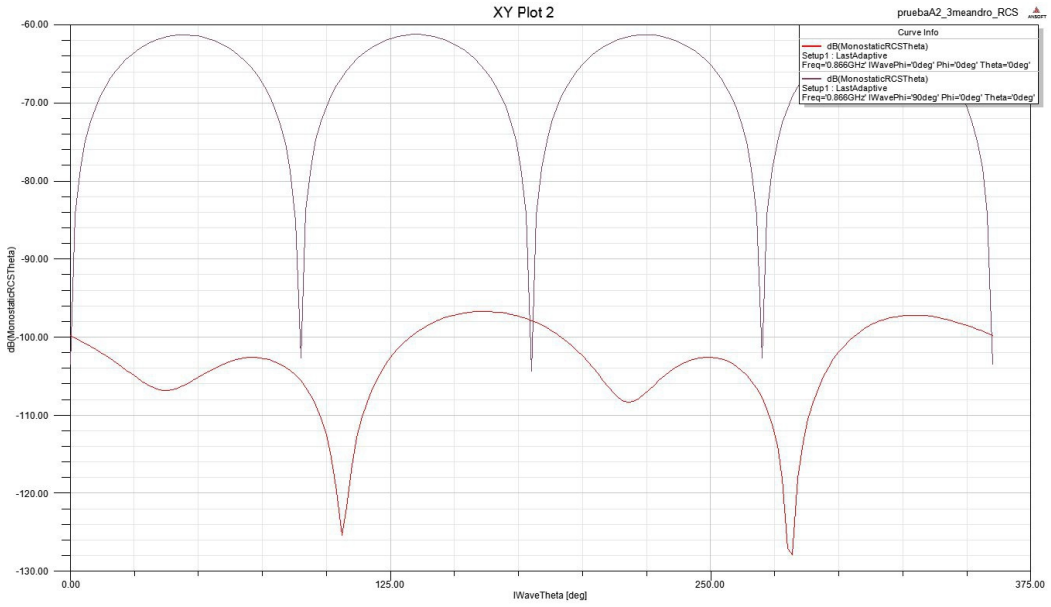

Figure 4.34: Reflected component (Theta) when reader interrogates with Phi polarization for both planes $\phi = 0$ deg and $\phi = 90$ deg

In this case we observed that the component (theta, cross-polar) in the plane $\phi = 90$ is much higher than the reflected in the plane $\phi = 0$. In both cases the two levels are low around 60 dB below the incident power.

In the next study the reader interrogates with a Theta polarized wave. Figure 4.35 shows the co-polar reflection obtained in the same Theta component, and the two main plane ($\phi = 0$ deg and $\phi = 90$ deg). In this case, we have again a similar performance. The co-polar reflected component is very similar in both planes, indicating that the antenna reflects energy in a very similar way regardless of the electric field orientation. Reflection levels are still very low around -50 dB. The analysis is

completed with the last cross-polar component shown in figure 4.36 which yields the same conclusions as aforementioned.

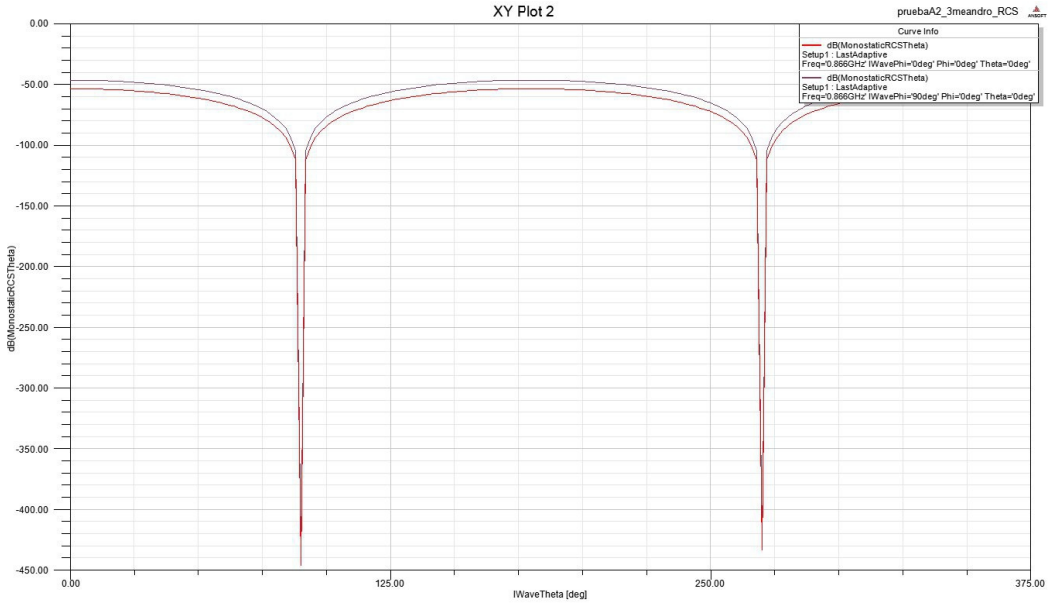

Figure 4.35: Reflected component (Theta) when reader interrogates with Theta polarization for both planes $\phi = 0$ deg and $\phi = 90$ deg

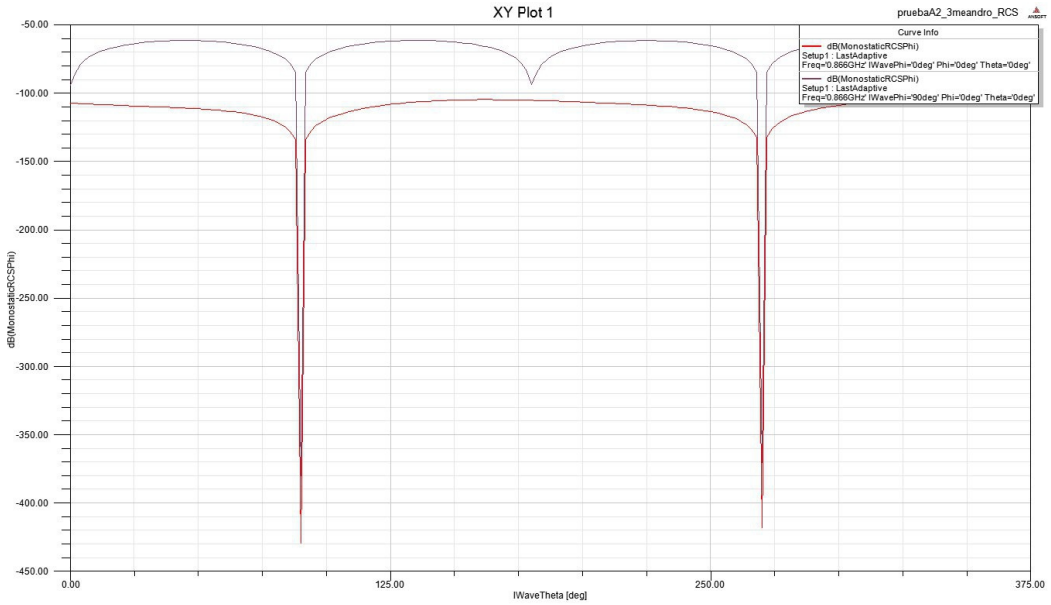

Figure 4.36: Reflected component (Phi) when reader interrogates with Theta polarization for both planes $\phi = 0$ deg and $\phi = 90$ deg

Chapter 5

Simulations and Results with GUI Software

As we have explained in previous chapters, creating an antenna structure is very complicated and requires a lot of time to define its geometry and even more time if we want to parametrize its dimensions in order to study the effects produced by the variation of these dimensions.

So, after creating the first antennas we realized that it would be much better to develop a software that automatizes all the antenna creating leaving to the user only the task to define the geometric parameters, making it possible to significantly reduce the design time and allowing to do many simulations and optimizations in a short time. All this software is explained in detail in chapter 3, so in this chapter we will focus in the simulations and results obtained with this software.

5.1 First Examples

The first antenna model generated with this software is shown in figure 5.1. As can be seen the figure shows the final optimized structure at RFID UHF European frequency and its S_{11} reflection coefficient. It has very good matching values at this

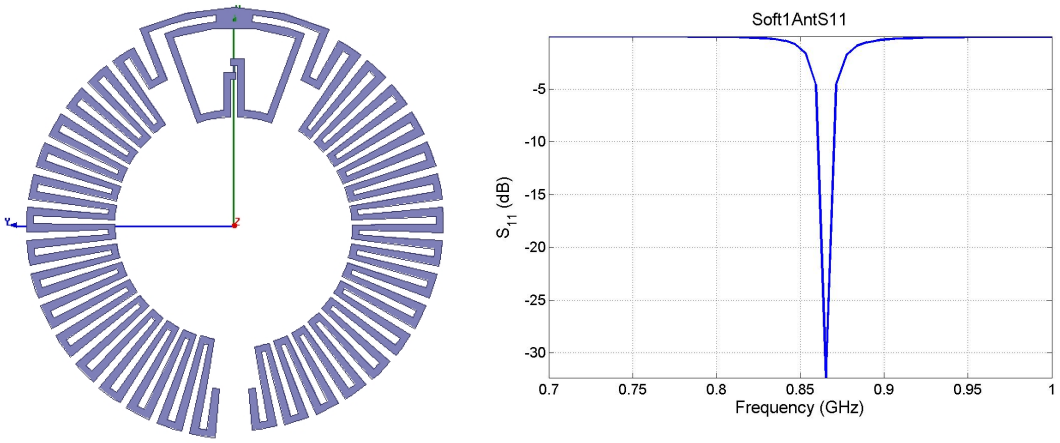

Figure 5.1: New optimized antenna at RFID UHF frequency

frequency. The only drawback is that it has a narrow bandwidth, hence the antenna could be susceptible to de-tuning when it is placed near other objects.

To get some idea on this software effectiveness, this last example might have needed 2 work days without the software but it only took about 4 hours to design and optimize the structure. In the next example we will show is another antenna model with a lower meander density, and performing a linear taper increasing the meanders length. The results are shown in figure 5.2. In this case the optimization have been performed to improve the antenna bandwidth trying to control the two resonances coupling. As can be seen this have been achieved but at a higher frequency (1.2 GHz) and worst matching level.

The following example is similar to the previous one, but introducing an asymmetry in the antenna arms. The idea is to shorten one arm almost completely, to check the influence of the second arm. In figure 5.3 we can observe the structure and reflection coefficient after the optimization process developed. We see that the effect of eliminating one arm has a greater control over the two resonances coupling, which are now very well optimized. The obtained bandwidth covers almost 400 MHz below -3dB. The disadvantage is that the eliminated arm makes the antenna electrically

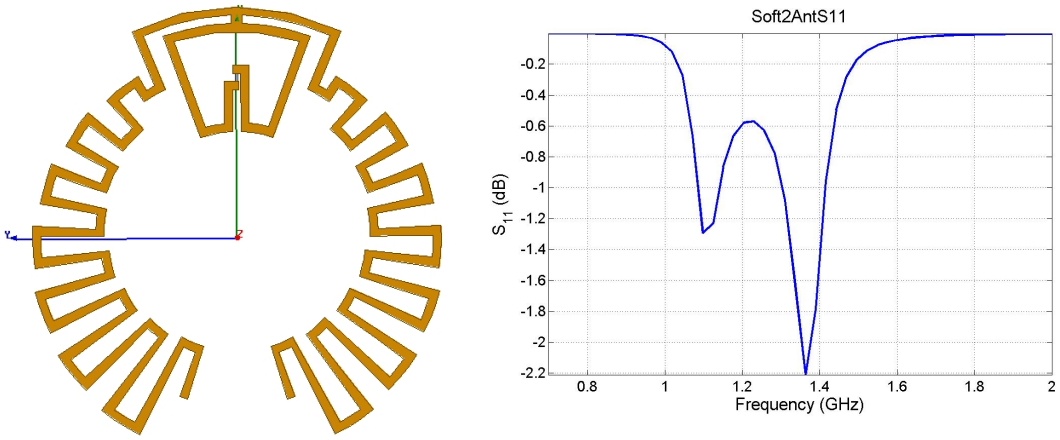

Figure 5.2: Optimized antenna with less meanders and increasing tapering

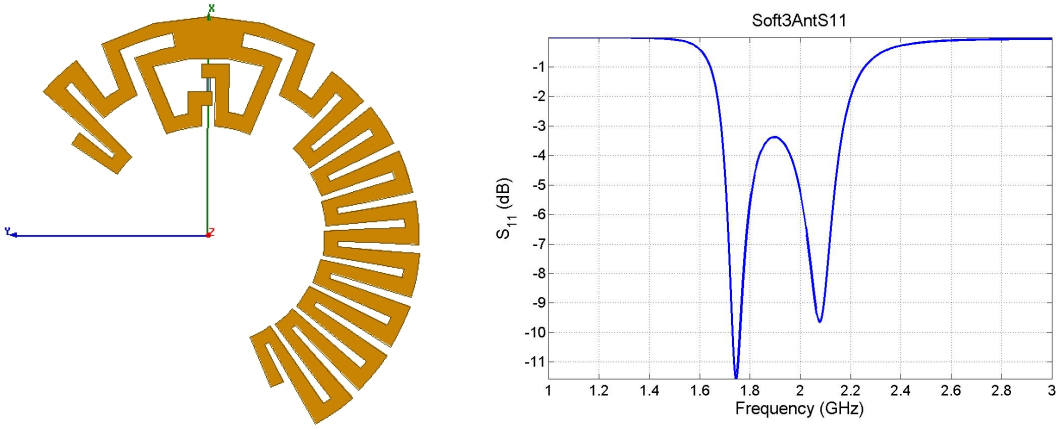

Figure 5.3: Optimized antenna with one arm shortened

much shorter, so that the operating frequency grows up to 2 GHz band, therefore the antenna operation band is not correct.

The created software also allows to generate automatically the CD structure to check its influence on antenna performance. On the basis of the last asymmetric antenna, figure 5.4 shows it only on a polycarbonate disc. We can observe that the polycarbonate has a positive effect. The 2 resonances keep coupled and the operation frequency has decreased due to the dielectric material effect at 1.8 GHz

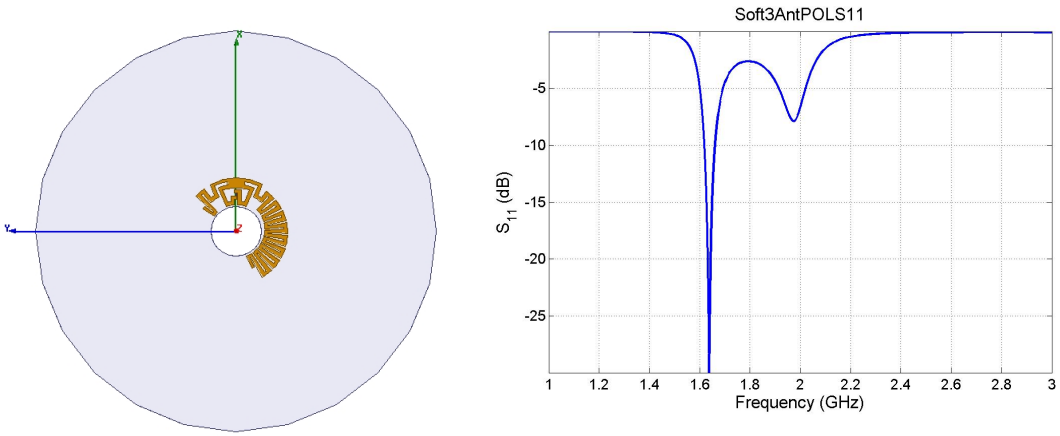

Figure 5.4: Optimized antenna with one arm shortened on polycarbonate

although is to high yet.

The next step is to check if this antenna could work when placed on a full CD (polycarbonate and reflective layer). The reflection coefficient is shown in figure 5.5. In this case we see that the strong coupling with the reflective layer causes a big variation on the resonances, whereby the coupling between them becomes uncontrollable. Even so, the antenna get good matching levels around -5 dB, however the operation bandwidth returns to be very narrow. Operation frequency also remains very high (about 1.5 GHz).

Another tested strategy is shown in figure 5.6. This consists in a similar antenna but with its arms short-circuited to create another loop bigger than the connection loop. This antenna also has much more meanders than the previous ones in order to increase its electrical length. The result shows a good operation bandwidth with a very good matching level around -10 dB, but the operation frequency is still very high. This could be caused by the large number of meanders which causes a lot of couplings between them because they are close together spoiling the capability to do the antenna electrically bigger.

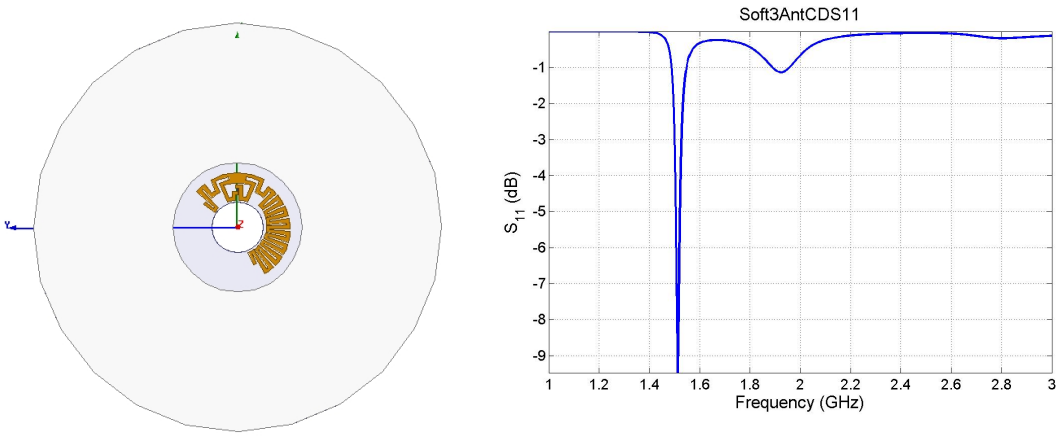

Figure 5.5: Optimized antenna with one arm shortened on CD

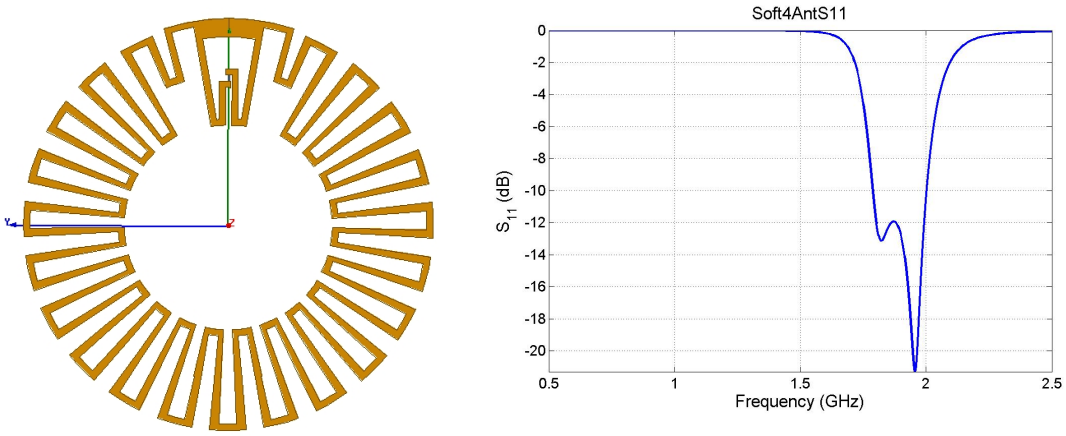

Figure 5.6: Optimized antenna with short-circuited arms

5.2 New Design Strategies

After this first contact with the software, we started to test some strategies with the objective of achieving a better performance for the antennas response such as the desired operation frequency and the matching level. We will explain all these strategies, showing the last antenna for each one, because it would be very long to show all the tested antennas which have been created in order to reach the final one, which is the best optimized one with each strategy.

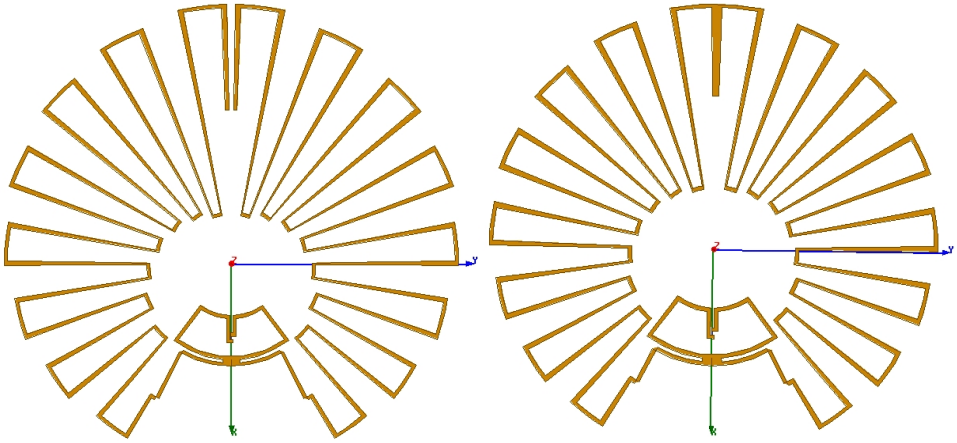

Figure 5.7: 8 meanders antennas with open arms (Left) and closed arms (Right)

5.2.1 Free Space Meanders Antenna

After realizing that having a big number of meanders is ineffective to increase the antenna electrical length and even deteriorates it due to increased couplings, we tried to do some simulations trying to make an antenna with the minimum possible number of meanders. We concluded after a few simulations that the minimum is 8 meanders for each arm, because if we put less than 7 the resonant frequency begins to grow. With this information we optimized 2 antennas with the aforementioned models, one with its arms opened and other with its arms closed. We can see this 2 antennas in figure 5.7. Other important thing is that the meanders size is bigger than the polycarbonate central part, so that we have designed these antennas with the connection loop inside the central part hoping that this will reduce the metallic layer effect when it is put in the CD.

Results obtained for these antennas are shown in figure 5.8 for the opened arms antenna and in figure 5.9 for the closed arms antenna. We can notice that this time we have drawn the Smith chart and the real and imaginary impedance plots. This is because the antennas performance can be best analyzed with all these results. The Smith chart shows a loop of which shape will depend on the antenna bandwidth

and position will determine the matching level. The same conclusion can be reached if we observe the real and imaginary impedance plot. We can notice that in these plots there are oscillations that will indicate a matching zone. For the real part, the desired value is 13Ω, so as closer the curve is to 13 and more wide range covers it would be better for the matching level and bandwidth respectively. Regarding the imaginary part it normally has an oscillation that we would need to situate near 151Ω by varying the antenna geometric parameters. Therefore these 3 plots together will help us to tune the antenna to the desired resonance frequency with a good matching level.

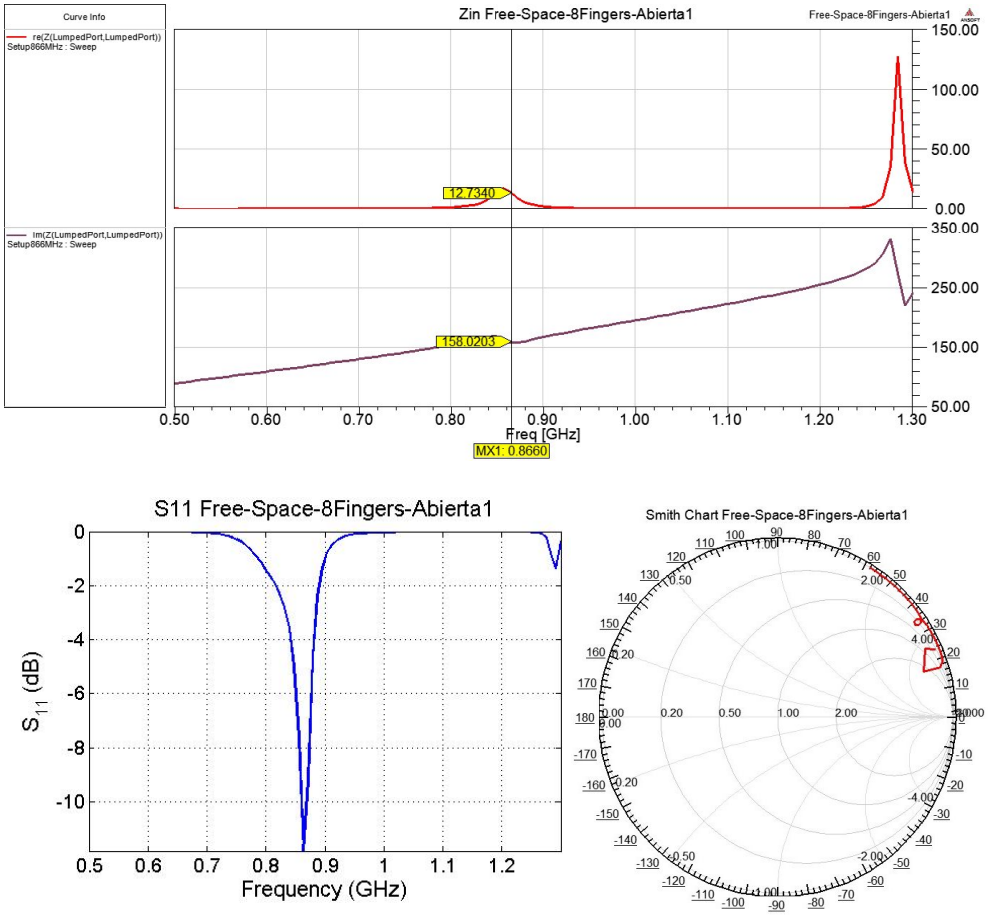

Figure 5.8: 8 meanders antenna with open arms results on free space

For the antenna with its arms opened we can see that it has a good matching

levels reaching values of -12 dB at the working frequency of 866 MHz and a bandwidth of 100 MHz at -2 dB. It is also important to notice that there is another resonance at 1.3 GHz and it can be seen in the three plots as another loop in the Smith chart and another oscillation in the real-imaginary plot. This other resonance is not important for our purpose.

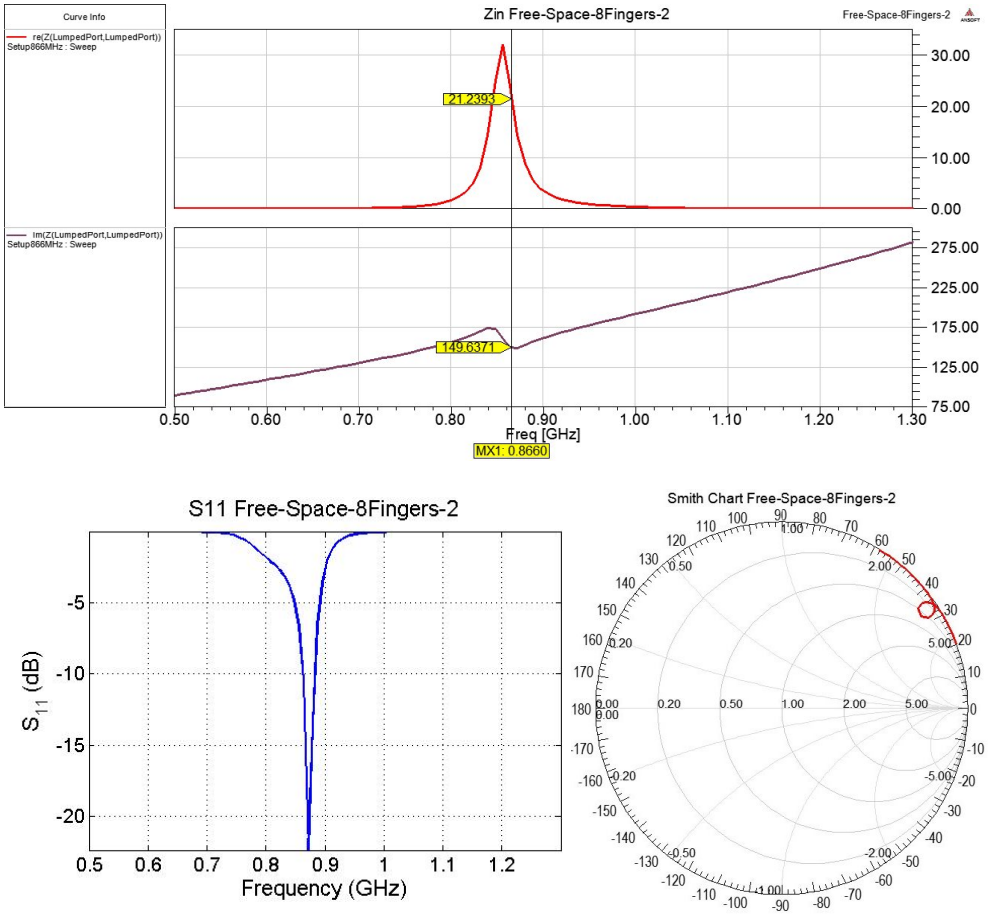

Figure 5.9: 8 meanders antenna with closed arms results in free space

For the other antenna (with closed arms) we can see that it has a better matching levels reaching values of -22 dB although it has the same bandwidth and the same response except for the single resonance frequency of this antenna. Both antennas could work very well due to these results and they are very good candidates for manufacturing and testing.

5.2.2 Meanders Antenna on Dielectric

As the previous antenna had so good response but it had its meanders upon the metallic layer we proposed a new strategy which consists of including a dielectric disc between the antenna and the CD to avoid the negative interactions between them. So we performed some simulations with different dielectric materials (different permittivity and thickness) to check the influence on our antenna which we hope that would be good as we have studied in others simulations explained in previous chapters.

After some simulations we achieved good results with two types of antennas shown in figure 5.10. They are basically the same antennas but they are placed on a dielectric material of $\epsilon_r = 6$ and 0.5 mm of thickness.

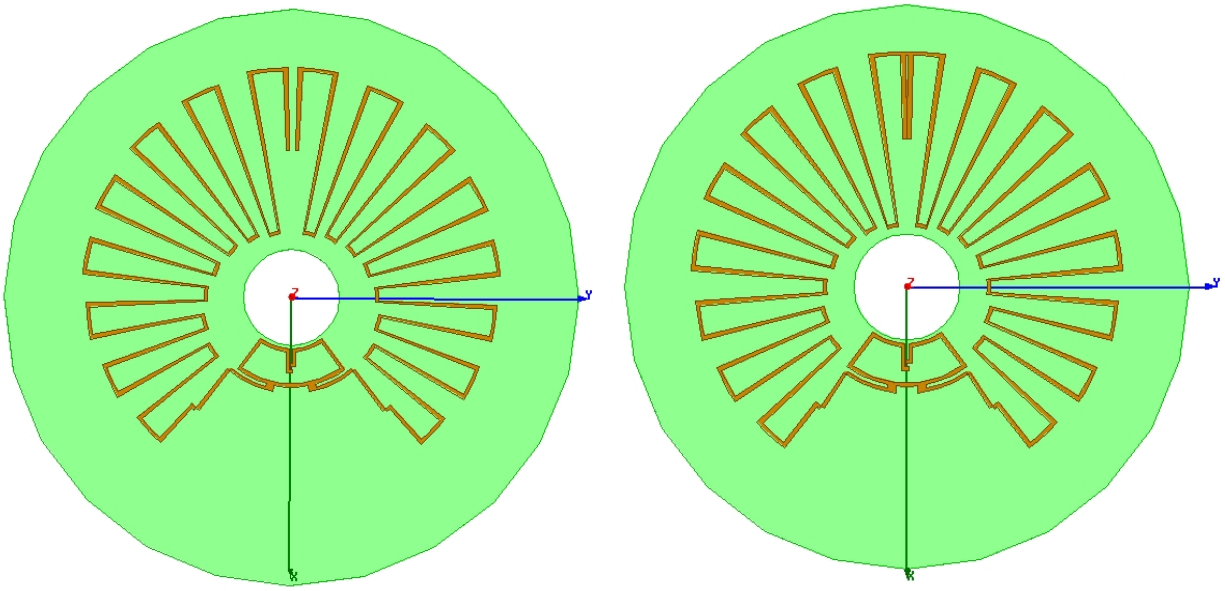

Figure 5.10: Meanders antennas on dielectric with open arms (Left) and closed arms (Right)

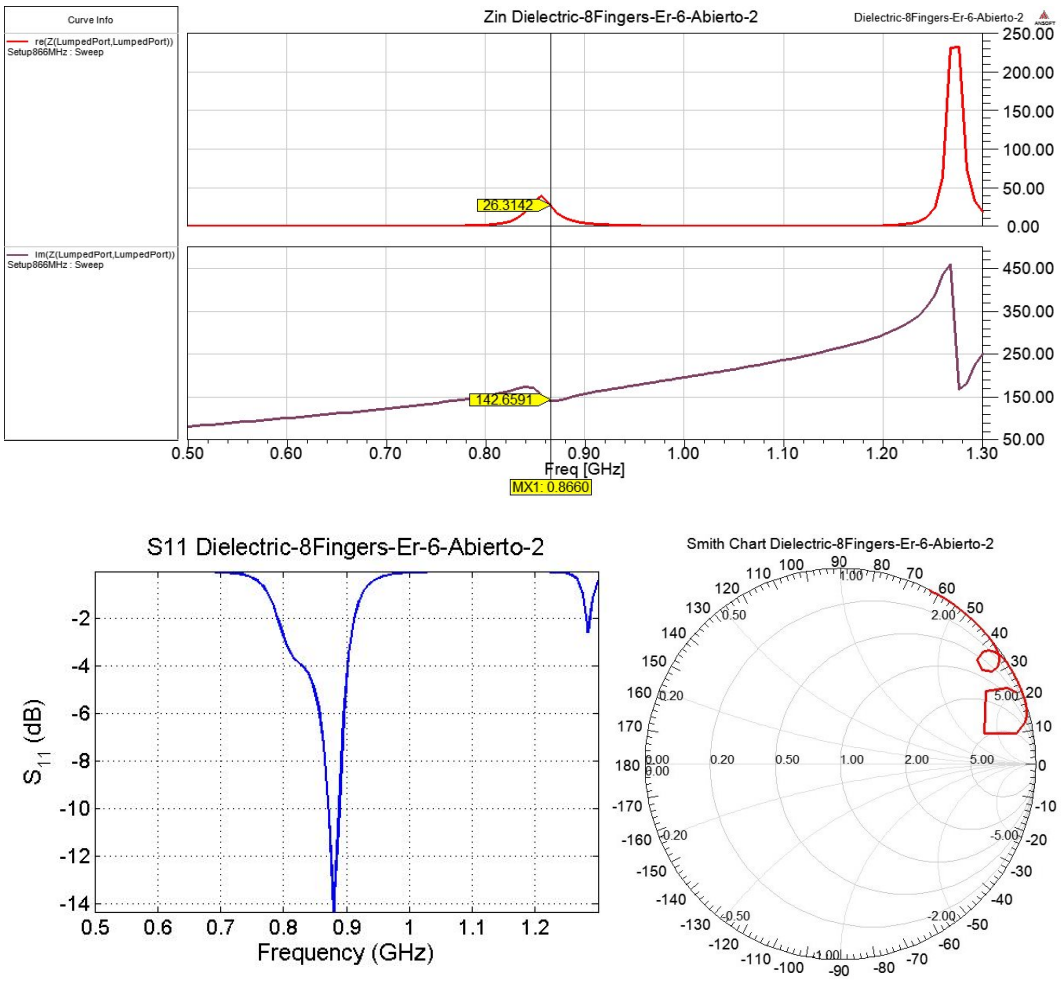

Figure 5.11: Meanders antenna with open arms results on dielectric

We can see the results obtained for the first one (opened arms) in figure 5.11. This antenna has better bandwidth than the no dielectric one (about 100 MHz at -4 dB) because of the aforementioned dielectric material effect (it reduces the resonance frequency and improves the bandwidth). We can see that the resonance frequency has not changed, this is because the dielectric thickness is very small so it has a small effect on the resonance frequency. The maximum matching level for this antenna is -14 dB and it is tuned to the correct frequency. Other aspect to remark is that with opened arms the other higher resonance frequency still appears.

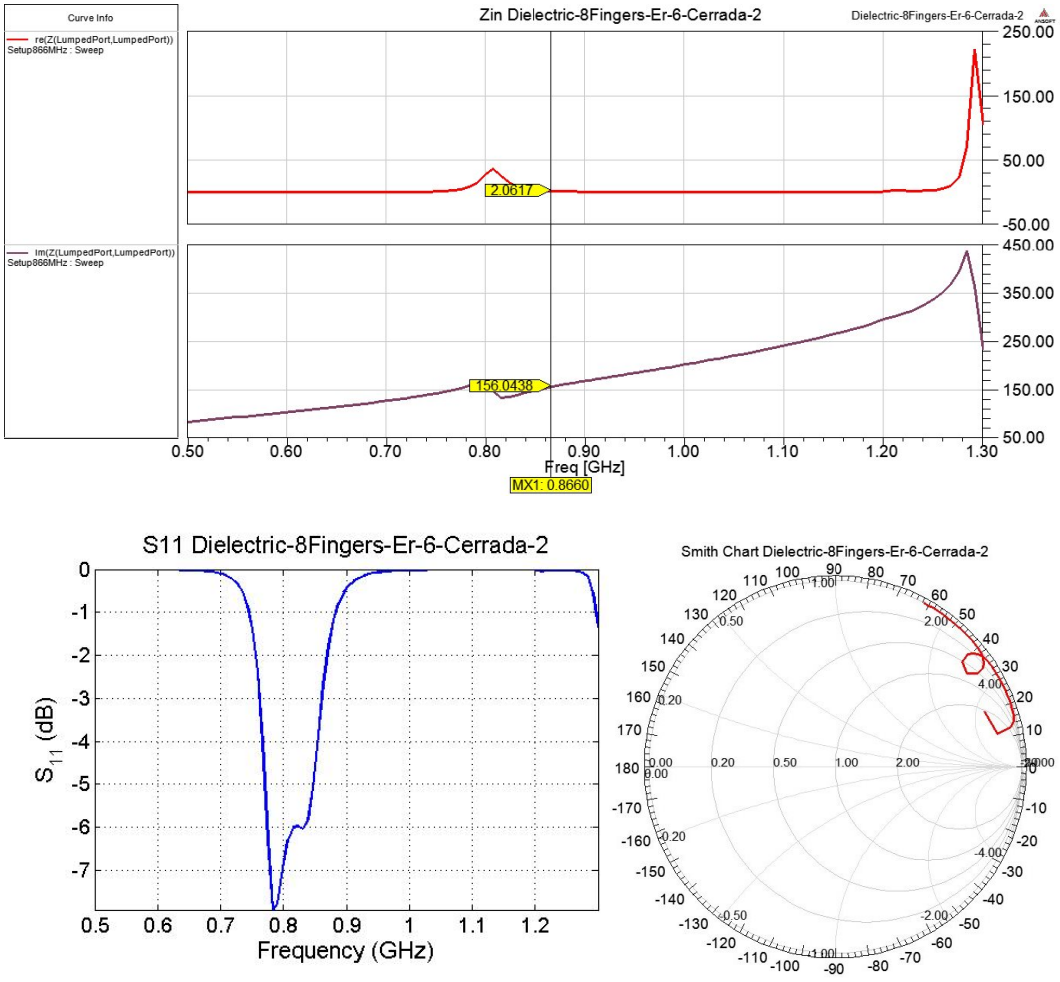

Figure 5.12: Meanders antenna with open arms results on dielectric

For the antenna with its arms closed we can see that it has worst matching levels reaching values of -6 dB at the working frequency of 866 MHz and a bandwidth of 100 MHz below -2 dB. It is also important to notice that this time the resonant frequency has decreased a little. Generally both antennas has similar performances so this strategy could lead to a real antenna development.

5.2.3 Meanders Antenna on CD

Given the last results the next step in the investigation was placing the studied antenna, which seemed to work well, on a CD. First we started with a dielectric of 1 mm and $\epsilon_r = 20$ which was unsuitable for our objective, but after a few simulations

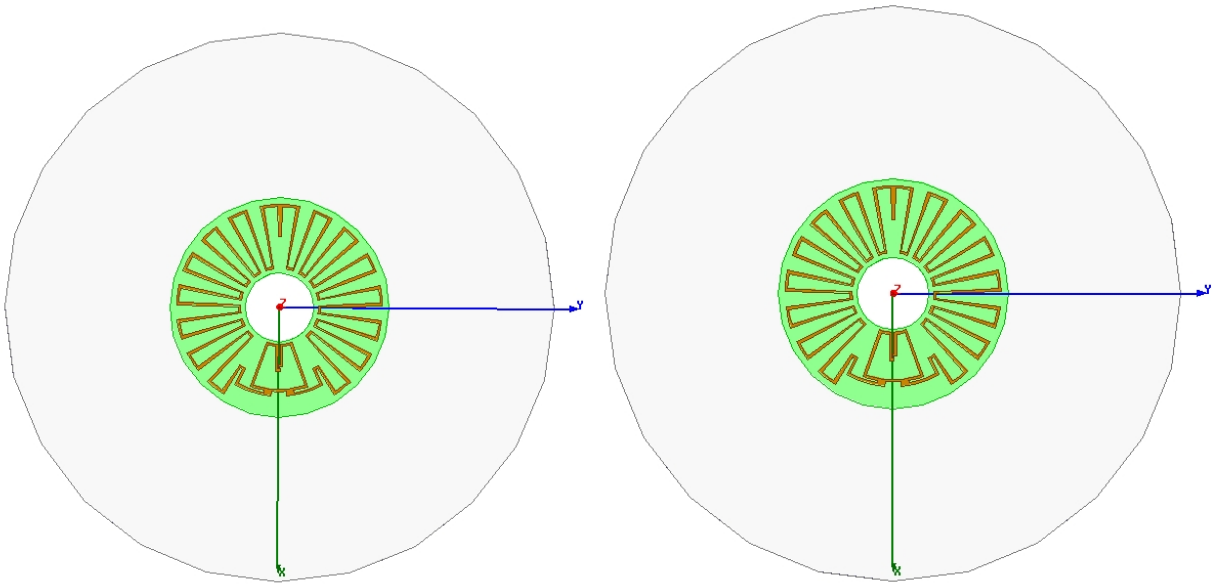

Figure 5.13: Meanders antennas on CD model 1 (Left) and model 2 (Right)

trying to achieve a lower permittivity and thickness we could reach a final solution for two models that in this case depends on the *junction angle length* (explained in chapter 2) with a dielectric of 0.13 mm and $\epsilon_r = 2.2$ which is a dielectric that we had at the laboratory. This geometric parameter permitted to increase the antenna bandwidth which is a conclusion that was used in following antennas. We can see these two final antenna models are very similar and are shown in figure 5.13.

For both results (model 1 is shown in figure 5.14 and model 2 in figure 5.15) we can notice that the Smith chart loop has become uncontrollable and it has an abrupt variation, this behavior lead to a de-tuning effect which can be appreciated on the real-imaginary and S_{11} plots. In the first one the variation for both stacked plots is not so soft as in previous cases and in S_{11} plot we can notice a matching level reduction for all the frequency sweep plus a resonance frequency reduction. One remarkable thing is that the bandwidth has been improved but with much less matching levels about -0.3 dB. As conclusion these antennas could work on a CD but with a very poor performance due to the spoiling caused by the reflective layer.

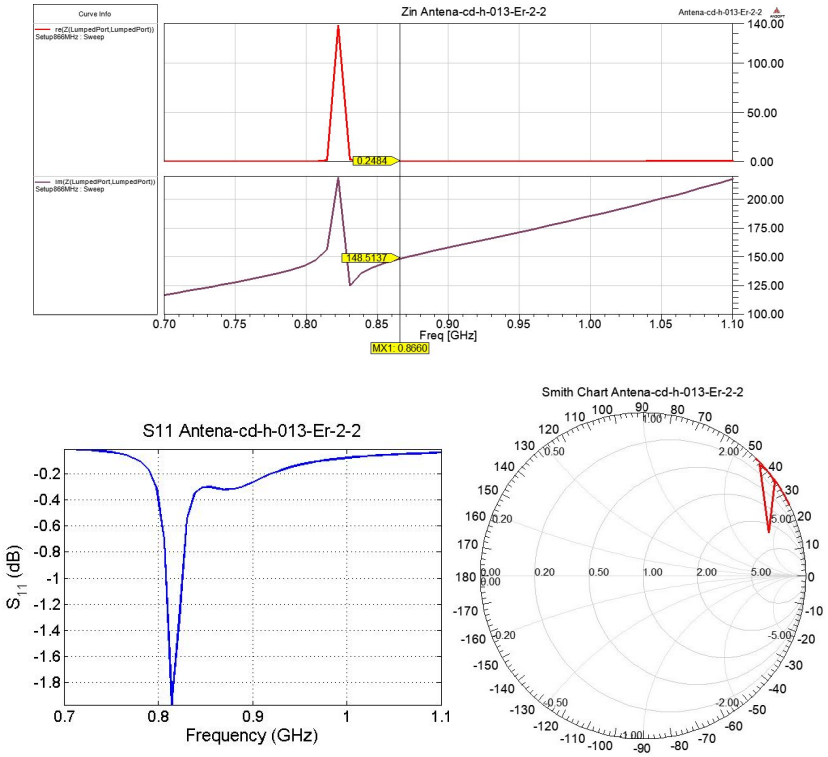

Figure 5.14: Meanders antenna model 1 results on CD

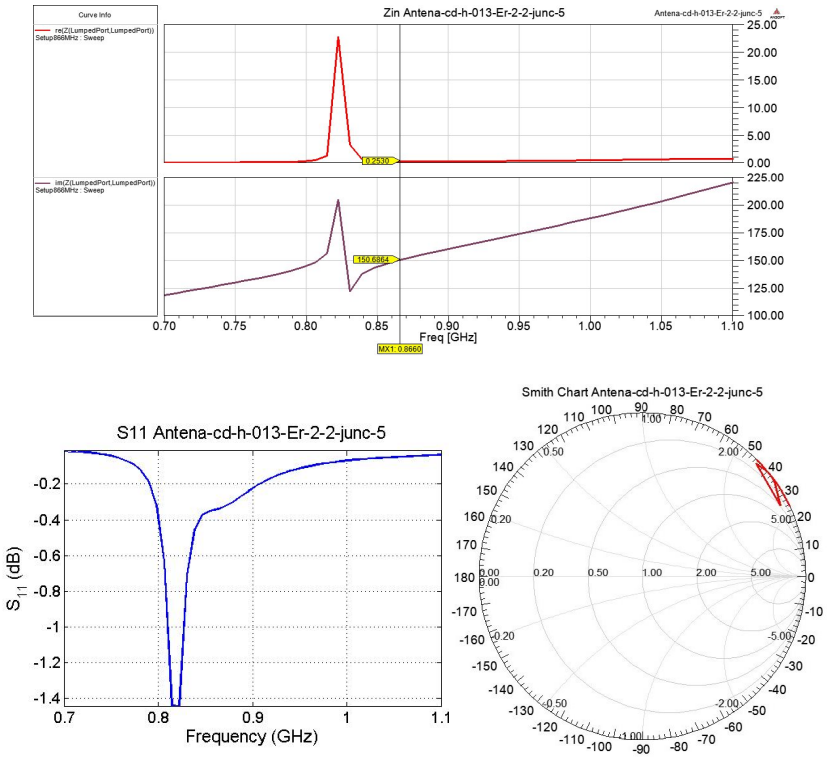

Figure 5.15: Meanders antenna model 2 results on CD

After this in depth investigation with this type of antenna we carried out some tests with other antenna models to compare our principal meander antenna to other alternatives in order to extract some conclusions about which is the best of all strategies to begin a real fabrication and testing. These are explained in following sections.

5.2.4 Ring Antenna

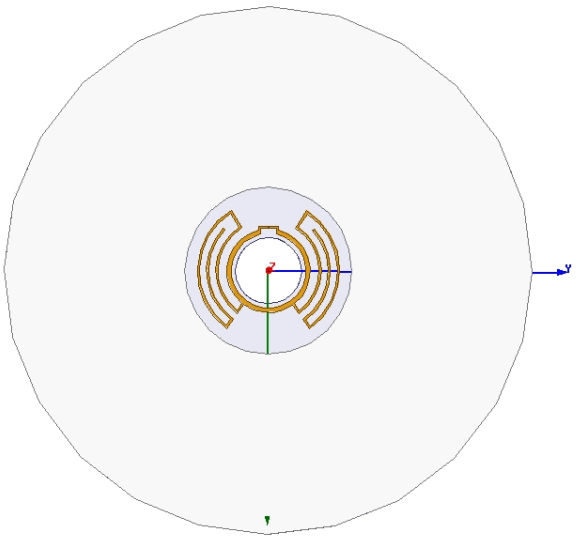

Figure 5.16: Commercial Ring Antenna on CD

Given the last antenna results, we thought about comparing them with an available commercial that we called commercial ring antenna. This antenna is basically formed by a central ring and two arms that are connected to it and which are folded several times to make the antenna electrically length. This structure is very interesting because it fits very well on the CD central part and is less prone to be affected by the reflective layer. We added this antenna to the software as explained in chapter 2 and obtained some interesting results that are explained below.

First we created the commercial antenna (Figure 5.16) on a CD. Figure 5.17 shows the results obtained for this antenna. We can notice that this antenna is

tuned to the American RFID frequency of 950 MHz and it has the same performance as the previous antenna with a better matching level about -1 dB but with a worst bandwidth. This behavior is unchanged if the antenna is not on a CD, so it seems that this antenna is less susceptible to the reflective layer effect but its performance is worst that our antenna since the less bandwidth could lead to more important de-tuning effects that might completely destroy the antenna operation. This poor bandwidth is due to the Smith chart loop that is too much open so it is better to achieve a closed loop even abrupt.

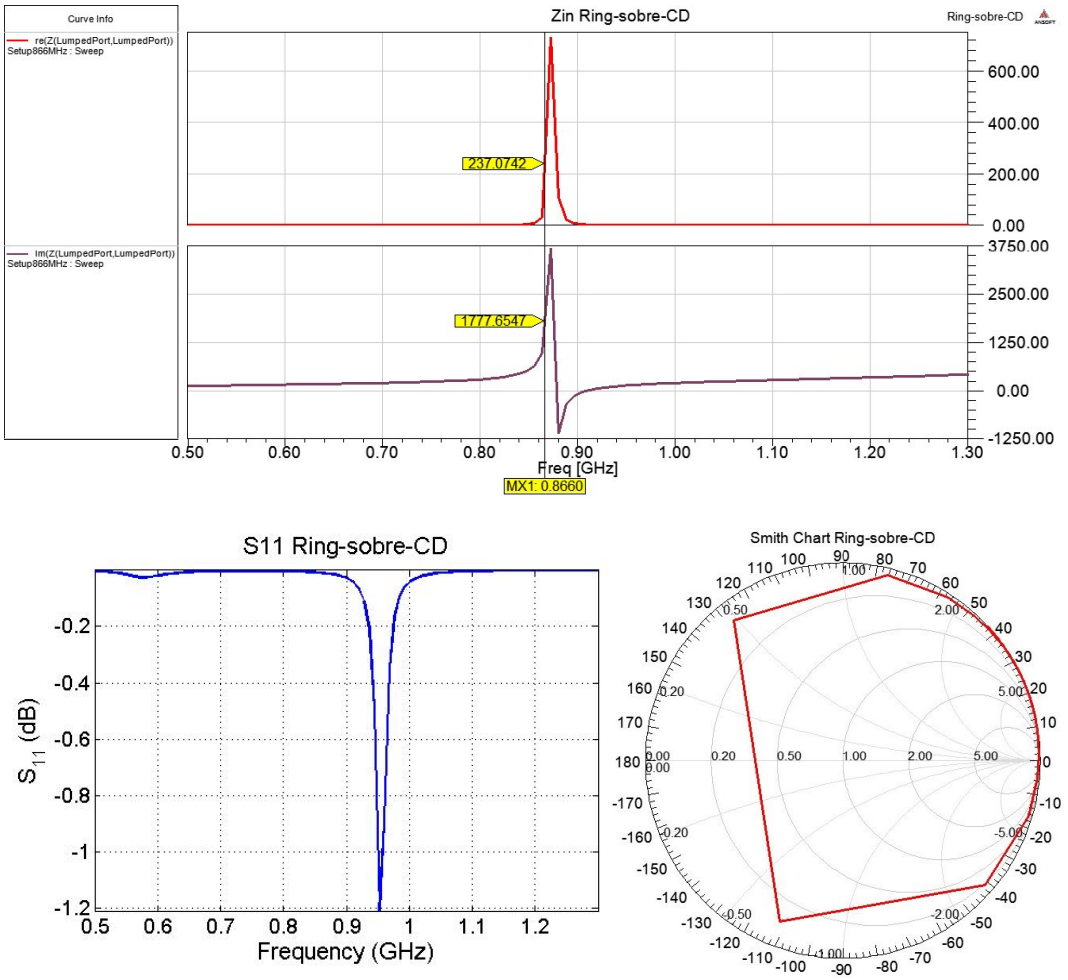

Figure 5.17: Commercial Ring antenna results on CD

After analyzing this ring antenna we tried to modify it with our software looking

for achieving a better performance with such structures but we always obtained the same results with poor bandwidth and better matching levels. Figure 5.18 we can see some of these designs. We have not shown all these results because are very similar to the original ring antenna and we would explain the same conclusions again. As can be seen in the figure these modifications are generally made in the antenna arms due to their more flexibility and including a dielectric.

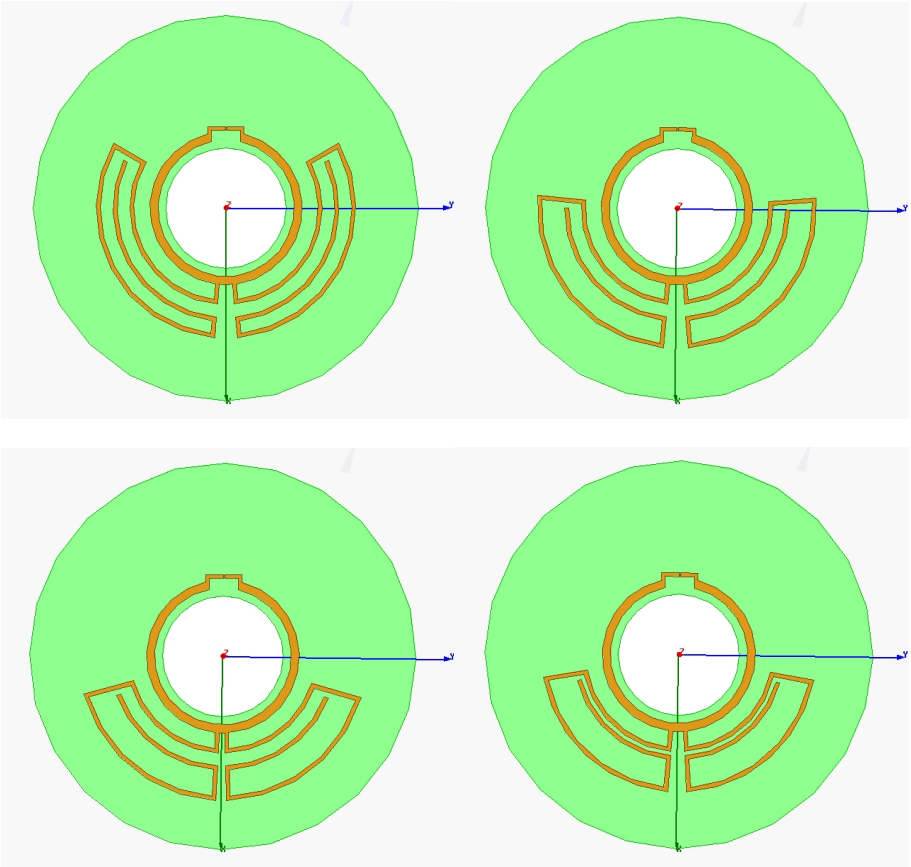

Figure 5.18: Ring antenna variations example

5.2.5 Arms Antenna

The next step after analyzing the commercial ring antenna was to try another mixed concept antenna which is formed by the connection loop of the meanders antenna connected to the commercial ring antenna arms. This strategy was tried

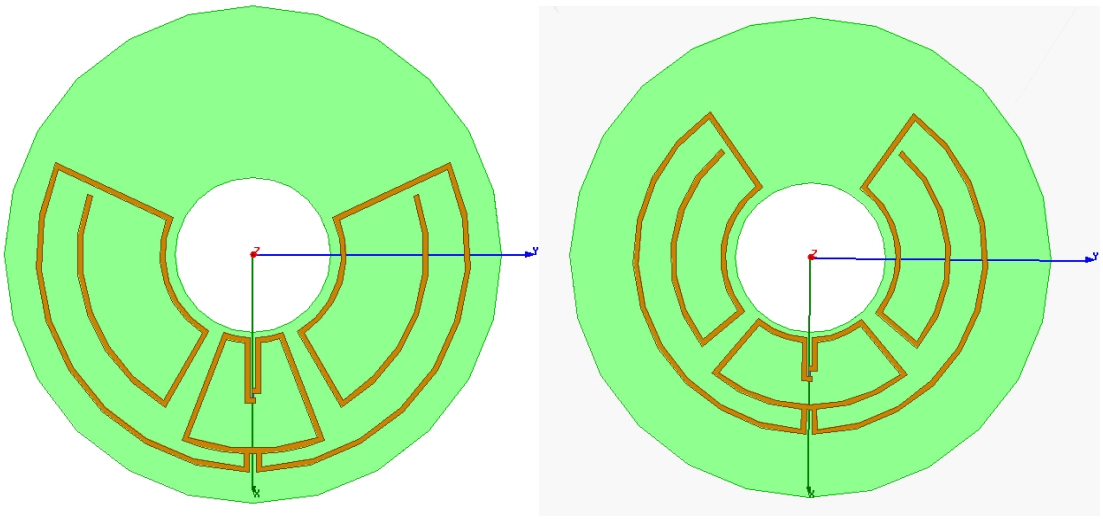

Figure 5.19: Arms antenna on dielectric (Left) and on CD (Right)

hoping that it would take advantage of the good characteristics of each antenna (the better matching levels of the commercial ring antenna and the better bandwidth of the meanders antenna) since as said before, this antenna parts seem to control these characteristics. We can see the final and best optimized model of this new antenna in figure 5.19 with and without CD.

We can see the results for this antenna in figure 5.20 for the non-CD model. As can be seen the results are not as we expected, the bandwidth is still very poor although the matching level at the resonance frequency has improved to -20 dB (we have to take into account that these results are on a dielectric with no CD so it is normal to obtain better matching levels). But this result leads to the same problem, the antenna is very susceptible to be de-tuned due to the narrow bandwidth. Regarding the better matching level, it is due to the achievement of a more closed Smith chart loop than the commercial ring antenna one, which it is probably achieved because the antenna is not upon a CD. As conclusion after the analysis of the previous antenna and this new one, the narrow bandwidth could be due to the utilization of the folded arms since when they are used the bandwidth is very poor.

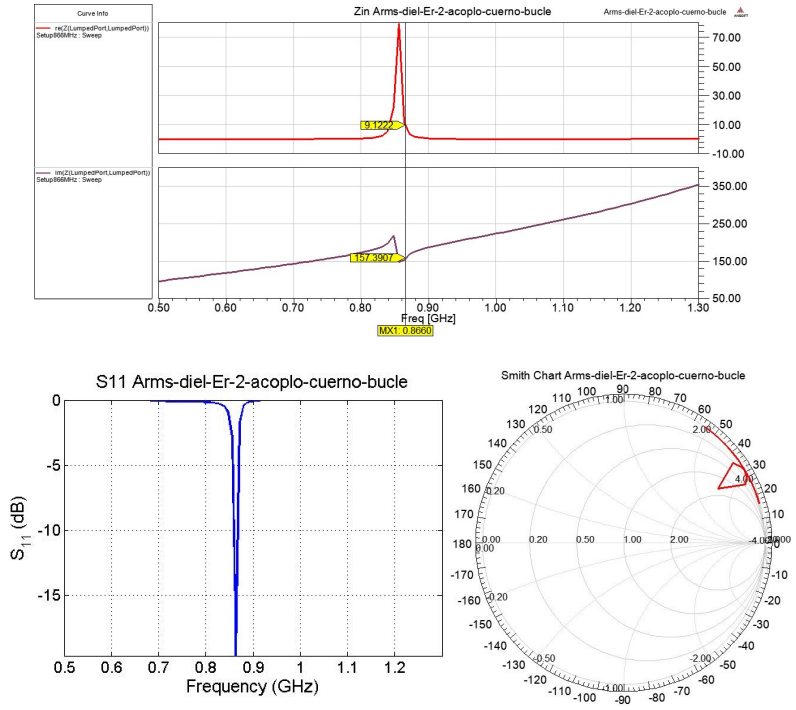

Figure 5.20: Arms antenna results on dielectric

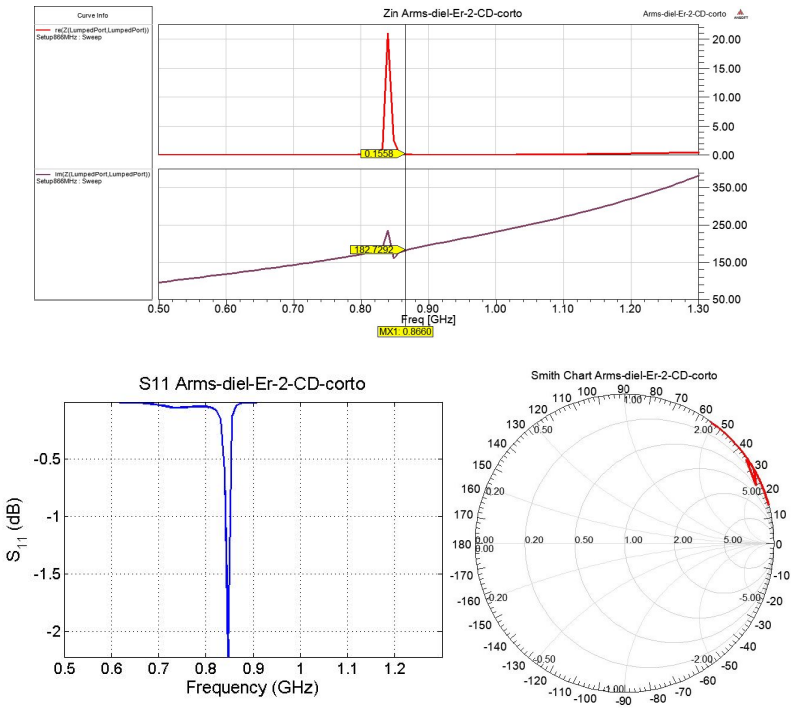

Figure 5.21: Arms antenna results on CD

If we put this antenna on a mini CD, the obtained results are shown in figure 5.21. These results are similar to the non-CD model except for the matching level which is very similar to the commercial ring previously analyzed, so as conclusion we can say that this two antennas are not so appropriated to proceed a further investigation as our meanders antenna due to their worst characteristics.

5.3 Meanders Antenna Improvement

After this point of the project and once rejected the last two antenna types, we focused on improving our meander antenna with some strategies trying to achieve a best performance that the previously obtained.

5.3.1 Meanders Antenna on Dielectric Cylinder

Leaving apart the aim to create antennas for CDs, we tried to study one possible solution for antennas on metallic surfaces that are not necessary CDs. To do this we tried to put the antenna on a dielectric cylinder to isolate the antenna from the reflective layer. This solution is not obvious for CD applications due to the need of a low profile antenna to avoid problems on the CD readers mainly with ejected-CD types.

The final antenna configuration obtained is shown in figure 5.22. As can be seen the antenna is located on a dielectric cylinder of 30 mm of heigh to avoid the metallic surface negative effect. The simulation of a metallic surface have been done using the CD structure but that does not mean that this antenna has been created for using it on CDs

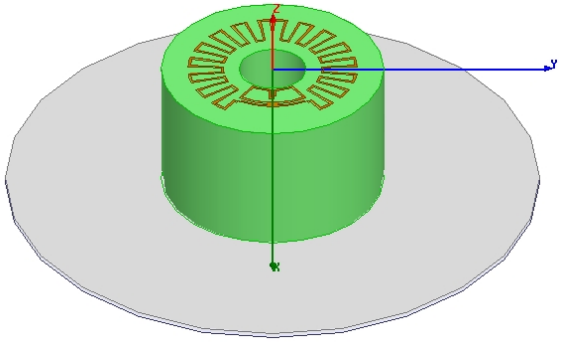

Figure 5.22: Meanders antenna on a dielectric cylinder

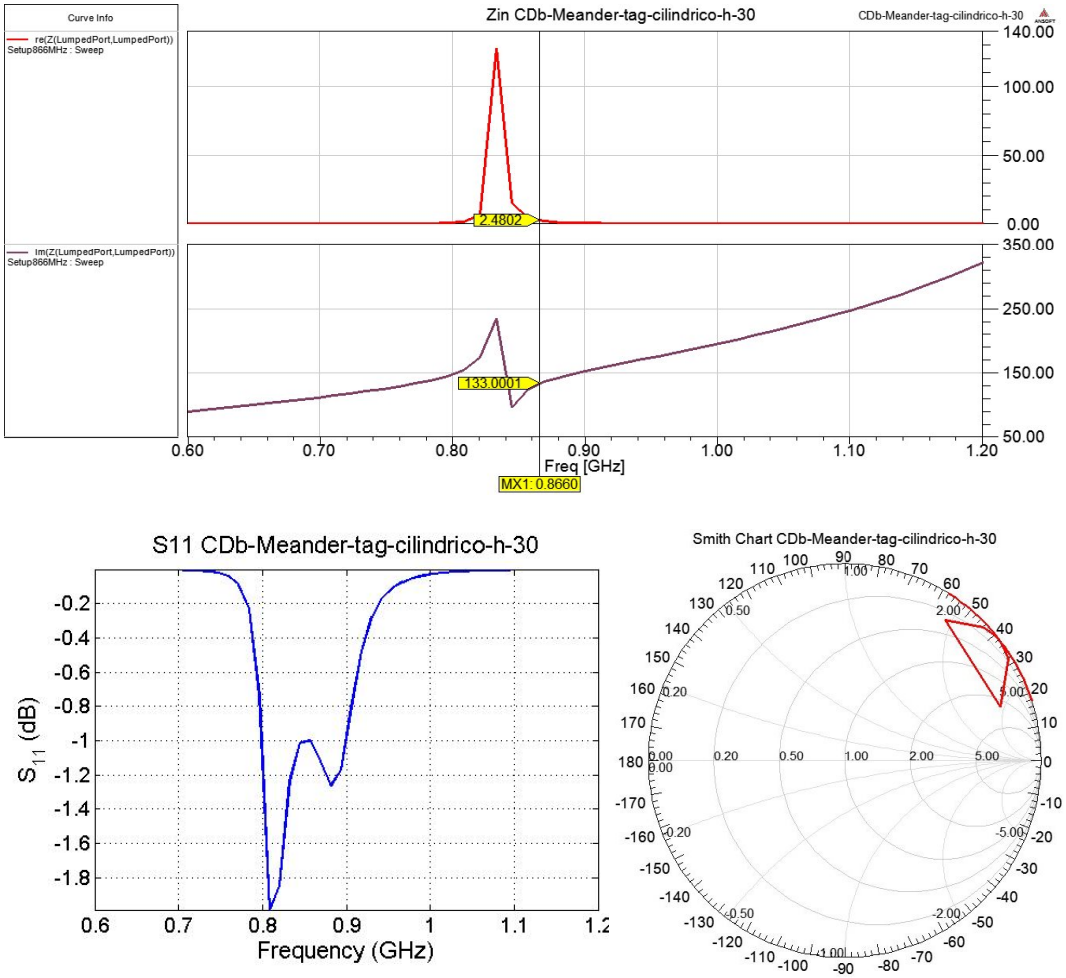

Figure 5.23: Meanders antenna results on a dielectric cylinder

The results for this antenna simulation are shown in figure 5.23. We can see that the antenna has a very good bandwidth of about 100 MHz (from 800 MHz

to 900 MHz) below -1 dB, so it seems that this strategy is useful for avoiding the aforementioned negative effects of the metallic surface proximity.

5.3.2 Meanders Antenna on Dielectric Foam

After this first test of dielectric cylinders utilization we realized that other commercial antennas are placed on a dielectric foam instead of a simple dielectric material in order to avoid the capacitive effect of the dielectric materials. Foams usually have very low permittivity ($\epsilon_r \approx 1$ as free space) and this leads to a separation between the metallic layer and the antenna as if they were nothing but air between them avoiding the characteristic capacities of the dielectric. After a lot of simulations trying to reduce the foam height and optimizing the antenna as best as possible we achieved a final solution that is shown in figure 5.24. This antenna is placed upon a dielectric foam of $\epsilon_r = 1.07$ and as can be seen its arms radius have been increased because we checked that this change improves the antenna performance because it makes the antenna electrically larger.

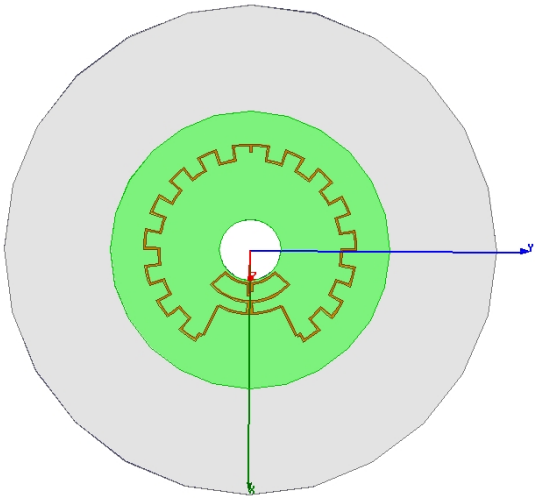

Figure 5.24: Meanders antenna on a dielectric foam

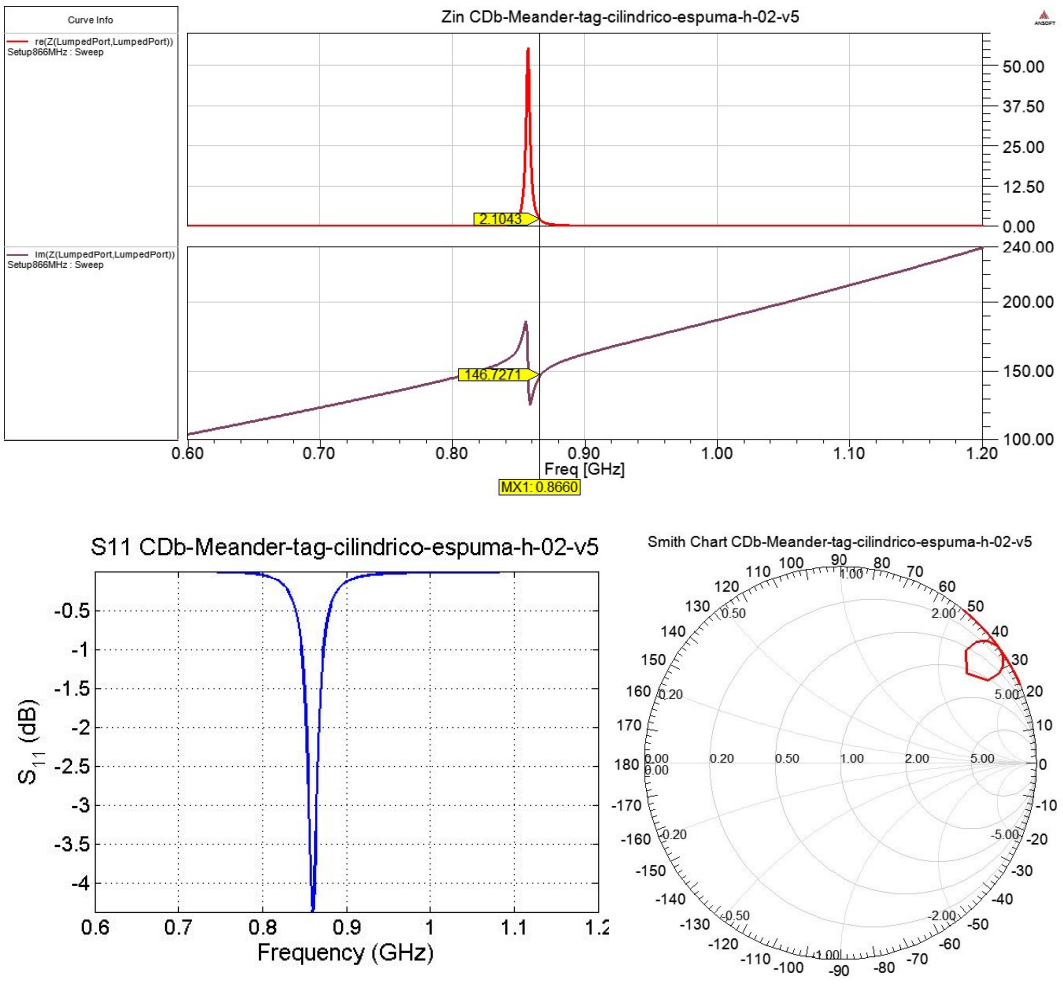

Figure 5.25: Meanders antenna results on a dielectric foam

Results for this antenna are shown in figure 5.25. As can be seen this antenna has a narrow bandwidth but it is better than the previous narrow bandwidth antennas as well as it has a much more controllable Smith chart loop which as can be seen is less abrupt than in precedent antennas as *Ring Antenna* and *Arms Antenna*. Due to this good control of the resonance frequency this antenna could be a good candidate for manufacturing and testing it.

5.3.3 Meanders Antenna on Available Dielectric

After this dielectric foam test we tried placing the antenna on a dielectric that was available in the laboratory of $\epsilon_r = 2.2$ and 0.13 mm of thickness. This is a very thin dielectric (it has similar thickness than a paper) so it is suitable for our purpose. The strategy of increasing the arms radius has been profitable to achieve a good results with this dielectric and with a low profile. The two antenna models optimized with this dielectric are shown in figure 5.26. The difference between them is that the left one has short-circuited arms and the right one has open-circuited arms.

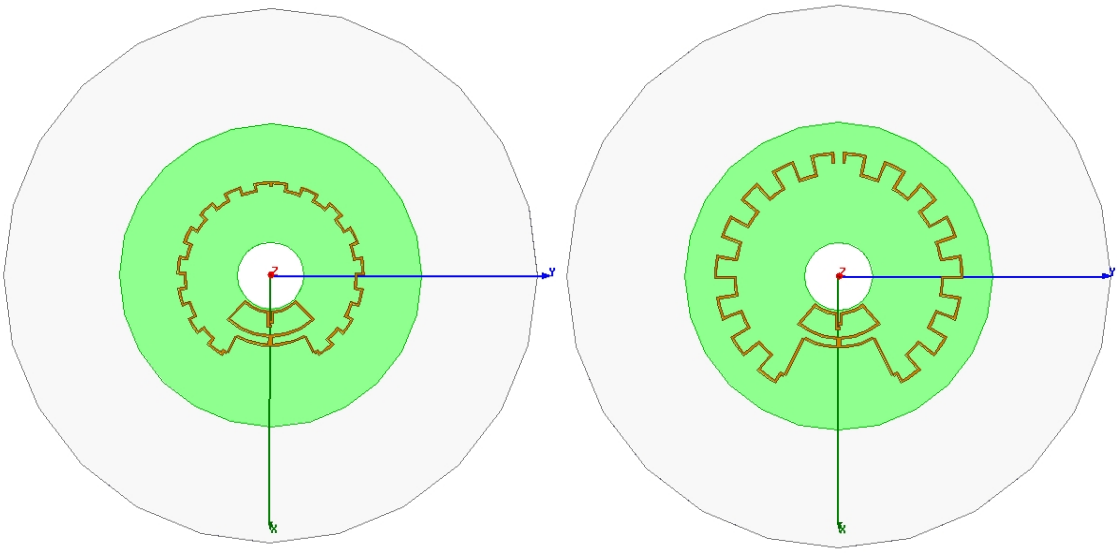

Figure 5.26: Meanders antenna on dielectric and CD (with available dielectric of $\epsilon_r = 2.2$ and 0.13 mm)

We can notice that the short-circuited antenna need a smaller meanders than the open-circuited antenna that is because as we have said before, when the arms are shortened the antenna becomes electrically longer. Results for these antennas are shown in figure 5.27 for the short-circuited arms antenna and in figure 5.28 for the open-circuited arms.

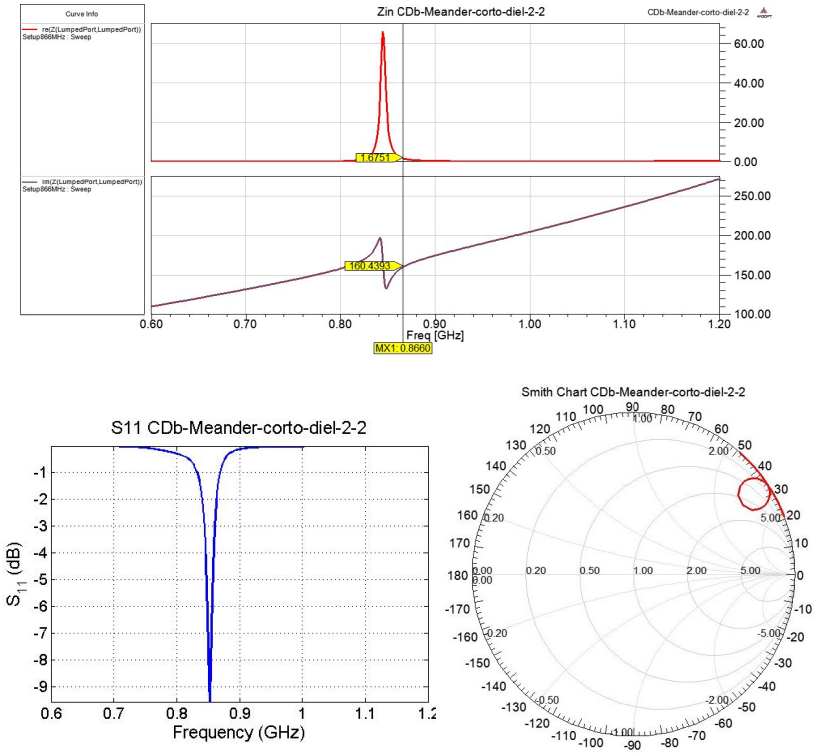

Figure 5.27: Meanders antenna with short-circuited arms results

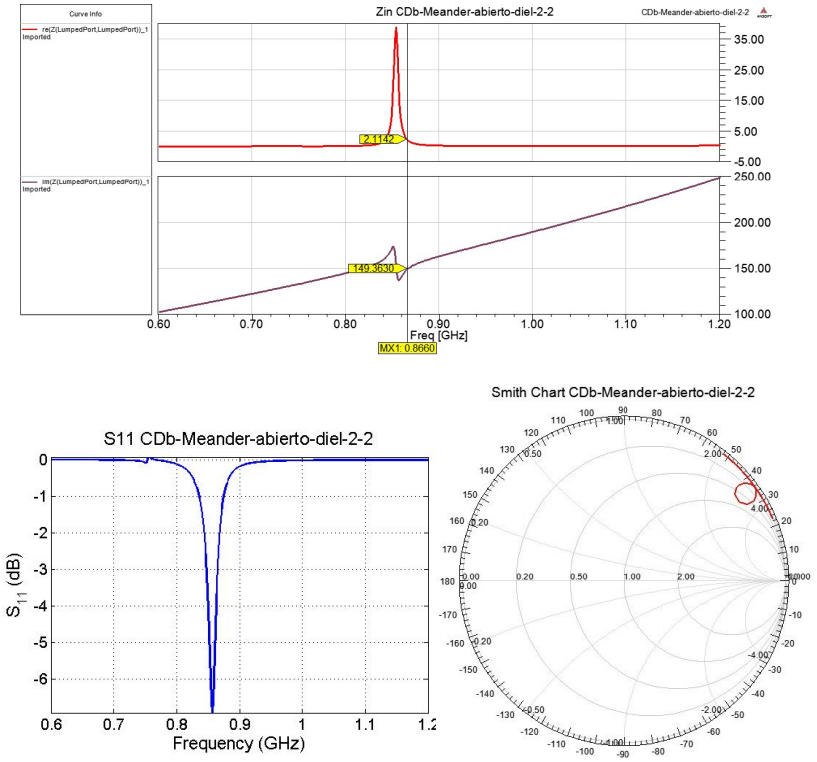

Figure 5.28: Meanders antenna with open-circuited arms results

As can be seen the results are very similar. Both antennas have a narrow bandwidth but nevertheless this bandwidth is wider than the other discarded antennas (ring antenna and arms antenna). Other advantage of these antennas is that their matching is much more controllable since although the Smith chart loop varies very fast, it is easy to control with the geometric parameters of the antennas. Therefore these two antennas are promising for a good performance on CDs although they do not have good bandwidth. If we look at the S_{11} parameter we can notice that the matching level at the resonance frequency for the short-circuited arms antenna is better (-10 dB) than the open-circuited arms antenna (-7 dB) as in previous short and opened arms antennas.

5.3.4 Meanders Antenna with 4 Arms

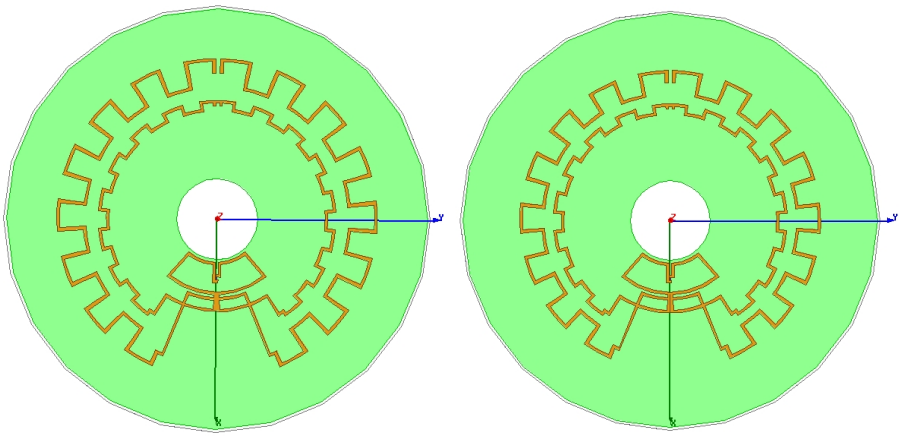

Figure 5.29: Meanders antenna with 4 arms on dielectric and CD model 1 (left) and model 2 (right)

It would be much better to improve the last antennas bandwidth so we decided to introduce a new option in the GUI software for creating a 4 arms geometry in order to obtain 2 resonances (1 for each arms loop) and achieve a wider bandwidth combining them. These simulations have been performed using a mini CD to reduce the simulation time due to the complex structure and are placed on the same

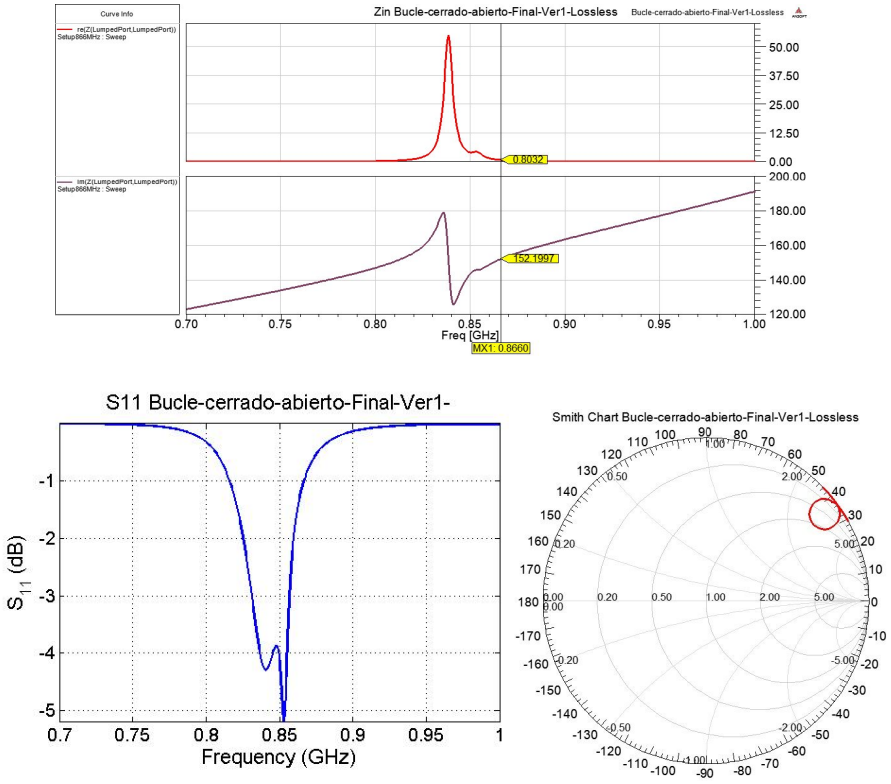

Figure 5.30: Meanders antenna with 4 arms on dielectric and CD results

dielectric available in the laboratory of $\epsilon_r = 2.2$ and 0.13 mm. After several antenna tests we obtained the final two models which are shown in figure 5.29 (model 1 at left and model 2 at right). As can be noticed both models have the inner arms short-circuited and the outer arms opened and than as we have seen in previous results, the closed arms are smaller than the opened arms.

We can see the results for the model 1 in figure 5.30. The bandwidth of this antenna has improved compared to the 2 last models with only 2 arms and it has a good matching level of -4 dB in this bandwidth range. This is due to the combination of the 2 resonances of the 4 arms. We can also see this effect in the Smith chart plot where there are 2 loops that correspond to the 2 resonances. The only drawback of this antenna is a low resonant frequency but this could be controlled with the geometric parameters.

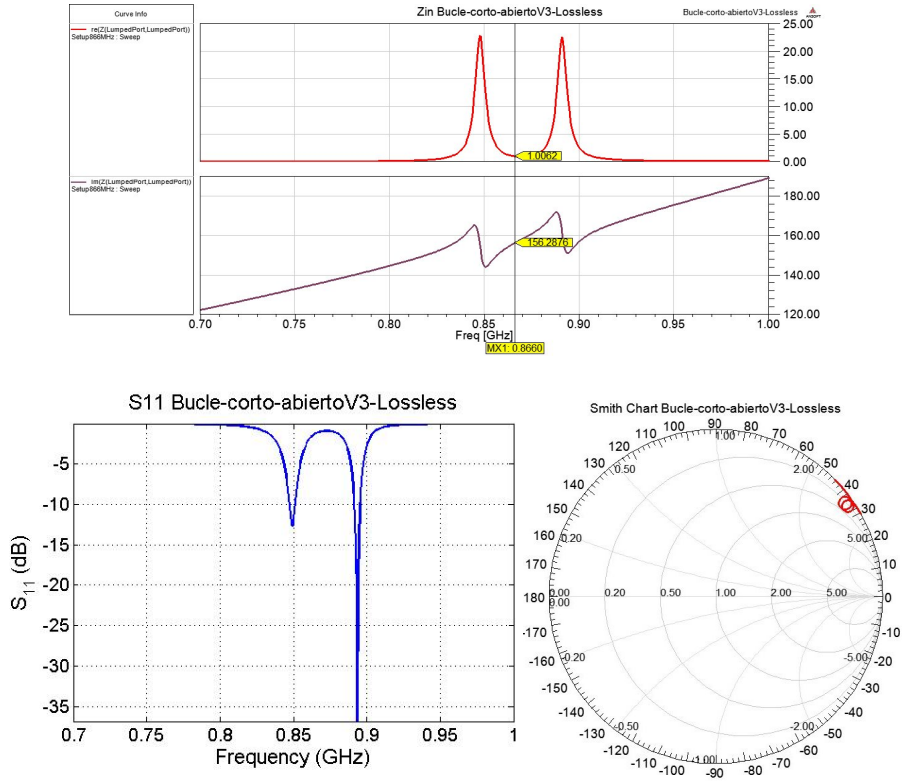

Figure 5.31: Meanders antenna with 4 arms on dielectric and CD results

Figure 5.31 shows the results for model 2. In this case we see 2 resonances separated in frequency which could be useful to creating dual-band antennas. This antenna improves the matching levels (-12 dB for the first resonance and -30 dB for the second resonance) compared to the previous one but with separated resonances. Even so, the bandwidth is also better than the 2 arms antennas.

5.4 Ideal CD Dilema

After all this simulations on CDs we realized that the CD model created by the software was not ideal since the reflective layer was made of aluminum instead of PEC and the polycarbonate had a given loss tangent different than zero. This fact made us repair this mistake and we performed some simulations to check if it was very influential in the obtained results. We found that it was a really important problem since the tested antennas with a non-ideal CD did not provide the same

results as the ideal CD simulations. This is caused by the real CD absorption produced by the lossy materials which may provoke a resonance in the results that is not a real radiation resonance but an absorption resonance caused by these materials. Therefore we needed to rethink which was the next step in the project due to this inconvenient

5.4.1 Tapered Antenna

The first step as we have said was to check the ideal CD problem. Once we realized that it was very important, we tried to design an antenna which could really work radiating its power instead of being absorbed by the CD. We achieved a solution doing a increasing tapering on the antenna arms in order to use the first meanders (which are inside the central polycarbonate part of the CD) to radiate the chip power and the last meanders to adjust the resonance frequency. This antenna is shown in figure 5.32. The dielectric used is the same as before ($\epsilon_r = 2.2$ and 0.13 mm) and the antenna is on a mini CD to reduce the simulation time.

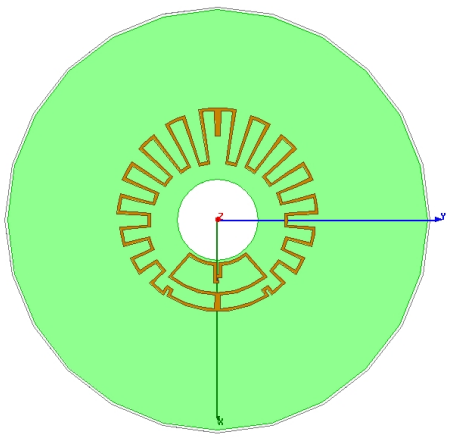

Figure 5.32: Tapering antenna

The results for this antenna are shown in figure 5.33. We can see that it has a good resonance frequency but the matching level is very low (around -0.4 in the

best peak) since the Smith chart loop and the Z_{in} plot became uncontrollable. This demonstrates that the ideal CD almost totally avoids the antenna.

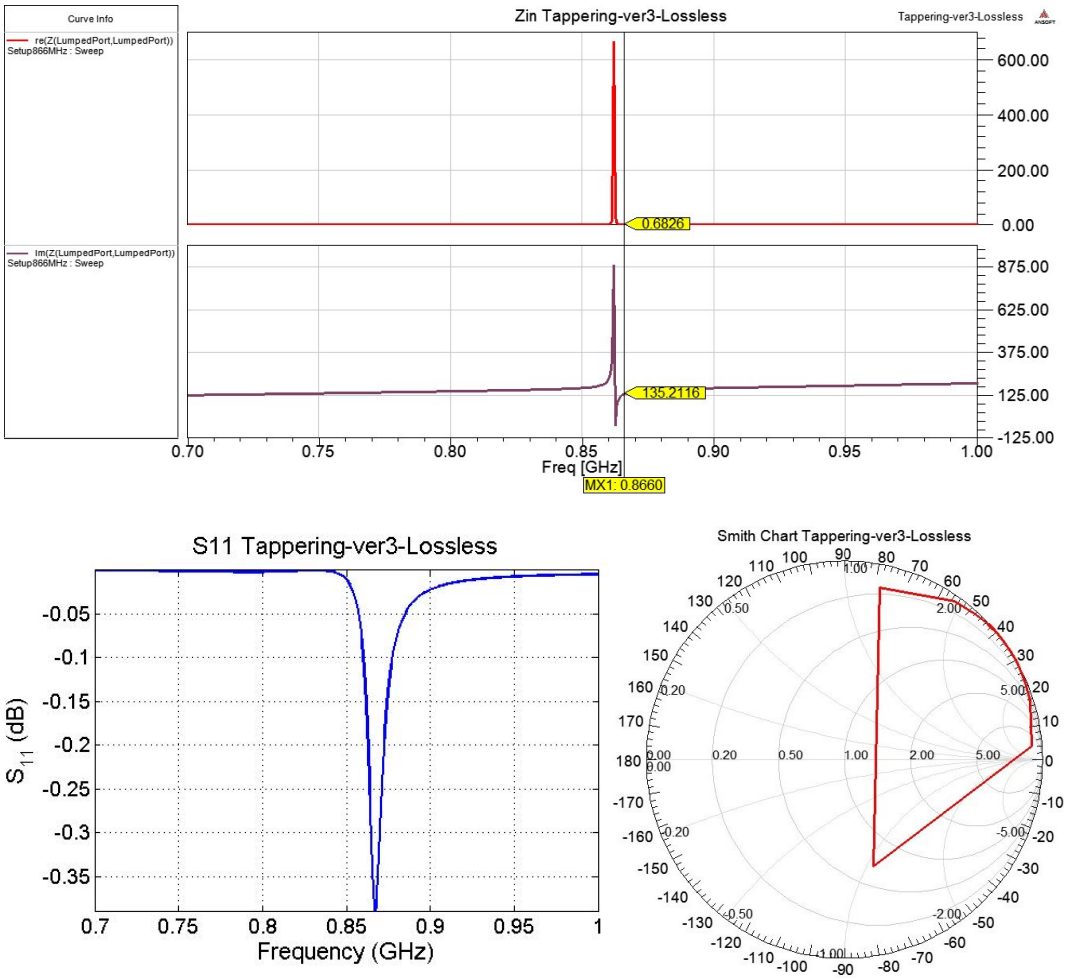

Figure 5.33: Tapering antenna results

5.4.2 Ground Plane Antennas

Thick Ground Plane

Given the last solutions we can conclude that there are not a simple solution for the CD application due to the complexity of placing the antenna on such structure, because the interaction with the metallic layer is very strong and is very complicated to avoid this effect. After this conclusion we tried to design an antenna which could deal with metallic surfaces although it was not planar. To this purpose we returned

to the dielectric cylinder idea and tried to reduce its thickness as we could.

We first started designing the antenna shown in figure 5.34. As can be seen this antenna is less curved than the other ones but is kept conformed to the curved shape of the CD. It is situated upon a dielectric of 27 mm and $\epsilon_r = 10.2$ which serves to separate the metallic layer from the antenna.

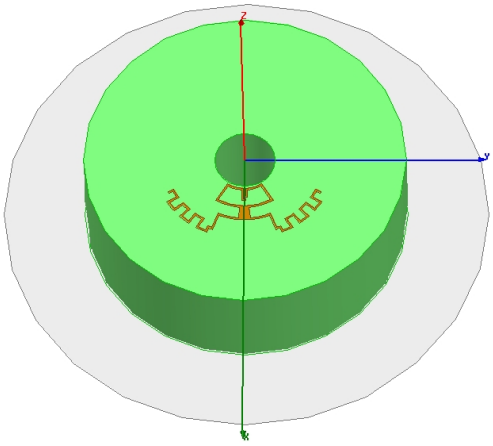

Figure 5.34: Thick dielectric ground plane antenna

The results obtained for this antenna are shown in figure 5.35. The Smith chart loop is very smooth and is very closed which leads to a very good bandwidth and matching level in all the frequency band of interest. The antenna shows a bandwidth from 850 MHz to 900 MHz with matching level around - 10 dB which is a very good result compared with the previous antennas. The only inconvenient of this antenna is the very thick dielectric.

At this point of the project we introduced the RCS calculation option in the GUI so we could obtain RCS results from this antenna. We have selected the most important RCS components that are the co-polar components in both planes XZ and XY. The RCS results for this one are shown in figure 5.36 for XZ plane. We can see that these components in plane XZ are very good, reaching values of -8 dB for the ϕ component and -13 dB for the θ component. This indicates that this antenna reflect the incident power very well but we have to take into account that the ground

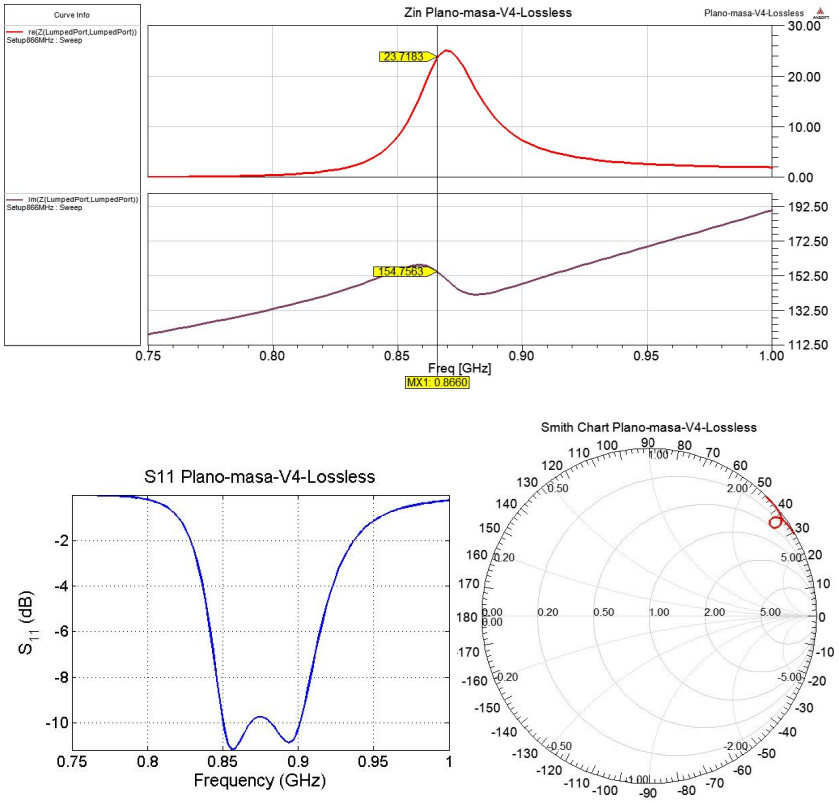

Figure 5.35: Thick dielectric ground plane antenna results

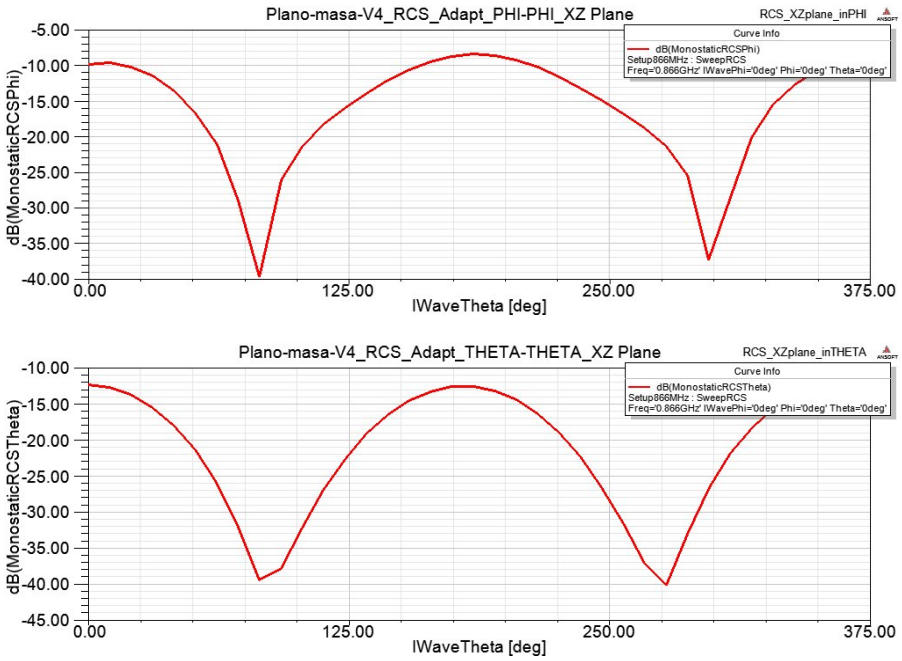

Figure 5.36: Thick dielectric ground plane antenna RCS results on XZ plane

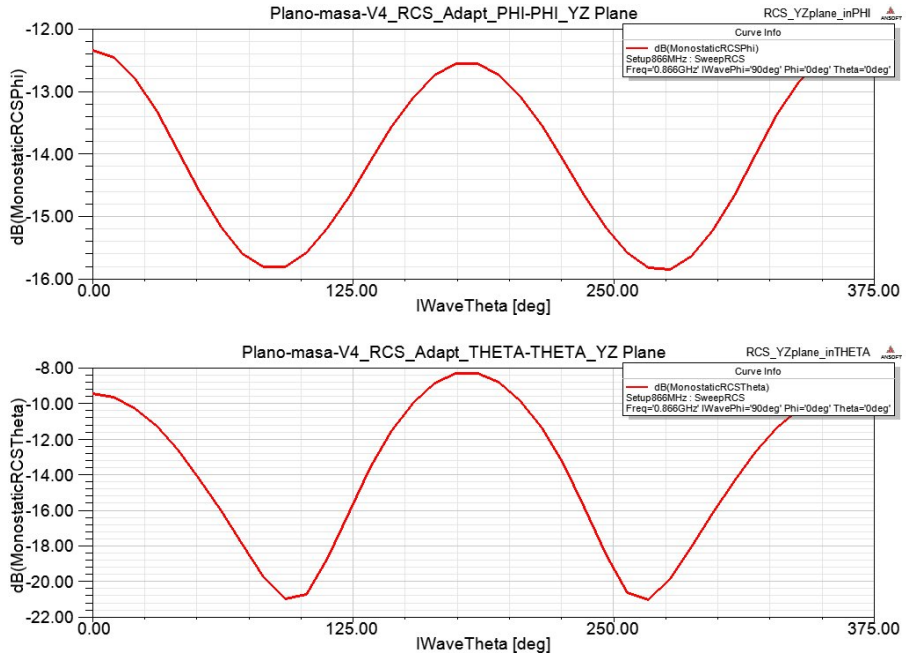

Figure 5.37: Thick dielectric ground plane antenna RCS results on YZ plane

plane could be reflecting power too.

For the other plane (YZ) we can see in figure 5.37 that the antenna shows a similar performance, but in this case the strongest component is the θ reaching values of -9dB. The other component ϕ is also well-reflected reaching values of -13 dB. As has been seen this antenna has a very good performance with the only disadvantage of the dielectric thickness so it could work well on other applications with metallic surfaces where a low profile antenna is not needed.

Thin Ground Plane

Given some results with a thick dielectric, we tried to reduce this thickness to the maximum possible in order to achieve a low-profile antenna which could work placed on a CD. The conclusion obtained is that when the dielectric thickness becomes lower than 1 cm the antenna performance begins to deteriorate. This conclusion is explained below. To demonstrate this conclusion we can see two antennas in figure 5.38, the first one (Left) is placed on a dielectric of 13 mm and the second one (Right) is placed on a dielectric of 4 mm both dielectrics of $\epsilon_r = 10.2$.

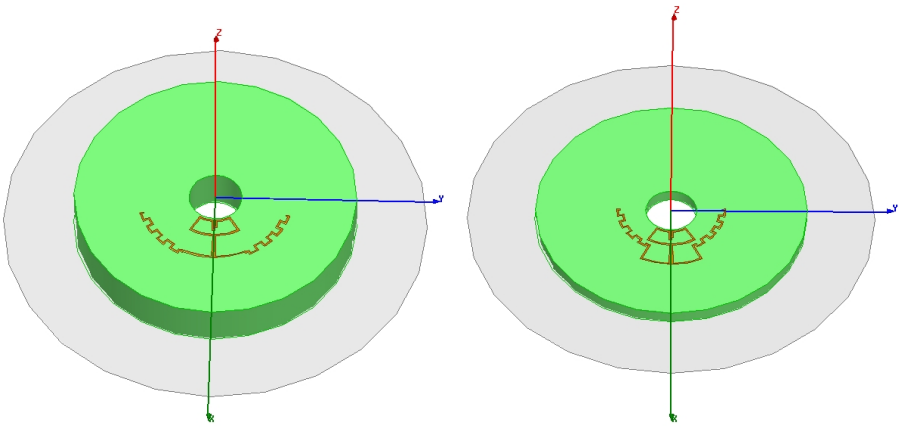

Figure 5.38: Antenna examples on thin dielectric of 13 mm (Left) and 4 mm (Right)

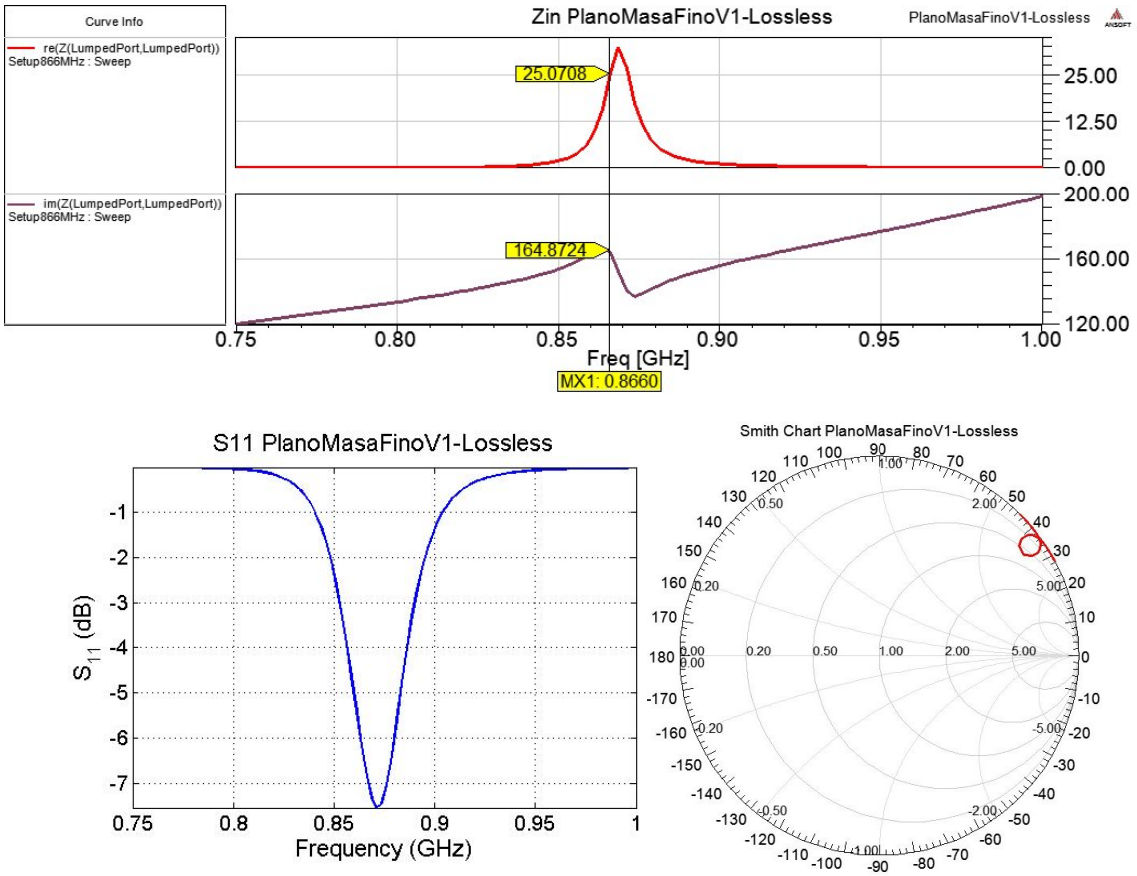

Figure 5.39: Antenna on 13 mm and $\epsilon_r = 10.2$ dielectric results

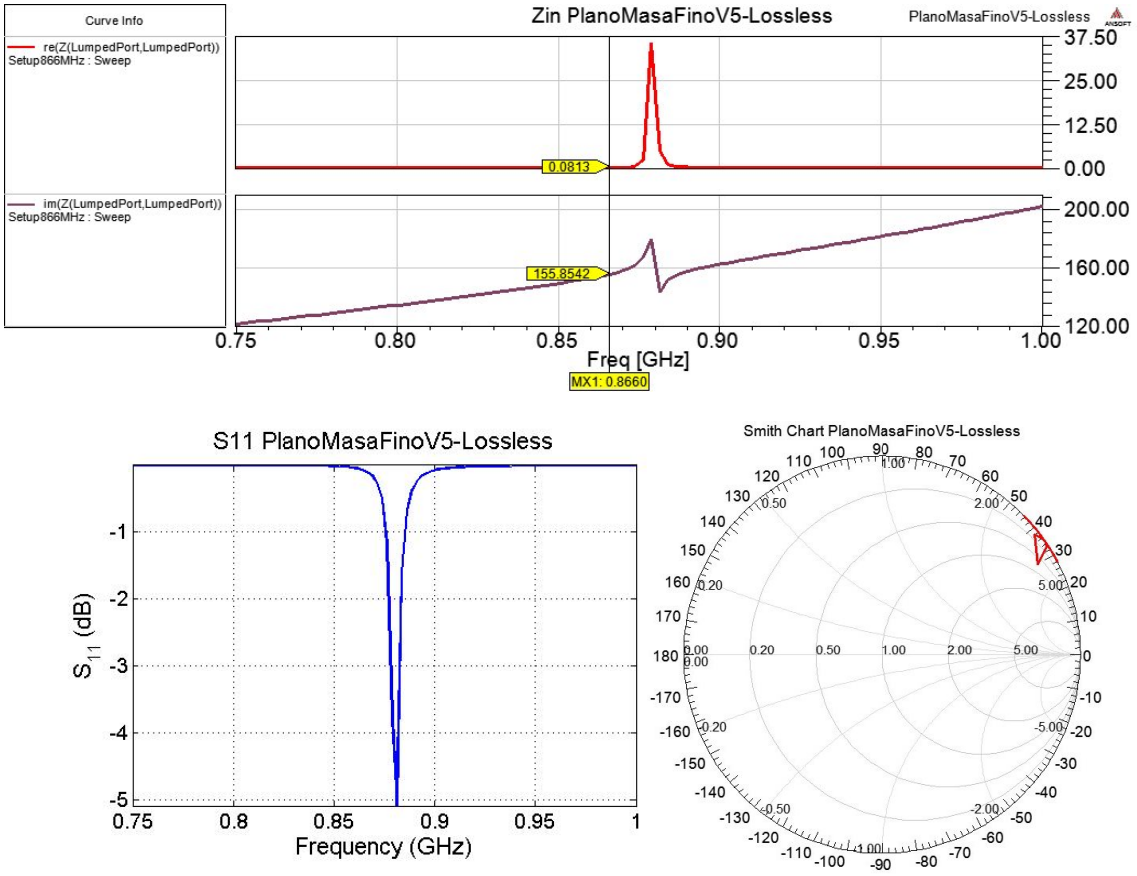

Figure 5.40: Antenna on 4 mm and $\epsilon_r = 10.2$ dielectric results

For the 13 mm dielectric results, shown in figure 5.39, we can see that the antenna have an acceptable performance since it has a good bandwidth and it has a good matching level in the resonance peak of -7.5 dB at 860 MHz and a average level of about -3 dB but it is obviously worst than the previous thick dielectric antenna due to the thickness reduction. Even so this antenna keeps a good performance as we have said but if we look at the second antenna results in figure 5.40 we can observe that the antenna performance has been deteriorated and now we have similar results as all the previous antennas when they was placed near the metallic layer. This antenna has a very narrow bandwidth with low matching level in the resonance peak of -5 dB at 870 MHz. This bandwidth reduction begins to be important when the dielectric thickness becomes lower than 1 cm and we have realized that it has a difficult solution after so much research.

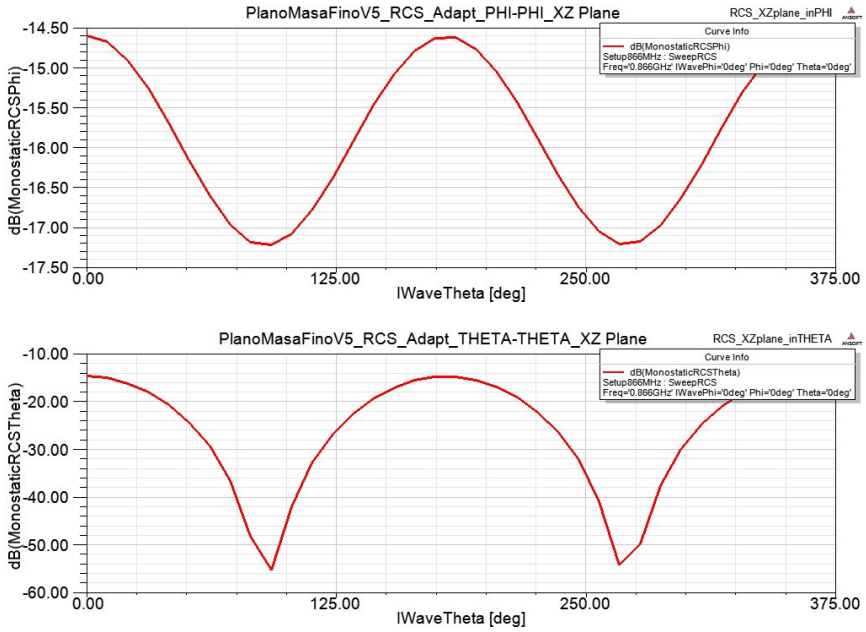

Figure 5.41: Thin dielectric (4 mm and $\epsilon_r = 10.2$) ground plane antenna RCS results on XZ plane

To complete the results for the last antenna which would be the more interesting if it could work (because it is less thick), we can see its RCS results on figure 5.41 for the XZ plane and in figure 5.42 both results for the co-polar components PHI-PHI and THETA-THETA.

As can be seen the results are very similar to the thick dielectric antenna, on the XZ plane the ϕ component is slightly higher with levels of -14.5 dB while the θ component reach -15.3 dB. For this antenna the RCS levels are clearly worst than with the previous antenna with thick dielectric, this is normal because of the proximity of the metallic layer.

For the other plane (YZ) the results are similar but this time the θ component wins with levels of around -14 dB. The ϕ component has a very similar value of -14.7 dB. These plane results are also worst than in the previous antenna so we can conclude the same as before, that this antenna is worst than the previous one due to the greater proximity of the metallic layer.

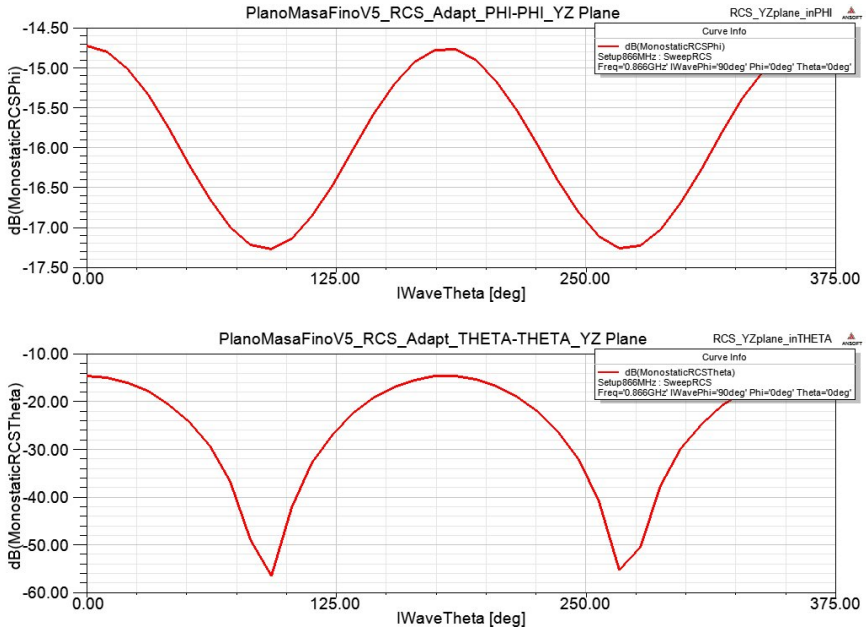

Figure 5.42: Thick dielectric (4 mm and $\epsilon_r = 10.2$) ground plane antenna RCS results on YZ plane

5.5 Last Meanders Antenna

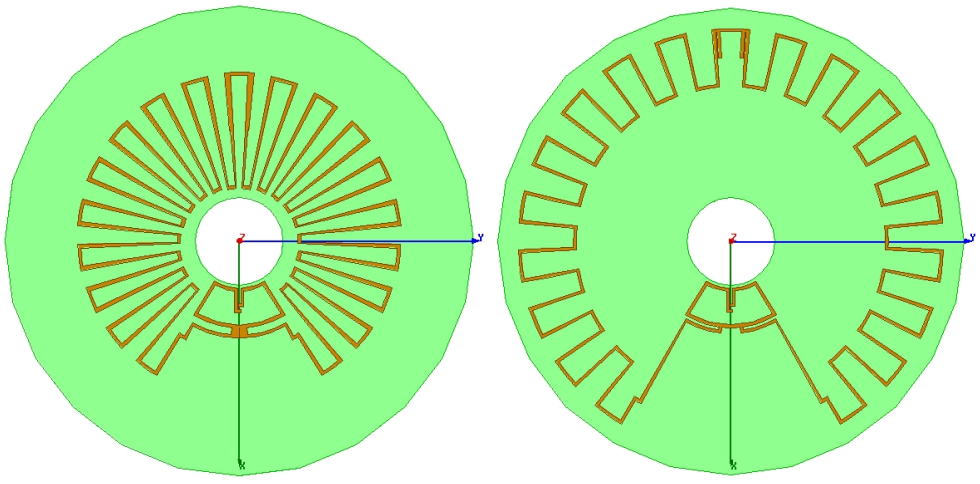

Figure 5.43: Last antenna meanders models with large meanders (Left) and small meanders (Right)

Once done all this research and and seeing that the solution is not trivial on CD we decided to focus on designing an antenna that could work at least on a dielectric substrate on free space with a circular CD shape. We retook the meanders strategy and achieved two good solutions with 2 models, both shown in figure 5.43.

5.5.1 Large Meanders Antenna

This antenna (the left one in figure 5.43) is the large meanders model. As can be seen it is simply the meanders antenna studied but using more area than the previous ones. This is because as more surface use the antenna the performance is better. This has a limitation which is that the antenna has to use the less area possible. The results obtained for this antenna are shown in figure 5.44.

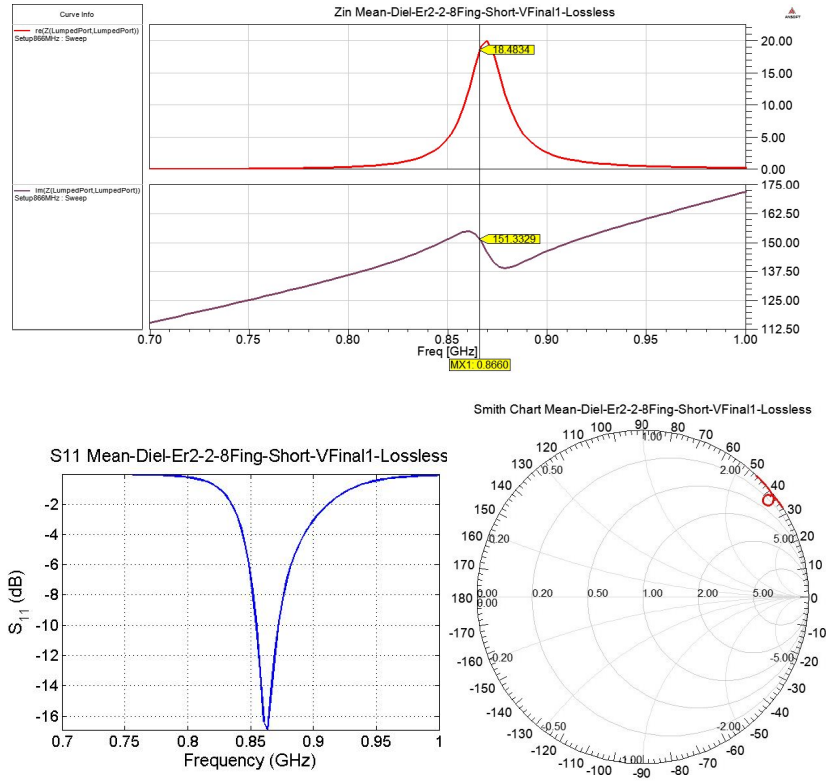

Figure 5.44: Last antenna meanders with large meanders results (dielectric 0.13 mm and $\epsilon_r = 2.2$)

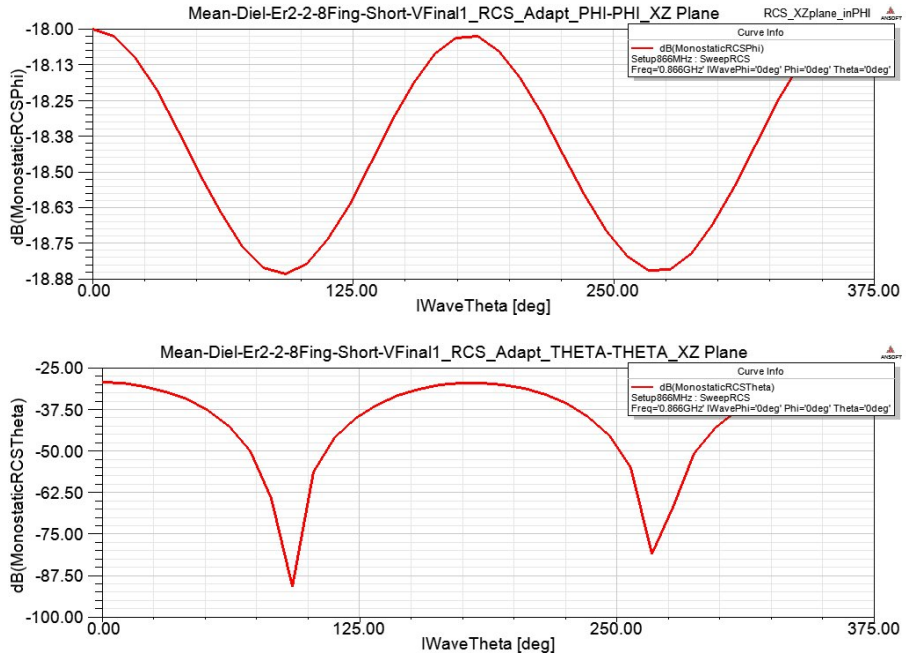

Figure 5.45: Last antenna meanders with large meanders RCS results on XZ plane

We can notice that these results are much better than other meanders antennas results as they have a very good bandwidth of 100 MHz below -4 dB and they are very well tuned at the desired frequency of 866 MHz with good matching level around this frequency. This is due to the good Smith chart loop that is very closed and with a smooth shape besides it is very controllable with the geometric parameters.

To complete the results for this antenna we can see the RCS components in figure 5.46. Once again the studied components are the co-polar since they are the more interesting for our aim. This antenna has worst RCS performance than the previous studied ones. As can be seen in plane XZ the best compoment is the ϕ reaching values of -18 dB and with a θ component that has maximum values of -26 dB. In the other plane (YZ) we have the opposite situation with a better θ component of -18 dB maximum value and a ϕ component with maximum values of -29.5 dB.

As conclusion this antenna seems to work well given the previous results but it

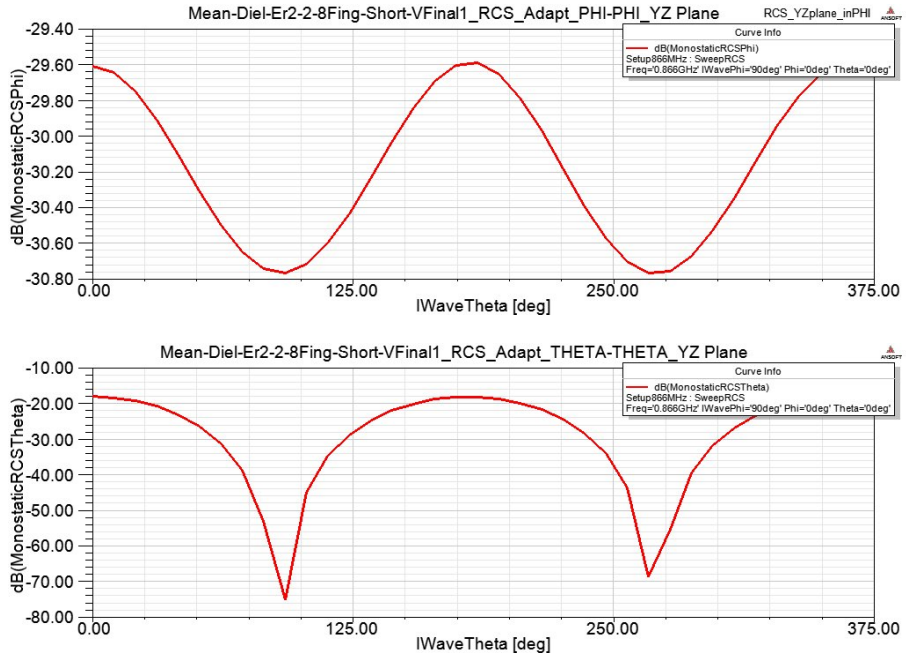

Figure 5.46: Last antenna meanders with large meanders RCS results on YZ plane

has a worst RCS than previous antennas so it could lead to a reading range reduction even in good environments.

5.5.2 Small Meanders Antenna

This other antenna that is on the right in figure 5.43, is the short meanders model. To achieve the same performance with smaller meanders we designed this antenna with a higher arms radius to compensate the surface reduction of the meanders. So this antenna occupies more area than the previous one. This could be negative for applications where a small surface antenna is needed.

Figure 5.47 shows the results for this antenna. We can see that this antenna has similar performance than the previous one but with a much better resonance. The bandwidth achieved by this antenna is about 100 MHz at -5 dB. We can notice that these better result is due to the soft variation of the Zin plot and the smaller Smith chart loop which is still very controllable.

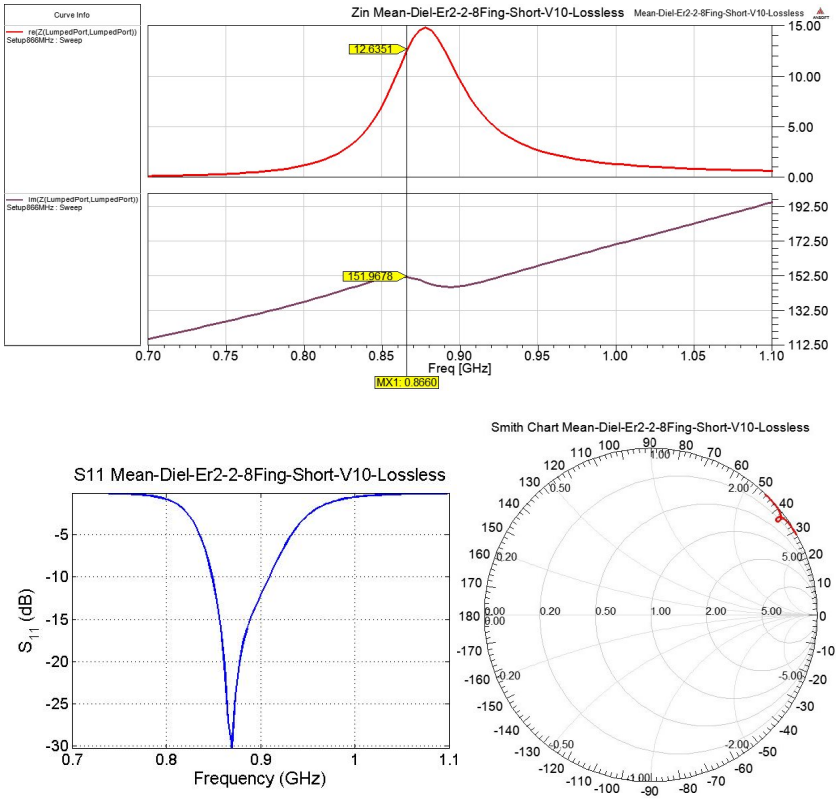

Figure 5.47: Last antenna meanders with small meanders results (dielectric 0.13 mm and $\epsilon_r = 2.2$)

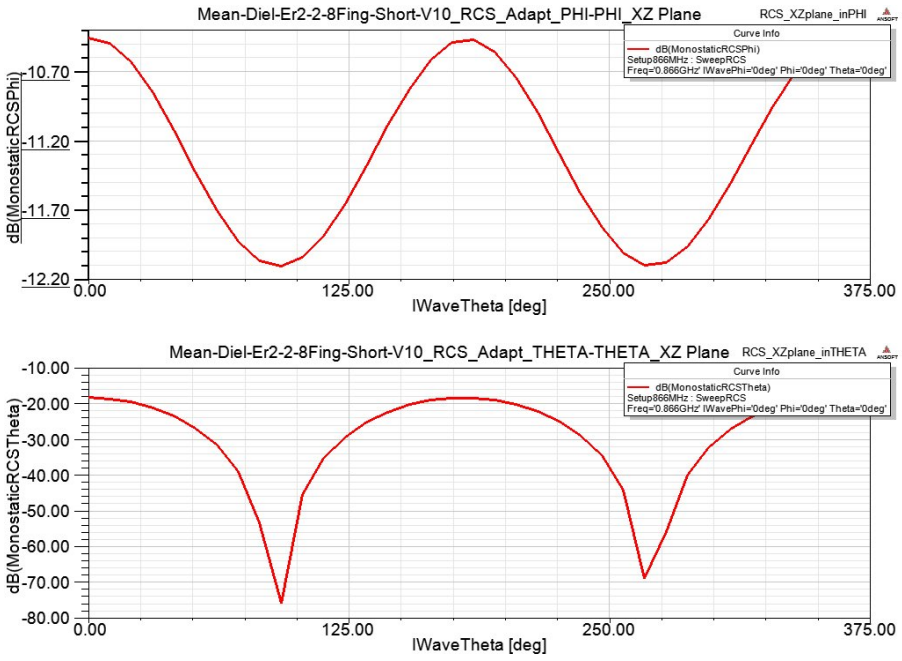

Figure 5.48: Last antenna meanders with small meanders RCS results on XZ plane

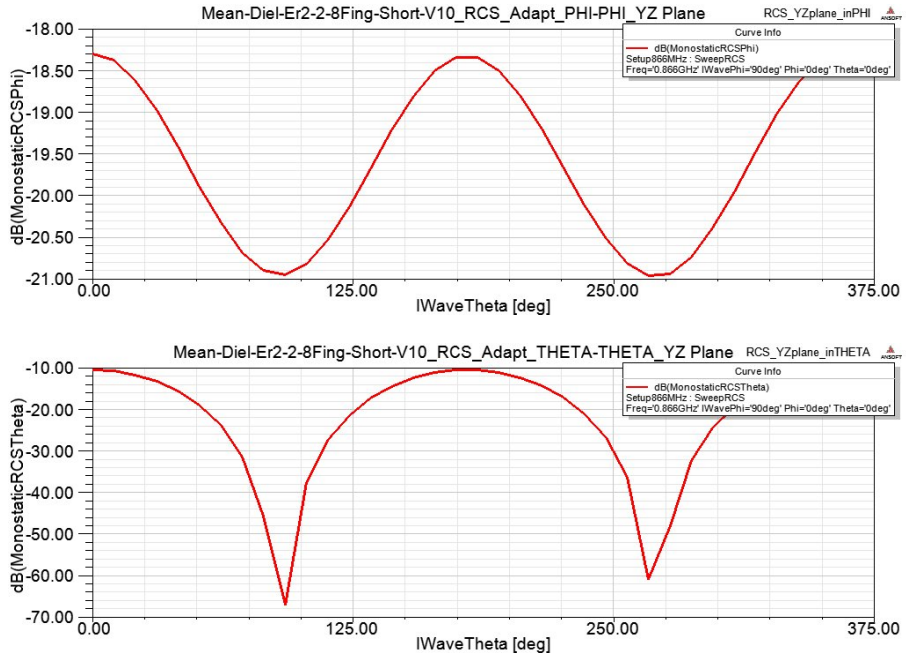

Figure 5.49: Last antenna meanders with small meanders RCS results on YZ plane

We can see the RCS co-polar components in figure 5.49. In this case the RCS results are better due to the greater surface occupied by this antenna. As can be seen in plane XZ the best compoment is the ϕ reaching values of -10.5 dB and with a θ component that has maximum values of -18 dB. In the other plane (YZ) we have the opposite situation with a better θ component of -10 dB maximum value and a ϕ component with maximum values of -18.3 dB.

As conclusion we can say that the last antenna with small meanders but higher arms radius is the best candidate to work well on a real situation due to its best RCS results. The other antenna with bigger meanders has also a good performance and could work well too.

Chapter 6

Conclusions and Future Research Lines

Throughout this project we have covered the investigation of antennas to be put on optical devices such CDs and DVDs. We have shown after a lot of tests that this is a very difficult scenario for an antenna to work on because of the metallic surface presence, which is a problem partially solved for general applications, but not in this case due to the other inconvenient, the very small available surface. It would be much better if the CD graphic layer is not covered (which is the most normal thing that a company would want to buy these antennas).

In chapter 2 we have explained all the theory studied for this project and the techniques used to obtain the results for the antennas. It is important to remark here that the formula used to obtain the reflection coefficient S_{11} has the numerator Z_{chip} conjugated. As we said it is also important that in previous investigations researchers have only focused on studying the impedance matching for the antennas and not the radiation efficiency and the RCS which are very important too to determine the final antenna performance. In this chapter is also reviewed the CD and RFID chip characteristics which are very necessary to do the project properly.

In chapter 3 we have reviewed all the developed GUI software operation and how to use it. All the HFSS operations are controlled via scripts generated by this soft-

ware using many MATLAB functions, which not only allows the automation of the process, but also permits the optimization and testing of many antennas in a short period of time. The knowledge acquired and the developed software are combined in a MATLAB GUI that implements all the geometry design, HFSS simulation and results exporting processes and it is very important to remark that this software have been developed as a modular software which means that if someone would want to create a new antenna with it, is very simple to combine the software with it by creating a new function for this antenna and calling it with the GUI function and matching the parameters texts on the interface but leaving the rest of the GUI equal.

The last 2 chapters are a review of all the simulations and analysis processes followed to design all the antennas proposed in this project, from the first ones created without the software, which took a lot of time, to the last ones created with the software which are more numerous due to the facility to create a lot of different antennas in a few minutes. These last chapters show the difficulty of designing such antennas and the poor performance achieved with all of them even for commercial ones. Here is also explained the problem with the ideal CD and its importance in the designs although finally the CD results are very bad with ideal or non-ideal CDs. Many situations have been explored and finally he reached a partial solution with a thick dielectric and at last we show an antenna with the circular CD shape (with its center free) but that are optimized to work on a dielectric of 0.13 mm and $\epsilon_r = 2.2$.

As final conclusion we have developed a very useful software which saves a lot of time of designing and is prepared to be used for many other antennas just including a new function for each antenna and combining it with the GUI, and we have research a lot of different situations and studied the influence of a lot of parameters in such types of antennas although finally the conclusion is that is very difficult to develop an antenna with a very good performance in such scenario

Some lines of research after this project include:

- Studying the use of new antennas with different shapes that works better that these ones. We have focused on these types of antennas due to the similarity to other commercial antennas but it does not mean that other antennas could work better than these ones. So it could be interesting to try other designs and if there would be some promising one, include it in the software to do a deep investigation.

- Exploring the use of dielectric or magnetic materials in these antennas.

- Further studying the idea of a dielectric since there are commercial antennas for metallic surfaces that work well. Although these antennas does not have the surface and shape limitations than our antennas have, it could be possible to use the CD thick in some way to exploit this advantage. For example we could use the CD border to adapt an antenna using the CD thick as a dielectric. One example of this antennas that work in CDs but has the inconvenient of being very thick to ejected-CD readers is shown in figure 6.1.

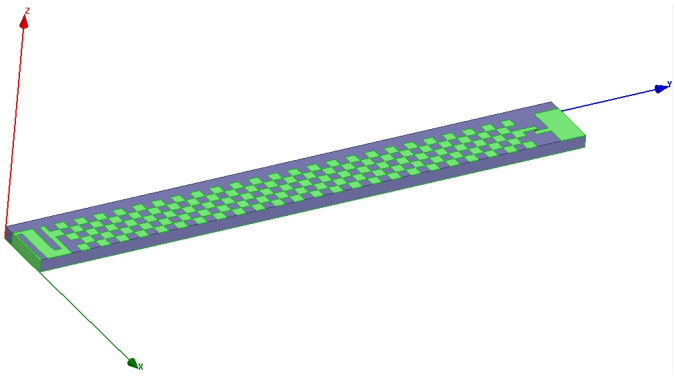

Figure 6.1: Thick antenna example

Bibliography

[1] ANSYS, "Ansoft HFSS 13.0," http://www.ansys.com/Products/Simulation+Technology/Electromagnetics/Signal+Integrity+&+Power+Integrity/ANSYS+HFSS.

[2] *Getting the most out of RFID. A starting guide to radio frequency identification*, July 2006.

[3] K. Finkenzeller, *RFID Handbook. Fundamentals and applications in contactless smart cards and identification*, 2nd ed. John Wiley & Sons.

[4] N. C. Karmakar, *Handbook of Smart Antennas for RFID Systems*, Wiley, Ed. John Wiley & Sons.

[5] Impinj, *Monza 4 Tag Chip Datasheet*, rev 5.1 ed., December 2012.

[6] R. E. Collin, *Foundations for Microwave Engineering 2ND Ed.*, McGraw-Hill, Ed.

[7] A. Galehdar, D. V. Thiel, and S. G. O'Keefe, "Antenna Efficiency Calculations for Electrically Small, RFID Antennas," *IEEE Antennas and Wireless Propagatiion Letters*, vol. Vol. 6, pp. 156–159, 2007.

[8] H. A. Wheeler, "The Radiansphere Around a Small Antenna," *Proceedings IRE*, pp. 1325–1331, 1959.

[9] A. Álvarez Melcón, F. D. Q. Pereira, and J. A. G. Pérez, "Printed Antenna Investigation for RFID tags for CDs and DVDs Identification," *URSI*, 2012.

[10] V. Ramasami, "HFSS script generation using MATLAB," https://www.cresis.ku.edu/~rvc/projects/hfssapi/doc/hfss-matlab-api.html, 2004.

[11] J. A. G. Perez, "PFC JAGP. Final GUI Example," http://www.youtube.com/watch?v=dHWWzKsq7pE, 2013.

[12] W. T. Luk and K. N. Yung, "Bending Dipole Design of Passive UHF RFID Tag Antenna for CD / DVD Discs," *Microwave Conference, 2008. APMC 2008. Asia-Pacific*, pp. 1–4.

[13] A. S. Andrenko, M. K. T. Maniwa, and T. Yamagajo, "Compact Printed-On-CD UHF RFID Tag Antennas," *Antennas and Propagation Society International Symposium, 2007 IEEE*, pp. 5455–5458, 2007.